Statistical Modeling of the Human Sleep Process via Physiological Recordings

A Dissertation
Presented to
The Academic Faculty

by

Jacqueline Antoinette Fairley

In Partial Fulfillment
of the Requirements for the Degree
Doctor of Philosophy in the
School of Electrical and Computer Engineering

Georgia Institute of Technology
December 2008

STATISTICAL MODELING OF THE HUMAN SLEEP PROCESS

VIA PHYSIOLOGICAL RECORDINGS

Approved by:

Dr. George Vachtsevanos, Advisor
School of Electrical and Computer Engineering
Georgia Institute of Technology

Dr. Mark Clements
School of Electrical and Computer Engineering
Georgia Institute of Technology

Dr. Gary May
School of Electrical And Computer Engineering
Georgia Institute of Technology

Dr. David Rye
Department of Neurology
Emory University School of Medicine

Dr. Bonnie Heck-Ferri
School of Electrical and Computer Engineering
Georgia Institute of Technology

Date Approved: December 19,2008

Blessings on him who created sleep.-It covers a man all over, thoughts and all, like a cloak.-It is meat for the hungry, drink for the thirsty, heat for the cold, and cold for the hot.-It makes the Shepard equal to the monarch, and the fool to the wise.-There is but one evil in it, and that is that it resembles death, since between a dead man and a sleeping man there is but little difference.

DON QUIXOTE
By Saavedra M. de Cervantes

This dissertation is dedicated to my oldest sister Dr. Benetta E. Fairley-Johnson and the Reed Sister's of Monticello Arkansas Bessie, Bennie, and Bobbie whose prayers and love have consistently strengthened me physically, mentally and spiritually to help me move ***closer to my dreams****.*

ACKNOWLEDGEMENTS

Allow me to take this opportunity to extend my gratitude to the individuals and institutions that were instrumental in the development of this work:

The National Consortium for Graduate Degrees for Minorities in Engineering and Science, Inc., Motorola, IBM, National Science Foundation, and the Geogia Institute of Technology programs: CETL, FACES, and SURE for providing financial support; Dr. George Vachtsevanos for supplying guidance and technical equipment for this project; David Rye, M.D. for providing the opportunity to learn so many great and priceless things about the clinical aspects of the human sleep cycle; Dr. Gary May, Dr. Mark Clements, and Dr. Bonnie Heck-Ferri for participating on my dissertation committee; Brian Litt, M.D., Susan Herman, M.D., and Dr. Lichu Zhoa for introducing me to a research area that has provided me with an excellent conversation starter; Nicholas Butkov, RPSGT for graciously allowing me to adopt his illustrations in this work; Dr. Hiram Firpi, Dr. George Georgoulas, Dr. Javier Echauz, Dr. Lauren Burrell, and Dr. Otis Smart for supplying me with much needed technical assistance and emotional support; Ashley Johnson for her assistance in publishing the pre-processing results for this work; Lonnie T. Parker for assisting me with the oral presentation during the proposal of this work; Sekou Remy, Brett Matthews, and George Stefopoulos for providing feedback regarding the oral communication of this work; Karolyn Babalola for consistently offering a listening ear regarding my research methods; Ajia Mignon-Tenney for showing me how a few simple words can solve complex problems and offering to edit the written portion of this work; Adrianne Prysock for inspiring me to reach each milestone needed to complete this work and helping me to celebrate accomplishing them; Paula Ann and Ardell Fairley for encouraging my **passion** for learning at a young age; Bennie Mae Rayford for teaching me by example where true **strength** resides; Also, to all that have been referenced throughout this work because we do indeed “stand on the shoulders of giants”. Lastly, to the person this work is dedicated, Dr. Benetta Fairley-Johnson, in the words of Kindred the Family Soul “we’ve come so far the stars look up at us” without your unconditional love this work would not have been conceivable or achievable, for that I am forever and gratefully indebted to you.

TABLE OF CONTENTS

LIST OF TABLES

LIST OF FIGURES

NOMENCLATURE

** Terms adapted from Butkov[1].*

***Amplitude:** Represents the peak-to-peak voltage measurement of a signal. In biological signal analysis voltage values are often provided in micro-volts and found by comparing the measure signal with a calibration signal of a known voltage value.

***Artifacts (Noise):** Undesirable signals captured in any sleep parameter. Example: eye activity recorded in the brain signal.

***Bandwidth:** The available spectrum of frequency values in a system.

Bradykinesia: Represents a slowed ability to start and continue physical movements.

***Canthus:** The area located at the corner of the eye.

***Channel:** The components creating an input to output pathway used to record the biological signal.

Confusion Matrix: A visualization tool used to display classification confusion for multiple classifications. Rows in the matrix represent the actual class labeling and columns show the predicted class labeling. A perfect classifier is displayed when all matrix values contain zero except the central diagonal.

***Duration:** A time measurement that represents the interval between the start and end process of an event.

***Electrode:** An electrical device used for receiving and sending electrical signals.

***Electroencephalogram (EEG):** A recording of electrical activity generated within the brain.

***Electromyogram (EMG):** A recording of electrical activity generated within the muscle tissue.

***Electrooculogram (EOG):** A recording of electrical activity generated by eye movements.

***Electrocardiogram (EKG):** A recording of electrical activity generated within the heart.

***Epoch:** Polysomnogram signal recordings with a 20 or 30 second duration.

Feature: A distinct signal characteristic (ex. Amplitude) that is associated with a specific biological sleep state (ex. Wakefulness).

***Filter:** An electrical device that limits the range of frequencies permitted to pass through an amplifier.

***Frequency:** The number of wave forms that occur in one second.

***Hertz (Hz):** A measurement of frequency described in cycles per second.

***Hypnogram**: A graphical illustration of sleep stage sequences with respect to their occurrence in time.

***Impedance:** The prevention of the transmission of a specified range of frequencies, often measured in ohms or kilo ohms.

***Lead:** A wire located between an electrode and the polysomnograph.

***Movement Time (MT):** An unidentifiable epoch corrupted by excessive patient movement.

***NREM sleep:** Sleep lacking rapid eye movement activity.

***Peak:** Represents the maximum wave amplitude.

***Polysomnogram:** A graphical display of simultaneous physiological events recorded during sleep.

***Polysomnograph:** An instrument with multiple channels used to record sleep-related physiological events.

Processing window: The time duration used to calculate a signal feature.

***Quantitative data:** Recorded biological signals obtained from precise instrument calibrations.

***REM sleep:** Sleep containing rapid eye movements.

***REM sleep behavior disorder (RBD):** A sleep disorder marked by decreased muscle atonia during REM sleep, may also include increased motor activity and /or violent behavior in REM sleep.

***Signal:** An electrical quantity caused by the chemical reactions of charged ions.

***Sleep cycle:** A period of NREM sleep immediately followed by a period of REM sleep.

***Sleep scoring:** The method used to classify stages of a sleep cycle.

***Sleep stages:** Signature sleep intervals marked by specific EEG, EOG, and EMG characteristics.

***Sleep-wake cycle:** The arrangement of sleep and wakefulness segments within a 24 hour period.

***Slow wave sleep:** A term often used to describe stages 3 and 4 sleep.

***Surface electrode:** Electrodes attached to the surface of the skin.

Tonic: Continuous muscle tension or contraction

***Voltage (V):** An electromotive force caused by a difference in electrical potentials, represented in volts (V).

***Wave:** A graphical representation of periodic voltage variations

***Waveform:** The wave's shape

SUMMARY

The main objective of this work was the development of a computer-based Expert Sleep Analysis Methodology (ESAM) to aid sleep care physicians in the diagnosis of pre-Parkinson's disease symptoms using polysomnogram data. ESAM is significant because it streamlines the analysis of the human sleep cycles and aids the physician in the identification, treatment, and prediction of sleep disorders.

In this work four aspects of computer-based human sleep analysis were investigated: polysomnogram interpretation, pre-processing, sleep event classification, and abnormal sleep detection. A review of previous developments in these four areas is provided along with their relationship to the establishment of ESAM. Polysomnogram interpretation focuses on the ambiguities found in human polysomnogram analysis when using the rule based 1968 sleep staging manual edited by Rechtschaffen and Kales (R&K)[2]. ESAM is presented as an alternative to the R&K approach in human polysomnogram interpretation. The second area, pre-processing, addresses artifact processing techniques for human polysomnograms. Sleep event classification, the third area, discusses feature selection, classification, and human sleep modeling approaches. Lastly, abnormal sleep detection focuses on polysomnogram characteristics common to patients suffering from Parkinson's disease.

The technical approach in this work utilized polysomnograms of control subjects and pre-Parkinsonian disease patients obtained from the Emory Clinic Sleep Disorders Center (ECSDC) as inputs into ESAM. The engineering tools employed during the development of ESAM included the Generalized Singular Value Decomposition (GSVD)

algorithm, sequential forward and backward feature selection algorithms, Particle Swarm Optimization algorithm, *k*-Nearest Neighbor classification, and Gaussian Observation Hidden Markov Modeling (GOHMM).

In this study polysomnogram data was preprocessed for artifact removal and compensation using band-pass filtering and the GSVD algorithm. Optimal features for characterization of polysomnogram data of control subjects and pre-Parkinsonian disease patients were obtained using the sequential forward and backward feature selection algorithms, Particle Swarm Optimization, and *k*-Nearest Neighbor classification. ESAM output included GOHMMs constructed for both control subjects and pre-Parkinsonian disease patients. Furthermore, performance evaluation techniques were implemented to make conclusions regarding the constructed GOHMM's reflection of the underlying nature of the human sleep cycle.

Contributions from this work included a methodology for automatic removal/compensation of specific artifacts within the human polysomnogram, a quantitative based feature library for sleep event classification, and sleep models representing pre-Parkinsonian disease patients and normal age matched control subjects. These contributions are significant in understanding the human sleep cycle and aiding physicians in the identification, treatment, and prediction of sleep disorders.

CHAPTER 1: INTRODUCTION

1.1 Problem Statement

Quantitative sleep methodologies have been difficult to establish since sleep has been traditionally defined with quantitatively ambiguous rules. These rules are based on the 1968 sleep staging manual edited by Rechtschaffen and Kales [2]. A drawback of the R&K manual is that it neglects the micro-structure of sleep. Neglecting the microstructure of sleep has been shown to be problematic in medical treatment contributing to improper patient diagnosis in certain sleep pathologies. In 2004 Parrino et al. cited the importance of investigating the micro-structure of sleep to determine how depressive disorders affect the human sleep cycle [3]. The goal of this study was to bypass the need for ambiguous rule use in sleep analysis by establishing a computer-based expert decision system built upon sleep physician knowledge and a quantitative methodology.

Flexer et al's. continuous and probabilistic sleep classifier based upon a GOHMM addresses limitations of the R&K manual in quantitative and micro-structural sleep analysis [4] and does not rely on ambiguous sleep rule interpretation. For this reason, the Flexer Model was used as a benchmark for ESAM. Although Flexer's Model offered advantages in micro-structural sleep analysis it required further development in polysomnogram noise reduction/artifact removal and abnormal sleep analysis. ESAM expanded upon the Flexer Model by investigating noise reduction/artifact removal methods and evaluating polysomnograms of pre-Parkinsonian disease patients.

1.2 Purpose Statement

This work contained three aims. Aim one consisted of the development of an automated computer-based artifact removal/compensation methodology for specific artifacts within human polysomnograms. The second aim included the development of a quantitative computer-based sleep model based on human polysomnograms. Finally, the third aim focused on the application of the quantitative sleep model to a clinically relevant sleep problem. An illustration of the methodology used in ESAM to meet the three aims is provided in Figure 1.2 1 (module #1 reprinted with the author's permission [1]). The five module process implemented in ESAM is described in the bulleted list below:

- **MODULE#1**: Polysomnogram data collection, for both control subjects and pre-Parkinsonian disease patients, conducted at ECSDC
- **MODULE#2**: Pre-processing of polysomnogram data using noise reduction/artifact removal methods that included band-pass filtering and the GSVD algorithm
- **MODULE#3**: Polysomnogram processing window selection and feature extraction with window selection obtained from physician consultation and feature extraction conducted using sequential forward and backward feature selection algorithms, Particle Swarm Optimization algorithm, and *k*-Nearest Neighbor classification.
- **MODULE#4**: Sleep stage classification implemented using GOHMMs constructed for both control subjects and pre-Parkinsonian disease patients

- **MODULE#5**: Expert prior knowledge of the human sleep cycle provided by the sleep physician to enhance ESAM performance

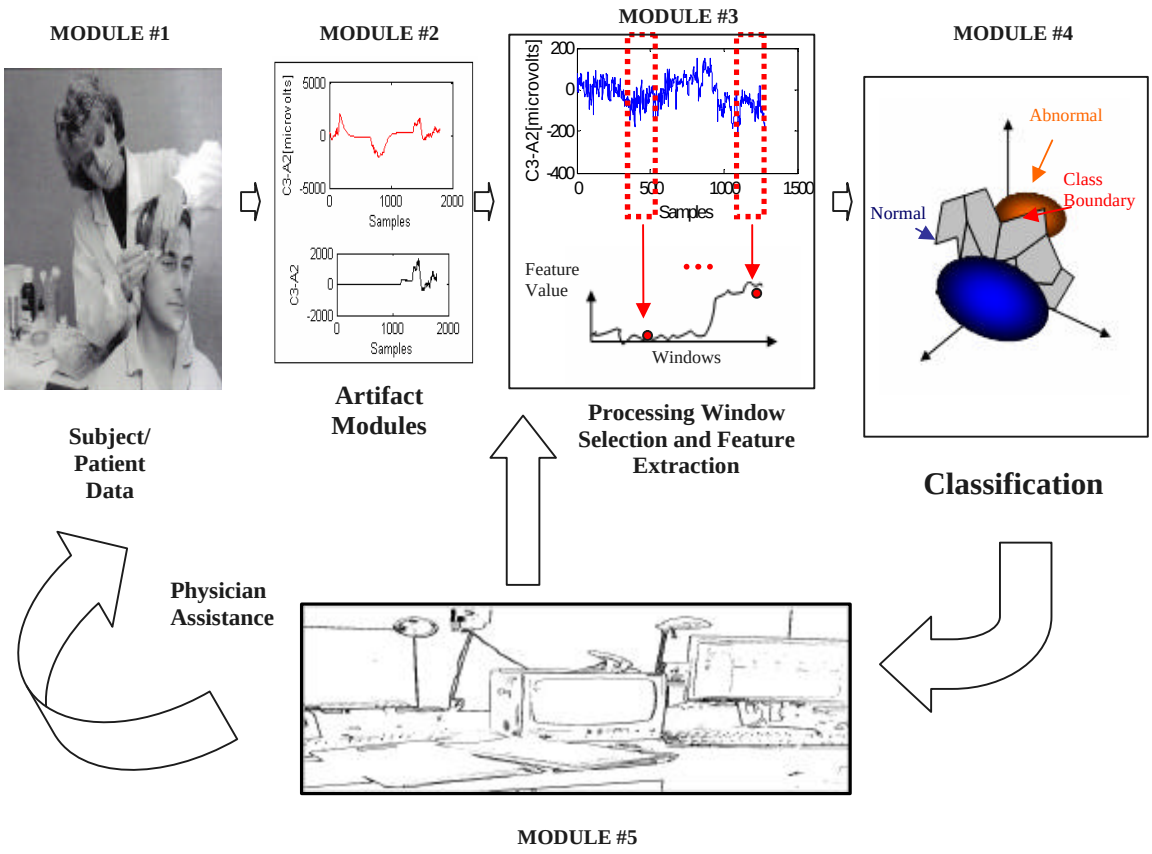

Figure 1.2 1: Illustration of the expert sleep analysis methodology (ESAM).

1.3 Research Questions

The research questions investigated in this study to meet the aims stated in Section 1.2 are included below.

1. What methodology should be incorporated to automatically remove/compensate for specific artifacts within the human polysomnogram?

2. What quantitative features should be extracted from the polysomnogram to best describe the human sleep cycle?

3. What GOHMM model parameters should be used to best differentiation between control subjects and pre-Parkinsonian patients?

1.4 Significance of Study

Sleep problems adversely affect daytime vigilance, job performance, and accident rates. Physiological changes during sleep also contribute to a wide variety of medical conditions. In 2005 the National Sleep Foundation found that 75% of American adults suffer from some type of sleep problem at least a few nights each week [5]. Understanding the human sleep cycle will aid physicians in the identification, treatment, and prediction of sleep disorders. Advancements in sleep research also provide potential cost savings along with improved health for thousands of Americans.

1.5 Delimitations

1. Polysomnogram data were collected for this study during 01/29/2007 through 03/16/2008.

2. All polysomnogram data for this study were obtained from the ECSDC located in Atlanta, Georgia.

3. The age range of subjects/patients included in this study was 54 to 76.

4. Manual artifact labeling for evaluation of the artifact methodology was conducted following proper training in visual polysomnogram artifact identification.

1.6 Assumptions

1. The size of the data set investigated was sufficient to extract significant conclusions regarding the application of ESAM to clinically relevant sleep problems.

2. The artifacts investigated were the primary polysomnogram signal degradation contributors in this study.

3. Artifacts not detected during manual labeling for artifact methodology performance validation did not significantly contribute to polysomnogram signal degradation.

4. The age range of subjects/patients utilized in this study significantly reflected the pre-Parkinsonian disease patient demographic.

5. Single night polysomnogram recordings for each subject/patient represented a sufficient sample set for pre-Parkinsonian disease classification.

1.7 Definition of Terms

1.7.1 Sleep Stages

According to R&K there are two cycles of sleep: REM (Rapid Eye Movement) and NREM (Non-Rapid Eye Movement). REM represents one stage of sleep that is

distinguished by physiological attributes such as increased brain activity, pronounced eye movement, hastened respiration, and muscle relaxation. NREM sleep consists of four stages (Stage 1, Stage2, Stage 3, and Stage 4). Wakefulness (Stage W) is often included as the sixth stage of the human sleep cycle.

Brain waves referenced during the characterization of sleep staging include: delta, theta, alpha, and beta bandwidths. The delta bandwidth tends to have the highest amplitude and slowest waves. These waves are usually found to reside below 4 Hz. Delta activity is often described as deep sleep because of the sleeper's low level of arousal. The 4 to 7 Hz frequency band includes theta brain wave activity and is present during sleep but may also be found in the wake state during stressful periods for adults. Alpha waves reside above 13 Hz bandwidth and are found when an individual is relaxed yet alert. Beta waves are located within the 14 to 30 Hz frequency band and are associated with normal waking consciousness. Figures 1.7.1. 1 - 4 taken from Butkov [1], and reprinted with the author's permission, display the brain wave activity found in the EEG signal during alpha, beta, theta, and delta activity respectively.

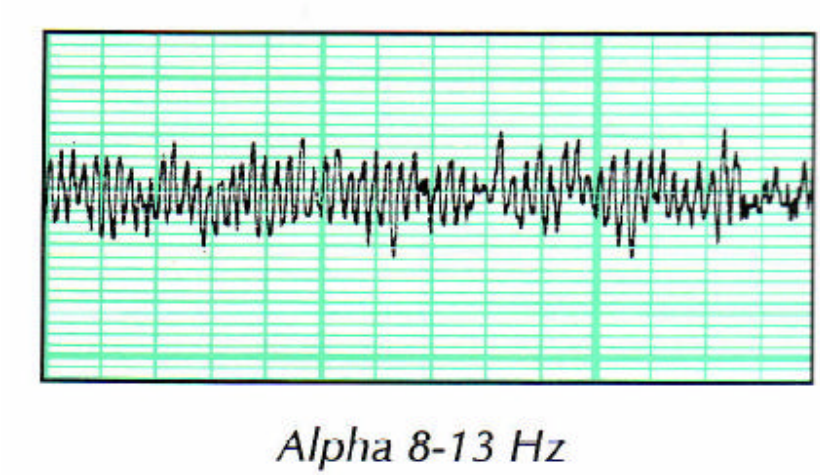

Figure 1.7.1 1: Illustration of alpha wave activity in the EEG signal[1].

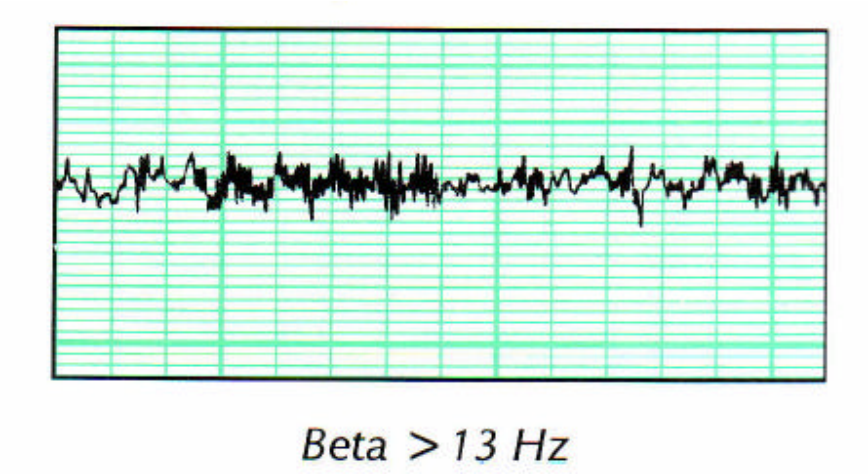

Figure 1.7.1 2: Illustration of beta wave activity in the EEG signal[1].

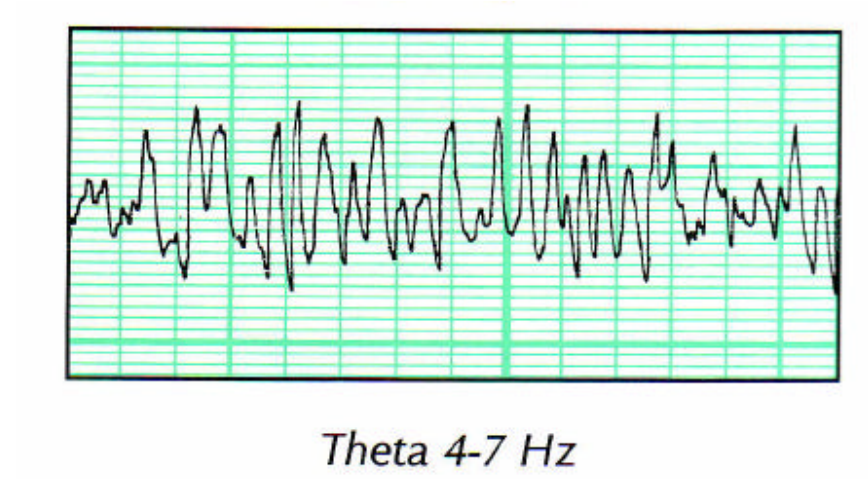

Figure 1.7.1 3: Illustration of theta wave activity in the EEG signal[1].

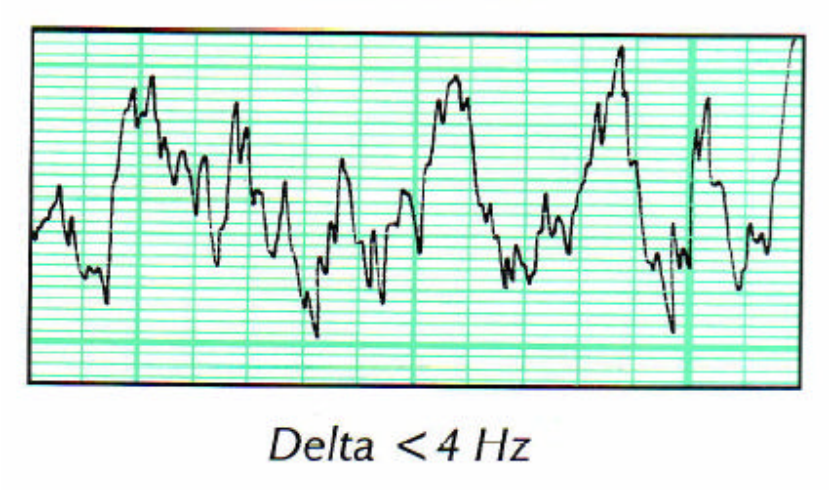

Figure 1.7.1 4: Illustration of delta wave activity in the EEG signal[1].

1.7.2 Scoring Criteria

The sleep stages with their prominent waveform characteristics taken from R&K [2] are listed below. These waveform characteristics were utilized as scoring criteria by the sleep technician in this study.

Wakefulness

This stage is represented by rhythmic alpha waves and/or low voltage, and mixed frequency activity in the EEG.

NREM Cycle

Stage 1: Considered a transitional stage of sleep, usually lasts for several minutes. Theta activity and sharp waves are prevalent with low voltage in the EEG. REM activity is absent in the EOG.

Stage 2: Consists of sinusoidal waves appearing in bursts of 12-14 Hz, commonly labeled as sleep spindles, residing within the EEG. K-Complexes (KCs) are also present, which are EEG waveforms defined by a negative sharp wave immediately followed by a positive component. The time duration of these waveforms should exceed 0.5 seconds.

Stage 3: The EEG is marked by low-frequency delta waves/slow wave activity.

Stage 4: This stage along with Stage 3 is often referred to as slow-wave sleep. The latter may be attributed to the increase in slow wave activity that dominates the EEG reading.

REM Cycle

Saw-tooth, theta, and slow alpha wave activity are commonly found in the EEG within this stage. REM activity is present in the EOG. Low amplitude activity is found in the EMG.

Table 1.7.2 1 adopted from Carskadon et al. summarizes the 20-30 second epoch-based sleep stage scoring criteria outlined by R&K for the adult normal sleep cycle [6]. Graphical representations of the polysomnogram activity and prominent waveforms presented in Table 1.7.2 1 are found in Figures 1.7.2 1 [7] and Figure 1.7.2 2 [1], respectively.

Table 1.7.2 1: Summary of sleep staging criteria outlined by R&K.

Stage	EEG Characteristics	EOG Characteristics	EMG Characteristics
Wakefulness	Eyes Closed: Rhythmic alpha activity (8-13 Hz) Eyes Open: Low voltage activity compared to baseline and mixed frequency waves	Rapid or no eye movements, plus slow eye movements during drowsiness	Tonic activity high
NREM Stage 1	Low voltage activity compared to baseline and mixed frequency waves Theta activity may be present (3-7 Hz) along with sharp vertex waves	Slow eye movements	Tonic activity low
NREM Stage 2	Low voltage activity compared to baseline and mixed frequency waves Sleep spindles (12-14 Hz) and KC events	Some slow eye movements near sleep onset	Tonic activity low
NREM Stage 3	Approximately half of the epoch contains high voltage activity(> 75μV) At least 20% of the epoch contains slow frequency waves (= 2 Hz)	None	Tonic activity low
NREM Stage 4	More than half of the epoch contains high voltage (> 75μV) Slow frequency wave activity present	None	Tonic activity low
Stage REM	Low voltage activity compared to baseline and mixed frequency waves Sawtooth, theta, and slow alpha wave activity present	Phasic rapid eye movements	Tonic suppression w/ phasic twitches

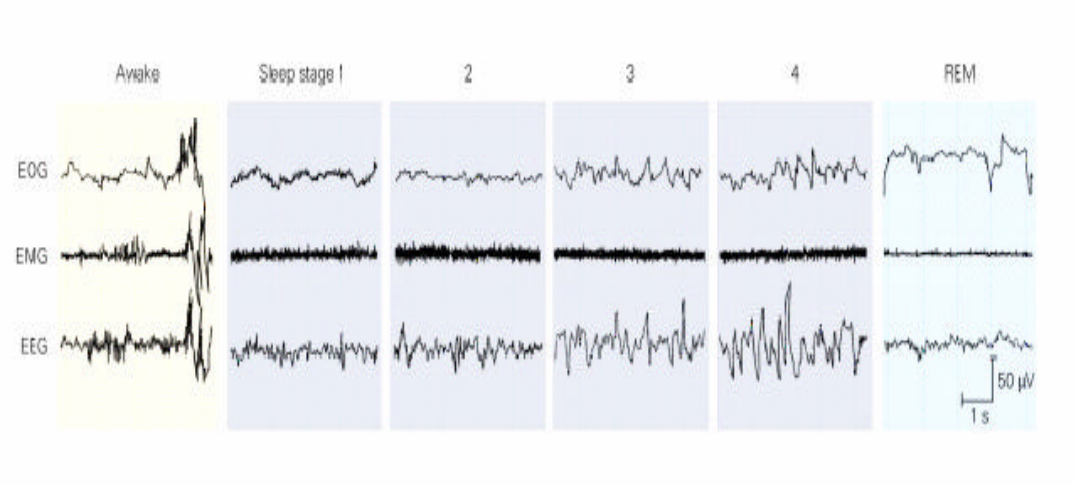

Figure 1.7.2 1: Illustration of polysomnogram data with respective sleep stages outlined by R&K (reprinted with the authors permission [7]).

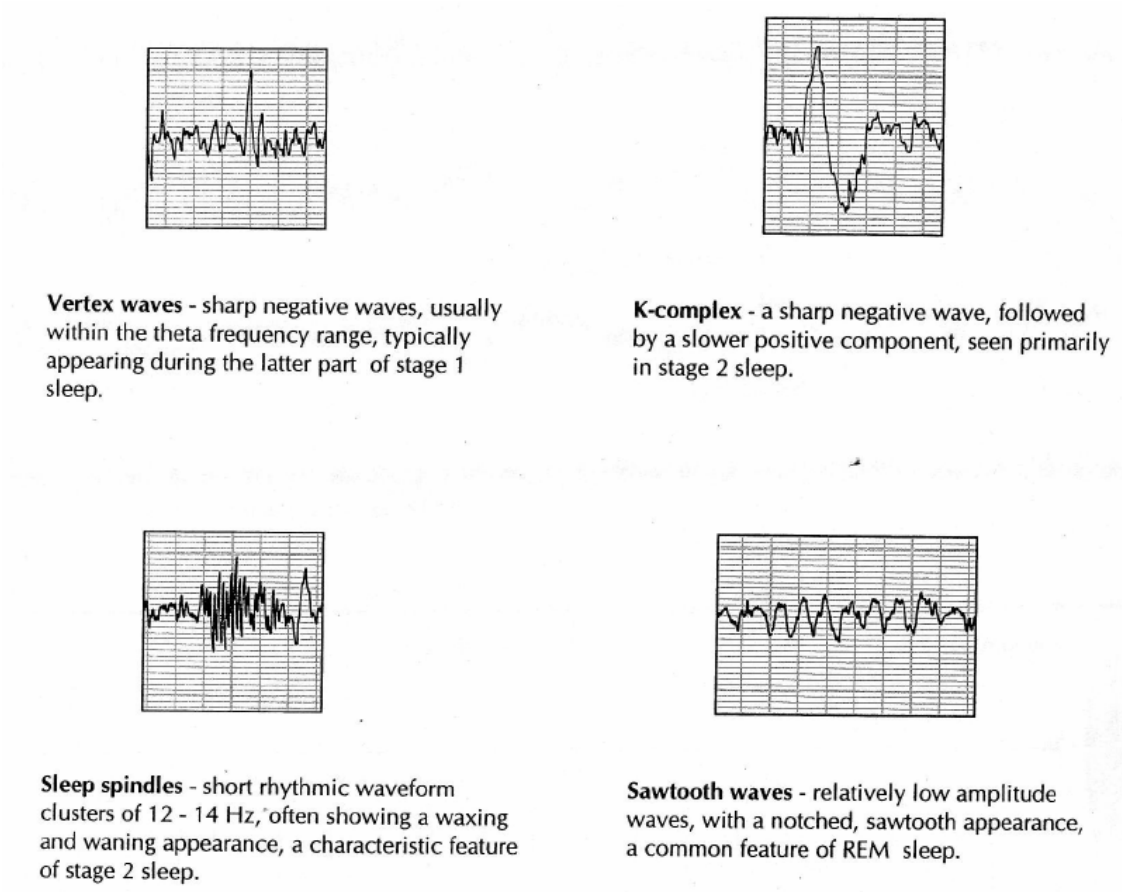

Figure 1.7.2 2: Prominent brain waveforms commonly found in the normal human sleep cycle (re-printed with author's permission [1]).

1.8 Organization of Study

The remaining portions of this study are organized into four chapters, appendices and references in the following order. Chapter 2 provides a review of relevant literature addressing concerns with R&K sleep scoring, artifact removal and compensation for polysomnogram data, computerized (automated) sleep scoring, and Parkinson's disease and the human sleep cycle. Chapter 3 presents the research design and methodology utilized to conduct the study. The data collection procedures, population and sampling procedures, instrumentation, study limitations, and research design are discussed. Presentation of the results obtained from ESAM polysomnogram intelligent feature selection, and ESAM model selection are provided in Chapter 4. A summary of the study, the relation of the study findings to the literature, study surprises, implications for action based on the study and how the study may be expanded to conduct further research are presented in Chapter 5. Appendices and references make up the final portion of the study.

CHAPTER 2: LITERATURE REVIEW

2.1 Chapter Introduction

This chapter focuses on four major aspects of human sleep analysis via polysomnography for computer-based human sleep modeling systems: interpretation, pre-processing, sleep stage classification, and abnormal sleep detection. The four major aspects of human polysomnogram analysis represent the benchmark for the development of efficient computer-based human sleep modeling systems.

Chapter 2 begins with a sub-section entitled *Concerns Regarding Rechtschaffen and Kales Sleep Scoring Manual*. Interpretation of the polysomnogram is the major focus of this sub-section. Ambiguities found in R&K that are interpretation dependent and may significantly affect computer-based human sleep modeling system performance are presented. Interpretation dependent ambiguities within R&K that may affect computer-based human sleep modeling system performance include the experimental procedure, epoch scoring procedure, and sleep stage characteristic definition.

Following the sub-section on ambiguities within the R&K sleep scoring manual a section on polysomnogram artifact removal and compensation is presented. Polysomnogram pre-processing is the major focus of this sub-section entitled *Polysomnogram Artifacts: Removal and Compensation*. Developments in artifact processing for polysomnogram signal processing are presented through the topics of artifact prevention, treatment, and recovery. This sub-section concludes with the author's

interpretation of the documents reviewed and how they relate to the development of computer-based human sleep modeling systems.

A sub-section on computer-based sleep stage classification is presented following the section on polysomnogram artifact removal and compensation. Polysomnogram sleep stage classification is the major focus of this sub-section entitled *Computerized (Automated) Sleep Scoring*. Computerized sleep scoring is discussed via three topics: feature selection, classification, and human sleep modeling. Feature extraction addresses the translation of visual data observed by the clinician in the human polysomnogram into quantitative values to be processed in a computer-based sleep analysis system. Classification of human polysomnogram characteristics is dependent upon the selected features. Lastly, computer-based approaches incorporating classification methods with human polysomnogram inputs to formulate quantitative-based human sleep modeling systems are presented.

Chapter 2 ends with a brief background on the clinical disorder Parkinson's disease entitled *Parkinson's Disease and the Human Sleep Cycle*. Abnormal sleep detection is the major focus of this sub-section. The detection of polysomnogram characteristics common to patients suffering from pre-Parkinsonian symptoms is an example case of the application of ESAM towards a clinically relevant sleep problem. Understanding this link between Parkinson's disease and the human sleep cycle displays the clinical relevancy of the pre-Parkinsonian case problem utilized in ESAM.

2.2 Concerns Regarding Rechtschaffen and Kales

Chapter 1 section 1.7.2 provided a brief overview of R&K sleep scoring criteria. Information regarding ambiguities associated with the R&K sleep scoring criteria are provided from Himanen et al., unless otherwise stated, and are presented in this section [8].

2.2.1 R&K Experimental Procedures

R&K's sleep manual was specifically developed for analysis of paper data recordings, which was the common polysomnographic collection method in 1968. Data collection specifications for the paper recordings included filter gains, paper speed, pen deflection, and number of channels. Advancements in digital signal processing and the utilization of digital equipment during the data collection process have made many of these specifications outdated.

Regarding electroencephalographic (EEG) recordings, the R&K committee did not find significant differences between regional areas on the scalp during sleep staging using EEG analysis. EEG channels C4-A1 and C3-A2 (refer to Section 3.2 Data Collection Procedures) were thought to be synchronous. Therefore, the committee suggested that the selection of one of these central EEG channels was satisfactory for sleep analysis. However, no experimental studies were conducted to validate these conclusions. Synchronicity of the C4-A1 and C3-A2 EEG channels were not the basis of ESAM. Therefore, uncertainties regarding this aspect of the polysomnogram collection procedure are not problematic to the development of ESAM.

2.2.2 R&K Epoch Scoring

Epochs of equal duration are individually assigned to a sleep stage using the R&K

criteria. If the epoch contains characteristics of two or more stages it is classified according to the sleep stage of the longest duration. Generally, if a 20 s epoch scoring approach is adopted, then an 11 s observation of a particular sleep stage is adequate for sleep scoring, while with a 30 s epoch scoring constraint a 16 s assessment is sufficient.

The above epoch scoring requirements are problematic since sudden stage transitions are often ignored, which prevents the study of the microstructure of sleep. Also, it is important to note that the ability to determine which sleep stage characteristics dominate an epoch is subjective. Studies have shown that the same individuals will score transitional epochs differently on separate occasions, especially for transitional stages such as sleep Stage 1 [9]. Normal sleep subjects contain electrophysiological characteristics that fit well within the R&K scoring criteria and have less immediate stage transitions; therefore these problems are less applicable to them. However, in disturbed-sleep subjects a larger number of sudden sleep stage transitions are present that may be overlooked when implementing the R&K scoring criteria. This can provide an improper representation of the subject's sleep cycle and lead to an incorrect clinical diagnosis.

2.2.3 R & K Stage Characteristics

The goals of the R&K committee did not include redefining the current approaches toward sleep analysis but rather linking them to create a more concise universally acceptable methodology. With this objective in mind the committee defined the sleep stages based on the state of the art that defined sleep polygraphically with sleep Stages 1, 2, 3, 4, and REM. The conscious state "Wake" was also defined. However,

scoring ambiguities exist within the sleep stages defined by R&K. The aforementioned ambiguities are presented below.

Wakefulness

Alpha activity and eye and muscle movement are the primary characteristics used to classify this stage. However, alpha activity has also been noticed in drowsy and sleep states so it is not always evident if the subject is experiencing an “alpha-sleep type” pre-arousal (micro-arousal) or a wake state.

Stage 1

This stage classification is defined by R&K as containing low-amplitude EEG with no sleep spindles or REMs within the EOG for time durations longer than 3 minutes. However, some studies have argued that the 3-minute rule is too long and causes many Stage 1 segments to be left unnoticed and scored as Stage 2 [10].

Stage 2

Initial indication of this stage is defined according to R&K as the first appearance of a sleep spindle or a KC lasting at least 0.5 seconds within low-voltage background EEG activity. The definition of the start of Stage 2 depends heavily on the sufficient recognition of spindle and KC events. However, the start and endpoint of the KC markings are not clearly stated within R&K criteria, which can cause confusion when defining Stage 2 epochs.

More confusion in Stage 2 scoring is found when episodes containing delta activity less than 75 μV in amplitude are commonly scored as Stage 2 despite a deficit of spindles or distinguishable KC events being observed. In this situation, if the R&K criteria were strictly enforced, this case would be scored as Stage 1, therefore displaying

the subjective nature of the R&K criteria.

Studies also show that sleep spindles and KC events tend to decrease in older healthy adults (average age=75.5±6.3 years) [11]. These findings are not addressed within the R&K criteria for scoring Stage 2 sleep.

Stages 3 and 4

Determination of sleep stages 3 and 4 according to R&K criteria is based on the presence of at least 20% but no greater than 50% of 2 Hz waves or slower with amplitudes larger than 75 μV peak to peak (measured by calculating the difference between the most negative and positive points of the wave) within the EEG epoch. The amplitude threshold of 75 μV appears to be sufficient for normal young adults (ages ranges = 25-35 years old) with delta amplitude usually being greater than 100 μV. Problems occur when applying the same amplitude threshold to the elderly. The literature has shown that slow wave amplitude decreases as an individual ages, especially within elderly men [12]. This indicates that the 75μV threshold may not be applicable for all age groups in scoring Stages 3 & 4 sleep. Also, application of R&K criteria in scoring these stages provides low inter-scorer confidence (23.5%) for patients with obstructive sleep apnea hypopnea syndrome [13].

Stage REM

An absence of KCs and sleep spindle events along with EMG (movement) activity may be indicators of sleep Stage REM according to R&K criteria. This stage is also defined by the occurrence of REMs within the EOG and possibly some saw-tooth waveform representation within the EEG. R&K criteria modifications are suggested within the literature when disease alters stage REM sleep of the polysomnogram. Bliwise

et al. have cited stage REM scoring methods beyond R&K criteria for patients with Parkinson's disease [14].

2.2.4 Revisions to R&K

Studies were not performed to investigate whether legitimate correlations existed between the polysomnogram results and the underlying morphological and physiological processes, during sleep, prior to the R&K manual's acceptance. This justified the committee's suggestions that revisions to the R&K manual be submitted. In 2004, the American Academy of Sleep Medicine (AASM) appointed a digital task force to update sections of the R&K manual. This task force focused on defining standards for digitally recording and scoring EEG phenomena, transient central nervous system arousals, sleep disordered breathing events, leg movement activity, sleep cycle alterations as a function of age, and other issues related to computerized polysomnography [15].

In 2007 the American Academy of Sleep Medicine (AASM) *Manual for the Scoring of Sleep and Associated Events: Rules, Terminology, and Technical Specifications* was published [16]. Shumard describes the AASM manual revisions to the R&K criteria regarding the scoring of sleep stages [17]:

- *The terminology has slightly changed with wake now being referred to as stage W, and stages N1, N2, and N3 referring to the "old" NREM stages 1, 2, and 3; REM should now be labeled stage R.*
- *Stage N3 represents slow wave sleep and replaces the R&K nomenclature of stage 3 and stage 4 sleep.*

- *Each stage now includes more detailed definitions and rules as well as procedural notes (figures are included in the manual to give some examples of the rules).*
- *The previous "3 minute rule" has now been abolished; therefore, the biggest impact will be noticed in the scoring of N2. N2 sleep can be scored as soon as one or more K-complexes unassociated with arousal or one or more trains of sleep spindle occur in the first half of the epoch or the last half of the previous epoch.*
- *Major body movements are now either scored as stage W (if more than 15 seconds of alpha is present for any part of the epoch or if an epoch of stage W precedes or follows the movement) or scored as the same stage as the following epoch.*

Section 2.2 of this study has presented problems associated with applying R&K criteria to the diagnosis of certain sleep pathologies. These problems may be attributed to the R&K manual's initial design specifications for the analysis of healthy adults. Despite the latter, R&K criteria remain the standard for the diagnosis of sleep-related illnesses, such as sleep apnea, narcolepsy, and restless leg syndrome. Although the AASM manual provides a new interpretation of the human sleep cycle and addresses some of the concerns presented it has yet to be accepted universally within clinical sleep laboratories. Section 2.2 of this study is not presented to obtain closure on all problems associated with applying R&K criteria to the diagnosis of certain sleep pathologies. This section is presented to display that further investigations are required to obtain substantial information on the best interpretation of the human sleep process regarding certain sleep

pathologies. An example investigation is displayed in chapter 4 of this study which illustrates the performance of ESAM in the discrimination between human sleep cycles of control subjects and pre-Parkinsonian disease patients.

2.3 Polysomnogram Artifacts: Removal and Compensation

2.3.1 Polysomnogram Artifacts

The establishment of an efficient computer-based ESAM relies on the creation of an efficient artifact processing methodology. Information regarding the application of artifact processing to computerized analysis of polysomnogram data has been provided by Anderer et al. unless stated otherwise[18].

2.3.2 EEG Artifacts

Artifacts (noise contributions) within EEG data are represented by any electrical potential difference source that is extra cerebral. EEG artifact has been shown to replicate that of standard EEG patterns [19], which may significantly influence computerized and manual sleep staging. Therefore, it is of extreme importance that the proper treatment of artifacts be incorporated when analyzing sleep EEG data. To provide the reader with a knowledge base regarding the area of artifact removal, the most well-known sources of sleep EEG artifact are addressed in this section: ocular (EOG), EMG, electro-dermal, EKG, pulse, movement, and technical artifacts.

2.3.3 Ocular Artifacts

Slow and rapid eye movements or eye blinks, which alter the external electrical field of the cornea-retinal dipole, are the primary causes of ocular artifacts. These artifacts may interfere with EEG and EMG channels during polysomnograph recordings.

2.3.4 EMG Artifacts

A mixture of swallowing and various body movements are responsible for EMG artifacts. Specifically, body and head movements may introduce slow potential shifts in the polysomnogram that may cause the improper interpretation of the EEG as delta activity [20]. Also, 60 Hz interference may be found in the EMG channels and is often observed in the leg EMG recordings. This artifact occurs when the EMG leads absorb 60 Hz line power as interference from the sleep laboratory environment [1].

2.3.5 Electro-dermal Artifacts

Modifications in the electrolyte concentration of the EEG electrodes resulting from sweat gland secretions are the sources of electro-dermal artifacts. Immediate arousals during light sleep (Stage 1/Stage2) may also contribute to these artifacts.

2.3.6 EKG Artifacts

EKG artifacts depend on the direction of the electrical dipole of the heart and may interfere with several polysomnogram data channels at once. Therefore, the electrical field generated by the heart may also corrupt the EEG data recordings.

2.3.7 Pulse Artifacts

Pulsating scalp arteries located directly beneath the electrode contribute to the pulse artifact. These artifacts are localized to the lead that maintains contact with the pulsating artery.

2.3.8 Movement Artifacts

Breathing-related chest movements that press the scalp electrodes onto the pillow, creating rhythmic slow potential shifts in the polysomnogram, contribute to movement artifacts. Of course, other types of body movements not mentioned may also contribute

to this type of artifact.

2.3.9 Technical Artifacts

Technical artifacts appear within any area of the recording system, specifically within the electrodes, leads, or the EEG instrumentation. An illustration of the electrodes and leads commonly utilized during a sleep study is provided in Figure 2.3.9 1 [1].

Immediate changes in the direct current potential between the electrode and the skin create technical artifacts. These artifacts may be viewed in the corresponding electrode channel by sharp rises of variable amplitude, with exponential decays dependent upon the time constant. The movement of electrode leads may create electrostatic activity that produces slow wave artifacts that are considered technical artifacts.

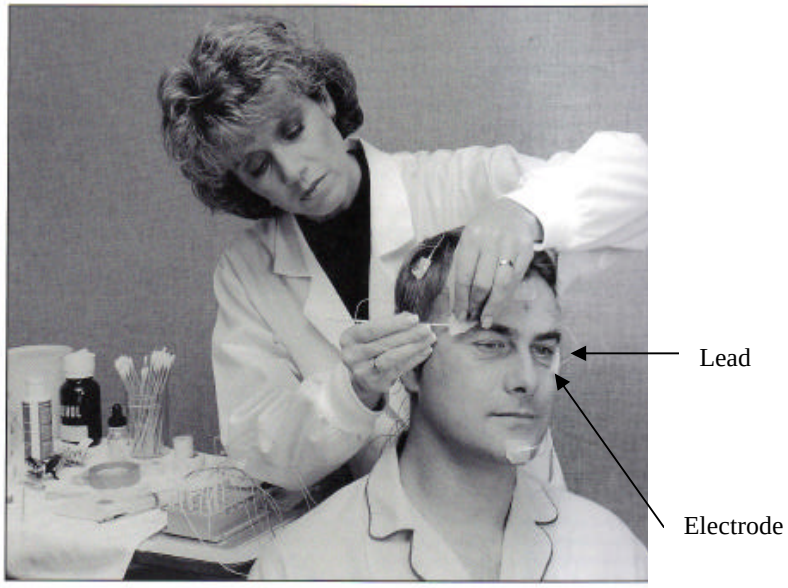

Figure 2.3.9 1: Illustration of electrode and lead connections commonly used during a polysomnograph recording(re-printed with author's permission[1]).

2.3.10 Artifact Processing

Polysomnogram artifacts may be handled by two main approaches, prevention and treatment. Methods regarding these approaches are presented in this section.

2.3.11 Artifact Prevention

Artifact prevention focuses on the avoidance of artifacts during experimental procedures applied to collect the polysomnogram. This requires a cool and relaxing recording environment coupled with high-quality polysomnographic recording devices to achieve optimal experimental results. Experienced polysomnograph technicians should be employed to properly setup the electrode connections to monitor and test the electrode impedance levels before and after the recording process. Sweat artifacts may be prevented by rubbing the skin with an abrasive paste and/or skin puncturing below the electrode location [21]. The EKG electrode may be relocated a few millimeters from the pulsating artery to eliminate pulse artifact.

2.3.12 Artifact Treatment

Artifact treatment focuses on artifact removal through data elimination or recovery. Data elimination requires that all data segments classified as artifact be removed from the data set. This method may result in an undesirable loss of data, making further polysomnogram analysis difficult if not impossible. A more effective scheme involves data recovery. Within this scheme data segments, classified as artifacts are processed algorithmically, eliminating only the undesirable noise components. Current data recovery methods require that the source of the artifact be observable via channel recordings or reconstruction methods. For example, these recording-and reconstruction-based schemes may be incorporated using EOG for ocular artifacts or

EKG for cardiovascular artifacts. Although these methods seem advantageous, it is important that each method undergo careful validation to avoid distortion of the waveform.

2.3.13 Artifact Recovery Methods

Artifact processing within ESAM focuses on artifact recovery methods. The three primary artifact recovery methods, digital filtering, linear combination, and reconstruction for polysomnograph data are presented below in further detail.

2.3.14 Digital Filtering

Low [22] and high [23] pass filters have been implemented in artifact recovery methods to eliminate the effects of muscle and sweat artifacts. However, digital filtering may cause major distortions within the EEG when filtering the artifact signals [19].

2.3.15 Linear Combination

The linear combination technique assumes that the original artifact source may be recorded and the "observed" EEG signal is a linear combination of the "true" EEG signal and the recorded artifact sources [24]. Artifact sources are subtracted from the appropriate portion of the "observed" EEG signal to conduct artifact recovery. Performing this technique depends on the quality of the recorded artifact sources. Signal loss may occur if artifact sources contain parts of the "true" EEG signal.

2.3.16 Reconstruction

Reconstruction of artifact sources is possible when topographic (spatial) data regarding electrode locations is available. This spatial information, which includes the physical locations of the electrode placements, may be mathematically modeled to identify and remove specific artifacts. A multiple source eye correction method created

by Berg and Scherg corrects for EOG artifact using reconstruction [25]. This approach requires that a model of brain activity be coupled with spatial information from eye activity to detect ocular artifacts. Casarotto et al. also used reconstruction to obtain ocular artifact sources although their approach, principal component analysis (PCA), requires no brain activity model [26]. PCA uses a linear transformation to project the high-dimensional polysomnograph data onto a lower-dimensional space [27]. A least squares error criterion is required for the projection. Components obtained from the projection are utilized to detect the artifacts within the polysomnograph data.

Independent component analysis (ICA) is another form of component analysis. This type of analysis seeks directions in lower dimensional spaces, which provide the highest independence between the measured signals [27]. It is assumed that brain and artifact activities are produced from independent sources. The retrieved independent components are utilized to detect the artifacts within the polysomnogram data. Vigario applied ICA to polysomnogram data to isolate EOG artifacts [28]. Problems associated with ICA include the assumption that the signal is stationary and a lack of an explicit noise model. The latter may prevent sufficient noise removal within the signal and the former prevents the automation of the algorithm unless (quasi-stationary) sliding windows are implemented.

2.3.17 Artifact Conclusions

The manual approach to the removal of artifacts is extremely time consuming and may detrimentally decrease the data set size for sleep analysis. Consequently, there is a compelling need for a reliable and efficient automated artifact processing scheme. It is also important to note that until a reliable artifact processing scheme is instituted a

reliable computer-based ESAM will not be possible for clinical application. Chapter 3 section 6.1 addresses the incorporation of a valid artifact processing scheme to ensure proper automated sleep scoring in the computer-based ESAM system.

2.4 Computerized (Automated) Sleep Scoring

2.4.1 Feature Analysis

Feature analysis consists of two components: feature extraction and feature selection. The first step in feature analysis is feature extraction. Feature extraction is a technique used to characterize an object for recognition via measurements whose values are very similar for objects within the same category, and are very dissimilar for objects in different categories [27]. Feature extraction measurements reduce the data size, which decreases device implementation costs, paving the way for commercial/clinical applications. Since, ESAM contains commercial/clinical prospects it is advantageous that feature extraction approaches be adopted.

Past feature extraction methods for sleep staging consist of, relative spectral energy estimation, harmonic Hjorth methods [29], statistical feature analysis of the mean, average power, standard deviation calculations, and ratio of the absolute mean value of wavelet coefficient sub-bands estimation [30]. Other feature extraction methods for sleep staging include calculating the Lem-Ziv complexity, spectrum entropy, and approximate entropy estimation [31], EMG frequency level, and autoregressive reflection coefficients [32]. The literature also cites feature extraction methods including discrete cosine transform coefficients, discrete wavelet transform coefficients, adaptive autoregressive parameters [33], stochastic complexity [34], spectral edge frequency, relative EMG power, skewness, kurtosis, 75^{th} amplitude percentile and mobility [35].

Previous feature extraction methods for artifact removal in polysomnographic data consist of maximum absolute amplitude measurements [36], autoregressive modeling coefficient extraction along with power spectrum analysis for high pass and adaptive notch filtering [37], and correlation measurements [38].

2.4.2 Feature Selection

The second step in feature analysis is feature selection. Feature selection is a technique used to construct and select subsets of features that improve data visualization and interpretation, storage, training and computation time reduction, and prediction/classification performance [39]. This section presents two groups of feature selection methods as described by Holder et al. [40] followed by an overview of a dimensionality reduction optimization technique based on Particle Swarm Optimization (PSO). The section concludes with a description of how the presented feature selection methods are incorporated in ESAM.

Group one of feature selection methods described by Holder et al. [40] involves filtering/ranking the original extracted features. It is expected that the filtering/ranking process be executed such that sufficient feature dimensionality reduction be obtained for the final learning task. Filtering/ranking methods utilize metrics to determine the relevance of each feature. The correlation coefficient and mutual information are common metrics used in the filtering/ranking of features. For example, features with the same correlation coefficient value may be given a lower rank and considered less important to the final learning tasks over features with very dissimilar correlation coefficient values. However, it should be noted that the correlation coefficient and

mutual information metrics may not provide the optimal performance in dimensionality reduction when conditional dependence between features is present.

Group two of feature selection methods described by Holder et al. [40] involves using the learning algorithms as metrics to identify optimal subsets of the original extracted features. Two common approaches used in group two include the embedded and wrapper feature selection methods. In embedded methods feature subsets are evaluated and selected based on the training process of the classifier (see Section 2.4.3 for more about classification). Wrapper performance metrics unlike embedded methods are not dependent on the classifier training process. The classifier in a wrapper feature selection approach is treated as a black box and is only used to evaluate the performance of the feature subset at representing the final learning tasks. Both embedded and wrapper methods have the potential to obtain final feature subsets by using sequential forward selection or backward elimination. In sequential forward selection, features are added to a small initial subset of features as long as the performance of the final learning tasks improves. Sequential backward selection starts with all the original features and continues to eliminate features that provide the least promising performance for the final learning tasks [39]. Further information regarding the methodology of sequential forward and backward feature selection algorithms are provided in Section 3.6.2.1.

Promising feature selection for polysomnogram analysis is ultimately dependent upon the data domain and final learning tasks. Past approaches toward feature selection for polysomnogram analysis have included Bayesian wrappers and sequential forward selection [41]. Feature selection may also be approached using optimization techniques

to create feature subsets. An optimization technique used for feature selection is the PSO algorithm.

PSO was developed in 1995 by James Kennedy and Russell Eberhart as a population based stochastic optimization technique to obtain the "near optimal" minimum or maximum output value in a search space. The behavior of flocking birds was the inspiration for this algorithm. An analogous relationship between the flocking bird behavior and PSO strategy is often used in the literature. Hu et al. provides a good description of this analogy:

> *"Assume the following scenario: a group of birds are randomly searching for food in an area. There is only one piece of food in the area being searched. The birds do not know where the food is. But they know how far the food is and their peers' positions. So what's the best strategy to find the food? An effective strategy is to follow the bird which is nearest to the food.*
>
> *PSO learns from the scenario and uses it to solve the optimization problems. In PSO, each single solution is like a "bird" in the search space, which is called "particle". All particles have fitness function values which are evaluated by the fitness function to be optimized, and have velocities which direct the flying of the particles. The particles fly through the problem space by following the particles with the best solutions so far.* [42]

Particle Swarm Optimization

Initialization of the PSO algorithm in this study began with specifying a group of random particles. The length of the each particle was equal to the length of the feature vector. The fitness value of each particle was calculated in relation to the expert's sleep event scoring. The next step involved calculating the value *pBest.* The value *pBest* was

the location of the best solution (fitness value) a particle had reached throughout the running of the algorithm. PSO labeled the location of the best fitness that any neighbor of a particle has obtained as *nBest*. This was calculated after obtaining the value *pBest*. The values *pBest* and *nBest* represented the two "best" particle values utilized in the PSO iteration process to obtain the "near optimal" solution [42]. In the case where a particle considered the entire population as its neighbors, the best location was considered a global best and referred to as *gBest*. When the maximum number of iterations or the minimum fitness criteria had been reached, the PSO algorithm stopped and the feature(s) corresponding to the *gBest* particle were the output. A flowchart outlining this general approach to the PSO algorithm is displayed in Figure 2.4.2 1.

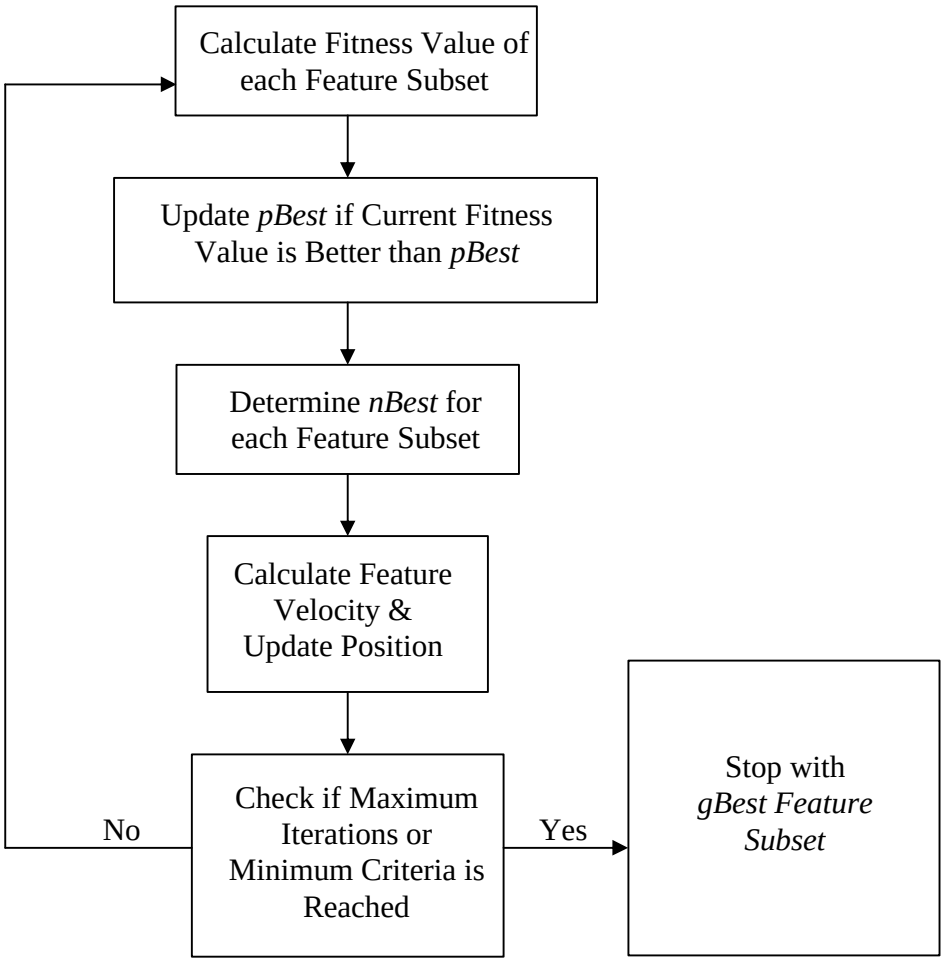

Figure 2.4.2 1: Illustration of the general particle swarm optimization algorithm.

Three main approaches exist for the implementation of the PSO algorithm. These approaches include binary, continuous numbers, and hybrid decision models. Binary and continuous numbers PSO decision models have been used by Shi, Eberhart, Firpi, and Agrafiotis to construct candidate subsets of features for classification problems [43-45]. Chapter 3 provides a detailed overview of the methodology behind the b-PSO. In chapter 4 of this study the b-PSO, and sequential forward and backward feature selection algorithms are compared for optimal feature sub-set selection for ESAM.

2.4.3 Classification

The primary objective of a classifier is to use the feature characteristics provided during the feature analysis process to assign an unknown object to a category [27]. Proper cataloging of input feature characteristics requires a training approach often incorporated under the guise of a general model that corresponds to the known data set. Training patterns allow the classifier to learn or estimate unknown parameters using the general model. Learning is represented by the reduction of an error function that describes the classification error on the training data within the model. The three primary types of learning algorithms include supervised, unsupervised, and reinforcement learning.

Supervised learning requires the user to provide a category label for each feature characteristic in the training set. For optimal performance, the learning algorithm at varying input parameter values should be evaluated. The user's goal is to reduce the labeling error of the learning algorithm.

Unsupervised learning is often referred to as clustering. The user supplies no prior category labels or training data but may supply a hypothesis regarding the number

of clusters prior for executing the algorithm. A natural cluster formation is expected to occur from the input feature characteristics. The selection of different cost functions for the learning algorithm will provide different cluster formations.

Reinforcement learning entails computing the tentative input feature characteristic category and comparing it to the known target category label. A binary approach is often incorporated in this method where the tentative labeling is correct or incorrect. Specific information regarding the amount of error between the tentative labeling and the correct labeling is not given. Reinforcement learning only provides information regarding the classifier's ability to correctly catalog input feature characteristics and does not provide information regarding the measure of error when classification is incorrect.

Supervised [46] and unsupervised learning [47] algorithms have been included in current automated sleep staging systems. Learning algorithms for artifact removal in polysomnograph data primarily use supervised methods [38, 48]. In this study supervised and unsupervised methods are utilized in the GOHMM evaluation within ESAM.

2.4.4 Modeling

Model selection requires deciding on a proper mathematical description of a known physical phenomenon. The physical phenomenon of interest in this study is the human sleep cycle. Model selection based on sleep onset has been presented in the literature since 1988 [49]. However, these models are behavioral based and primarily focus on wake-to-sleep transitions and do not address transitional occurrences within the sleep cycle. Models that attempt to not only address sleep-to-wake transitions but also incorporate transitional aspects of the sleep cycle based on biological signals contained in the polysomnogram have been presented by Kemp [50] and Flexer et al. [32].

In this study, attention is given to a continuous and probabilistic sleep stager based on a GOHMM, presented by Flexer et al. [4]. The Flexer Model aims to find a new description of human sleep based on comparably unambiguous "extreme" cornerstones of traditional sleep staging. These cornerstones represent a model of the human sleep cycle as a combination of three different processes: wakefulness "wake," deep sleep "deep," and REM sleep "REM." These stages were selected because of their lack of ambiguity among polysomnograph scorers.

Benefits of the Flexer Model include a finer temporal resolution and a probabilistic basis. Finer temporal resolution is obtained with a 1-second epoch analysis in contrast to that of the 30-second epoch analysis defined by R&K. This finer temporal resolution allows for the investigation of the microstructure of sleep, which is needed for the diagnosis of certain sleep illnesses. Solid probabilistic principles utilized within the Flexer Model allow the observation of transitions within the sleep cycle and easy model modification of the analysis of abnormal (i.e., sleep illness related) polysomnograph data. Chapter 3 section 6.3 provides information on how the Flexer et al. model is incorporated into ESAM.

2.5 Parkinson's Disease and the Human Sleep Cycle

Parkinson's disease (PD) is a brain disorder clinically marked by tremor (shaking), extreme slowness of movement, rigidity (stiffness), and lack of physical equilibrium. The rate of PD occurrence in the United States is 20 incidences per year per 100 000 population and affects up to 2% of the population over the age of 65 [51] [52].

It has been reported that as many as 80% of patients with Parkinson's disease complain of sleep problems[52]. Studies have shown the prevalence of specific sleep disorders such as obstructive sleep apnea syndrome (12%), restless legs syndrome (56%), and REM-sleep behavior disorder (13%) in PD patients[53]. Trenkwalder has stated the importance of the development of methods to assess sleep disorders linked to PD to guarantee the proper treatment and enhancement of quality of life for PD patients [54]. For this reason, chapter 3 section 6.4 addresses the significance of applying ESAM to process poylsomnograms of pre-Parkinsonian patients.

CHAPTER 3: METHODOLOGY

3.1 Chapter Introduction

Information to substantiate the computer-based ESAM is presented in this section. This chapter focuses on the data collection procedures, population definition, sampling procedures, instrumentation utilization, study limitations, and research design considered in the development of ESAM.

Section 3.2 entitled *Data Collection Procedures* discusses the data collection process for this study. Following the sub-section on *Data Collection Procedures* is a section that discusses the population definition for this study. This sub-section is entitled *Population and Sampling Procedures.* Details on the population sample for this study including: the number of subject/patient study participants, description of the subject/patient participants, and the selection criteria utilized to obtain the subjects/patient's sleep data are presented.

A sub-section on the instruments utilized in this study is presented following the section on *Population and Sampling Procedures*. This section entitled *Instrumentation* provides a detailed description of all equipment used to process the collected data. Following the section on instrumentation the system limitations of ESAM are presented in the section entitled *Limitations*. This section provides the reader with information on the clinical usability of ESAM as a decision support tool for physicians in sleep care.

Chapter 3 concludes with a detailed overview of the theoretical construct utilized in the development of ESAM. This section entitled *Research Design* presents information

on ESAM regarding: data preprocessing methods, feature selection techniques, quantitative model selection, and the relevancy of the selected quantitative model toward the selected applications.

3.2 Data Collection Procedures

Study data was obtained from adult polysomnogram (psg) recordings collected at ECSDC in Atlanta, Georgia, in association with the Department of Neurology within the Emory University School of Medicine. Special screening was implemented prior to data collection to exclude subjects taking medications that had the potential to influence study results. Sleep technicians attached electrodes to extract biological signals from human subjects and calibrated sleep monitoring equipment. Each subject's electroencephalogram, left and right electrooculogram, sub-mental electromylogram, right and left anterior tibialis electromylogram, and single bipolar electrocardiogram data were digitally sampled at 100Hz and 200 Hz and stored in real time on a personal computer using the sleep software program Somnologica® 2.0 (Medcare-Flaga, Reykjavik, Iceland) [55]. The 200Hz data was later re-sampled at 100Hz for computational ease.

Electroencephalogram data were extracted from central and occipital electrodes C3, C4, O1, and O2, respectively, according to the International 10/20 system. These electrodes were referenced to the ground electrodes A1 and A2 as follows C3-to-A2, C4-to-A1, O1-to-A2, and O2-to-A2. The latter were labeled as follows in the data set: C3-A2, C4-A1, O1-A2, and O2-A2. Figure 3.2 1 illustrates the International 10/20 scalp electrode placement system[56].

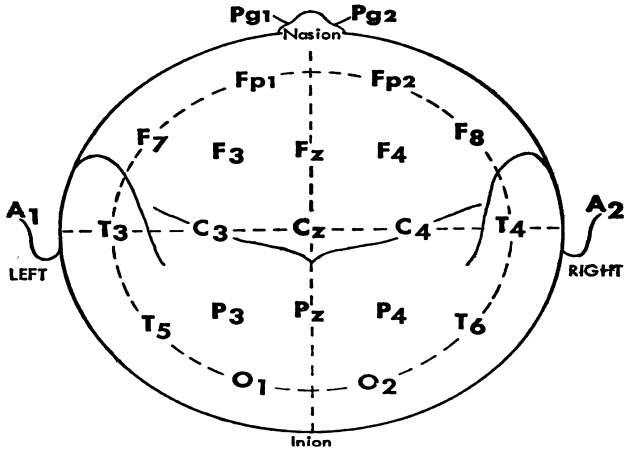

Figure 3.2 1: Illustration of the International 10-20 System for scalp electrode locations.

Electrodes were placed above and below the outer canthus of the subject's eyes to extract right and left electroculogram (R-EOG and L-EOG) recordings. EKG recordings were obtained by placing the positive electrode lead below the left pectoral muscle and the negative electrode lead under the right clavicle. The ground lead was placed below the right pectoral muscle.

3.3 Population and Sampling Procedures

The sleep population for this study consisted of patients diagnosed with presumptive pre-parkinsonism symptoms and normal control subjects. Purposive sampling was used by ECSDC physicians to identify psgs of patients displaying parkinsonism symptoms and normal control subjects. Selection criteria for the clinical diagnosis of parkinsonism has been outlined by deRijk et al. [57]. Physicians selected a psg as being Parkinsonian when REM-sleep behavior disorder (RBD) was observed.

Sampling Criteria Rationale

Parkinsonism primarily affects the older adult population. The prevalence of parkinsonism has been shown to increase with age. Prevalence rates from deRijk et al. for parkinsonism within the older adult population may be viewed in Table 3.3 1[57].

Table 3.3 1: Prevalence of parkinsonism within the older adult population.

Age Group	**Overall Prevalence of Parkinsonism (per 100 percent population)**
65-69	0.9
70-74	1.5
75-79	3.7
80-84	5.0
85-89	5.1

The sleep population for this study consisted of 6 whole night (7.265 hours ± 0.5929 hours) sleep records/psgs. Table 3.3 2 displays the demographics, clinical diagnosis, and data duration for the subject/patient psgs used in this study. The age range of subjects/patients included in this study was 54 to 76. This age range was selected from the available ECSDC data to reflect the overall prevalence of parkinsonism as observed by deRijk et al. [57].

Figures 3.3 1 – 3.3 6 display histograms indicating the number of occurrences of sleep events for each subject/patient included in this study. Table 3.3 3 indicates the relationship between the sleep event and sleep event classification numbers presented in Figures 3.3 1 – 3.3 6.

Table 3.3 2: Subject/patient psg demographics for this study.

Subject Number	**Data Duration (Hours)**	**Age**	**Gender**	**Clinical Diagnosis**
1	6.95	54	Male	Normal
2	7.79	60	Male	Normal
3	6.52	63	Female	Normal
4	8.04	76	Male	Sleep Related Parkinsonism Symptoms
5	6.83	72	Male	Sleep Related Parkinsonism Symptoms
6	7.46	73	Female	Sleep Related Parkinsonism Symptoms

Table 3.3 3: Relationship between sleep event and sleep event classification number displayed in Figures 3.3 1-3.3 6.

Sleep Event	Sleep Event Classification Number
Stage 1	1
Stage 2	2
Stage 3 and Stage 4	3
REM	5
Wake	6

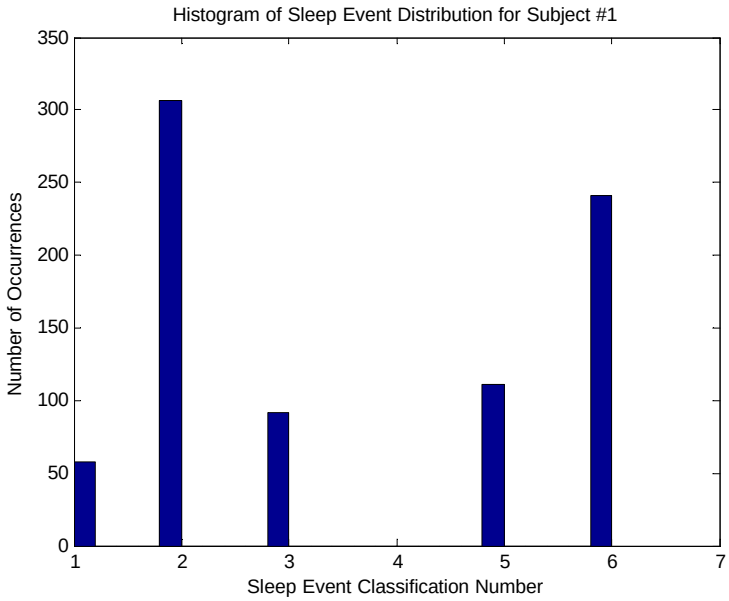

Figure 3.3 1: Sleep event distribution for Subject #1.

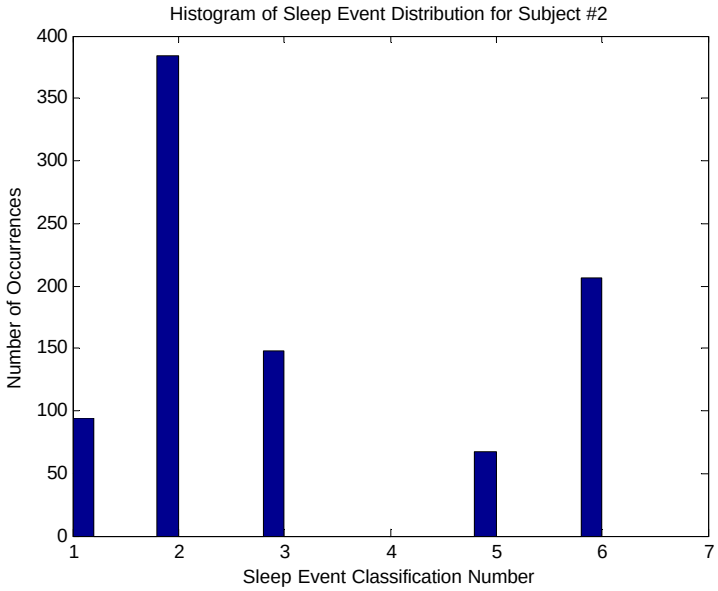

Figure 3.3 2: Sleep event distribution for Subject #2.

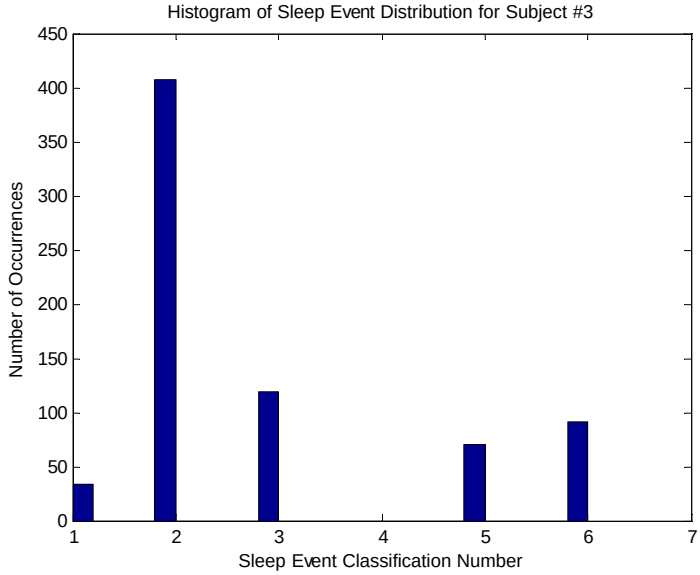

Figure 3.3 3: Sleep event distribution for Subject #3.

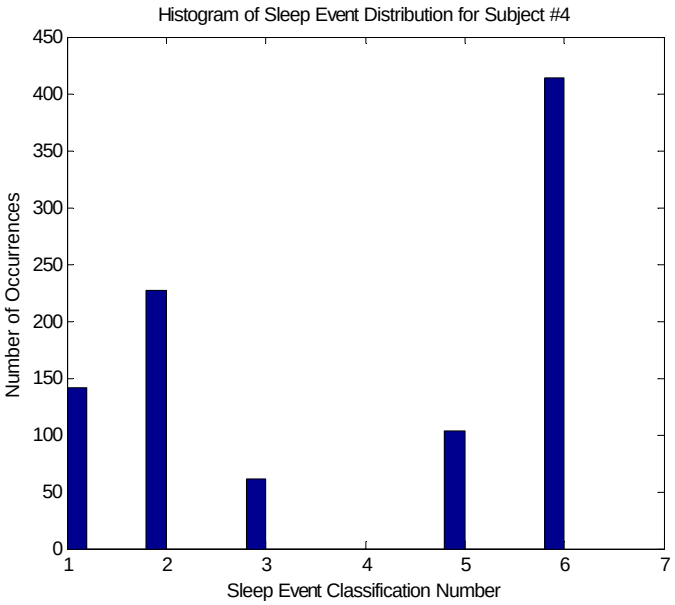

Figure 3.3 4: Sleep event distribution for Subject #4.

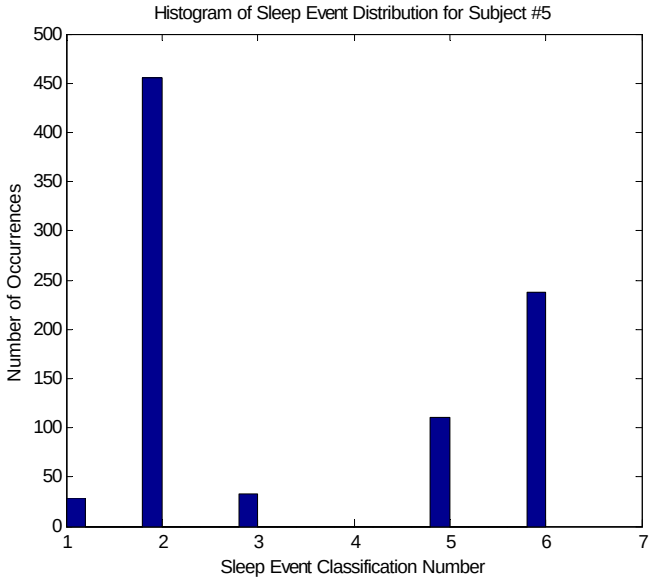

Figure 3.3 5: Sleep event distribution for Subject #5.

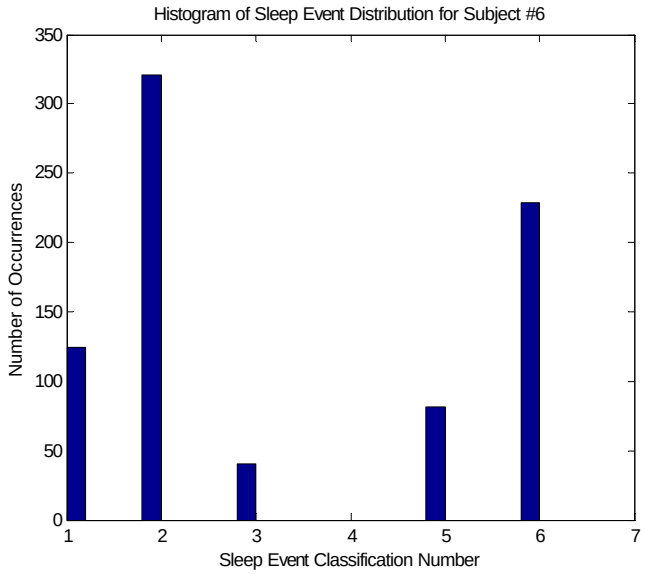

Figure 3.3 6: Sleep event distribution for Subject #6.

3.4 Instrumentation

Psg data for this study were processed on a DELL Precision 650 personal computer with two Intel® Xeon™ 2.8GHz and 2.79GHz processors and a Compaq Presario C700 laptop computer with a Dual-Core Intel® Pentium processor. The mathematical computational software program MATLAB version 7.0 (R14) was utilized to implement ESAM.

3.5 Limitations

The major limitations of this study are the data set size and intra and inter-rater reliability of the sleep technicians who labeled the psg artifacts and sleep stages. Resources did not allow for the collection of a large data set, >30 whole night psgs, and measurement of the intra and inter-rater reliability of the sleep technicians, so limitations exist in determining if and how these factors may bias this study and ESAM development.

3.6 Research Design

3.6.1 Data Pre-processing

Artifacts that prevent proper analysis of sleep data were identified by sleep physicians at ECSDC. It has been established from the physicians that 50Hz and 60 Hz line power absorption, excessive patient movement activity, and sampling interference are the major contributors to corruption of the psg data set described in Table 3.3 2. These artifacts prevent proper automated sleep stage classification.

The EMG chin electrode is the primary channel affected by 50Hz and 60 Hz line noise artifact. Excessive patient movement (EPM) activity which includes breathing related chest movements, pressing of electrodes on the pillow, and sudden body movements can create extreme amplitude values (> 200μV) and rhythmic slow potential shifts in the EEG, EMG, EOG, and EKG electrodes. The term sampling interference has been used to describe interference between electrodes. This interference may occur when data from the EMG channel is superimposed on the EEG channel. Sampling interference may occur between the EEG, EMG, EOG, and EKG electrodes.

Examples of psgs corrupted with 50Hz and 60Hz line noise, excessive patient movement, and sampling interference from the data set described in Table 3.3 2, are presented in Figures 3.6.1 1 - 3.6.1 3. VIEWEDF for MATLAB, (C) by Alois Schloegl 1998-2001, was used to obtain the plots presented in Figures 3.6.1 1 - 3.6.1 3.

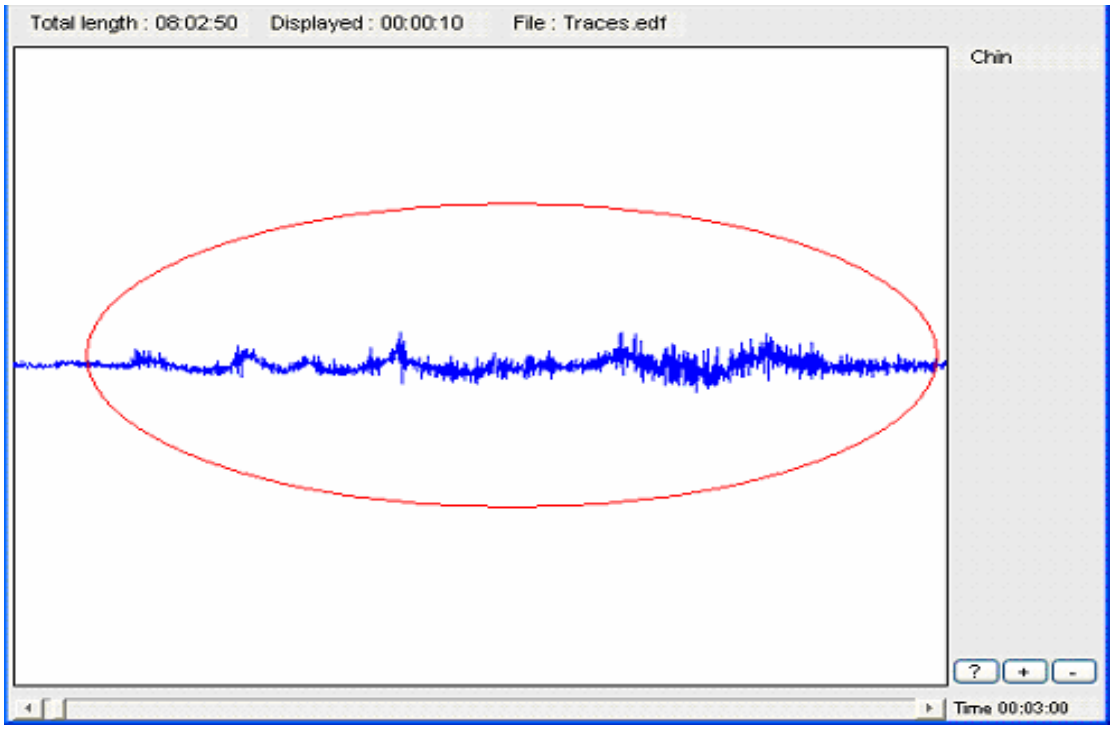

Figure 3.6.1 1: A 10 second example of 50 and 60 Hz line noise in the chin EMG electrode shown in the encirclement of the psg of subject #4.

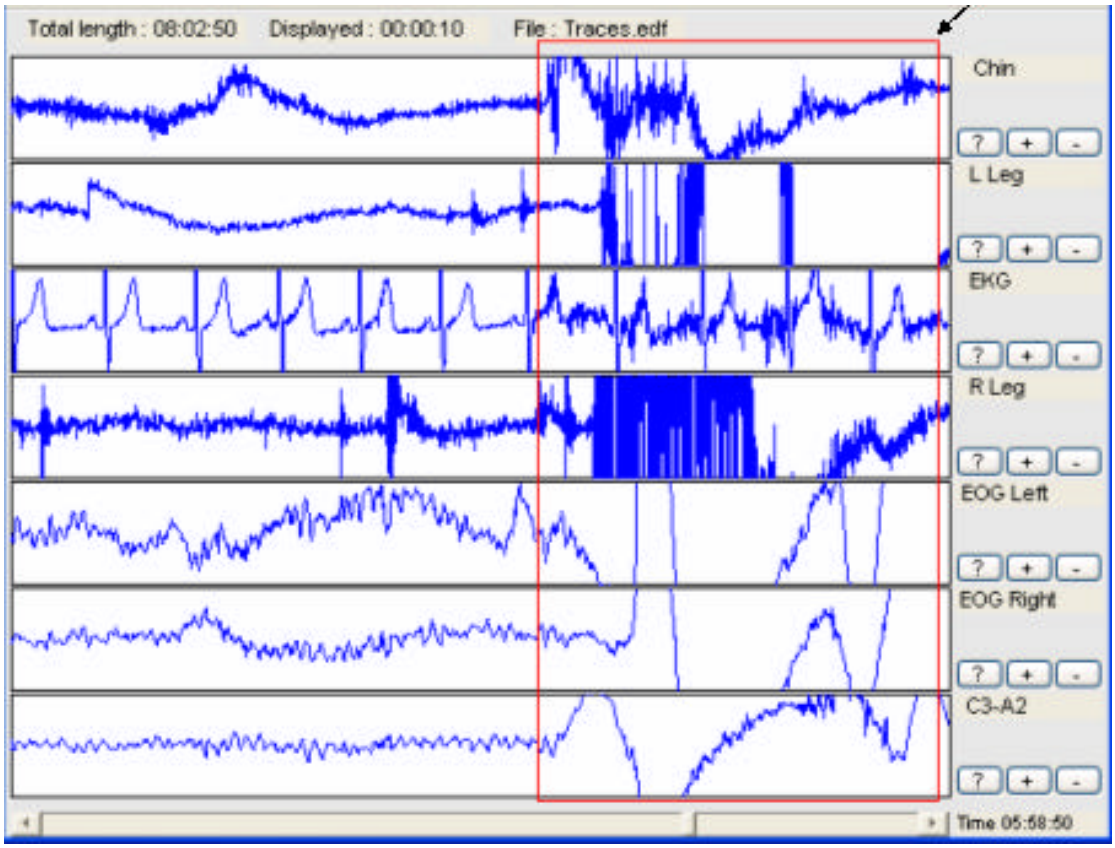

Figure 3.6.1 2: A 10 second example of EPM activity displayed in all electrode channels in the enclosed box and indicated by the arrow on
the psg of subject #4.

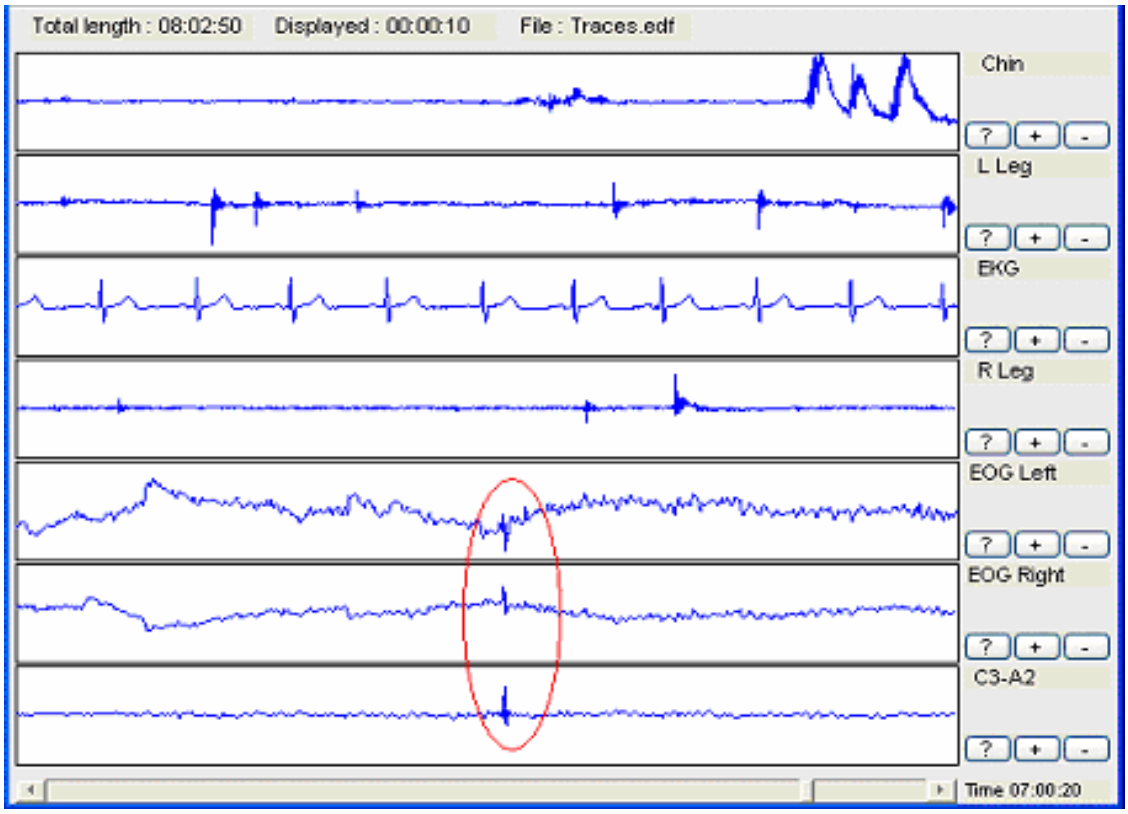

Figure 3.6.1 3: Illustration of sampling interference superimposed on the C3-A2 EEG electrode from the Left and Right EOG electrodes shown in the encirclement of the psg of subject #4.

Psg data was band-pass filtered using a 5^{th} order butter-worth filter to eliminate 50Hz and 60 Hz line noise from the psg chin data. A similar pre-processing approach has been utilized in psg signal processing techniques by Zoubek [35]. An example of the 50 Hz and 60 Hz line noise removal are provided using the psg chin data from Figure 3.6.1 1. Results from band pass filtering the 50Hz and 60 Hz line noise from the psg chin data are displayed in Figure3.6.1 4. The bandwidths and corresponding psg channels extracted during the band-pass filtering process are included in Table 3.6.1 1.

Table 3.6.1 1: Polysomnogram channels and associated bandwidths extracted during the band pass filtering process.

Channel	Bandwidth (Hz)
EOG	0.5-32.5
EEG	0.5-15
EMG	8-32
EKG	1-30

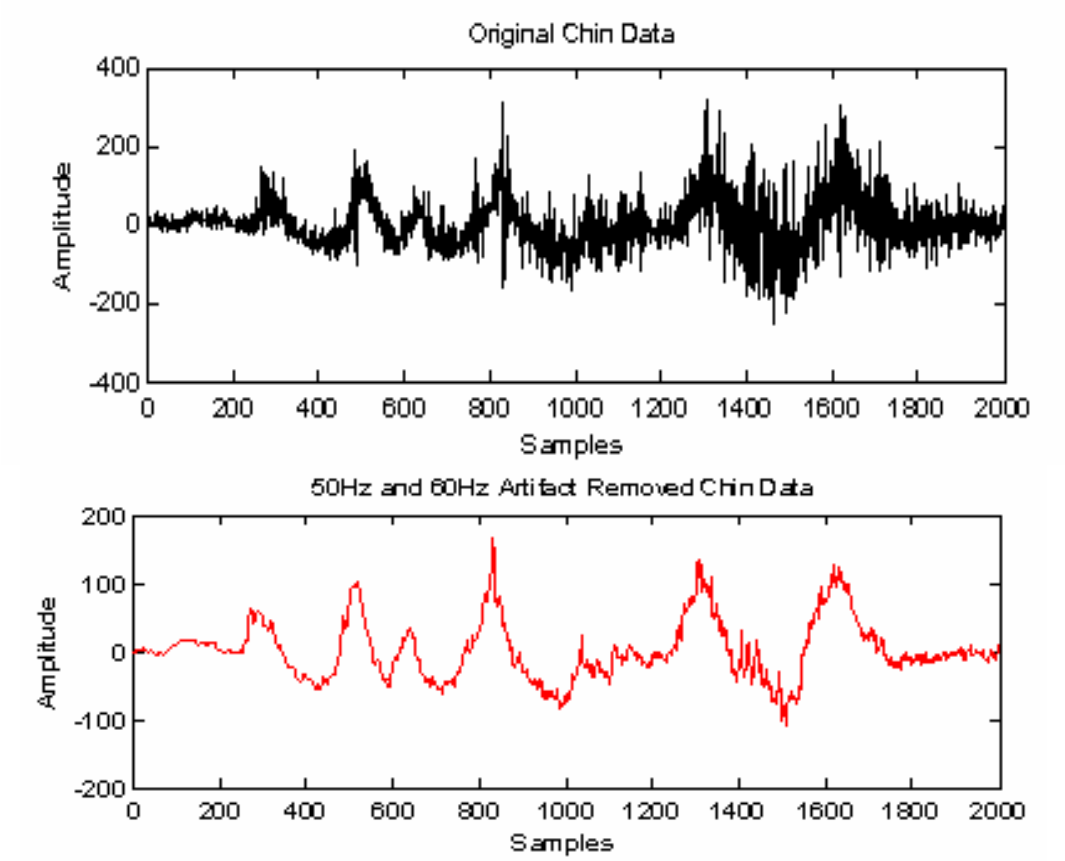

Figure 3.6.1 4: Top panel: Illustration of psg chin data from Figure 3.6.1 1. Bottom panel: Line noise removal of 50Hz and 60Hz from the top panel illustration.

EPM represented un-recoverable data and were identified using excessive amplitude detection and were clipped from the data sets. Sampling interference was identified using correlation analysis. Additionally, data compensation was conducted using the generalized singular value decomposition (GSVD) algorithm. Knight applied the GSVD algorithm to process blink artifacts in scalp EEG data used in brain-computer

interface technology (BCIT) [58]. Data compensation for sampling interference has been achieved by adapting Knight's methods to this work. Details on this approach are located in section 3.6.1.1.

3.6.1.1 Generalized Singular Value Decomposition

GSVD is a generalized matrix decomposition algorithm. This algorithm has been utilized in the literature to solve the maximum noise fraction (MNF) problem and is a signal separation technique developed to reduce noise in satellite imagery [59]. In solving the MNF problem a linear transformation maximizing the signal-to-noise ratio is obtained. The assumption is as follows:

$$X(n) = S(n) + N(n), \qquad (3.1)$$

where $X_i(n)$, $i = 1,\ldots,p$ is the observed multivariate data set, with p channels and n samples, generated by source signals, *S(n)*, and corrupted by additive noise, *N(n)*. Although, additive noise is assumed the presented approach may also be applied to multiplicative noise by taking logarithms of the observed multivariate data set. The assumption of additive noise follows Vigario's ICA approach where brain and artifact activity are assumed to be produced from independent sources[28]. Under this assumption the signal-to-noise ratio (*SNR*) may be defined as

$$SNR = \max_{y \neq 0} \frac{\| Sy \|}{\| Ny \|}, \qquad (3.2)$$

It is assumed that the signal is orthogonal to the noise with, $S^T N = 0$ and $N^T S = 0$ [60]. Therefore,

$$\frac{\| y'X'Xy \|}{\| y'N'Ny \|} = \frac{\| y'S'Sy \|}{\| y'N'Ny \|} + 1, \qquad (3.3)$$

From equation (3.3) the signal to noise ratio may now be expressed as

$$\text{SNR} = \max_{y \neq 0} \frac{\| Xy \|}{\| Ny \|}, \qquad (3.4)$$

such that, Xy and Ny provide a set of orthogonal maximum signal and noise fraction basis vectors, respectively.

Equation (3.4) is equivalent to that of equation (3.1) and leads to the optimization problem presented in equation (3.5) which may be solved by obtaining the generalized eigenvectors.

$$X^{\mathrm{T}}Xy = m N^{T}Ny , \qquad (3.5)$$

Where, m equals the eigenvalues. Eigenvectors for equation (3.5) may be obtained from the computation of the GSVD for *X* and *N*. Basis vectors obtained from (3.5) are sorted according to decreasing signal-to-noise ratio, which provides a straightforward approach for signal de-noising.

Previous research by Knight applies the GSVD algorithm to EEG signal analysis for artifact removal[58]. A single GSVD component was identified by Knight as contributing to signal corruption. However, this assumption could not be made in our application since preliminary results showed prominent artifact contributions in multiple electrode channels, therefore a single GSVD component could not be identified for artifact contribution.

Automation of the identification of sampling interference was conducted by utilizing the cross-correlation statistic via a covariance matrix. Cross-correlation measures the degree of similarity between two signals. Maximum and minimum

correlations occur at the values 1 and -1, respectively. For computational ease, a transformation was conducted to obtain a 0 to 1 range such that 0 indicates no correlation and 1 indicates maximum correlation.

The sampling interference example displayed in Figure 3.6.1 3 illustrated the utilization of correlation analysis and the GSVD algorithm for sampling interference psg data compensation. Two cross-correlation metrics were calculated during sampling interference psg data compensation. The first cross-correlation metric (CCM1) detected the primary channel of interference (i.e., EOG, EKG, or EMG) with the EEG signal. A second cross-correlation metric (CCM2) detected the GSVD component that suitably correlated to the sampling interference artifact.

A cross-correlation threshold value of 0.60 was found to be sufficient in detecting primary channels of interference and GSVD components containing significant sampling interference noise contributions. This threshold value coincided with Park's previous work of detecting EKG artifact within EEG data using cross-correlation analysis (cross correlation values greater than 0.50 considered artifact)[61].

GSVD components highly correlated with non-EEG signals were zeroed, eliminating their contribution to the EEG signal, and a transformation was conducted to obtain the artifact-reduced EEG signal. A diagram outlining the methodology for the sampling interference (SI) psg data compensation module is shown in Figure 3.6.1.1 1. Figure 3.6.1.1 2 contains the GSVD components obtained from the SI example using a 0.50 second processing window. Table 3.6.1.1 1 contains the cross-correlation matrix obtained from the CCM2 calculations between Figures 3.6.1 3 and 3.6.1.1 2.

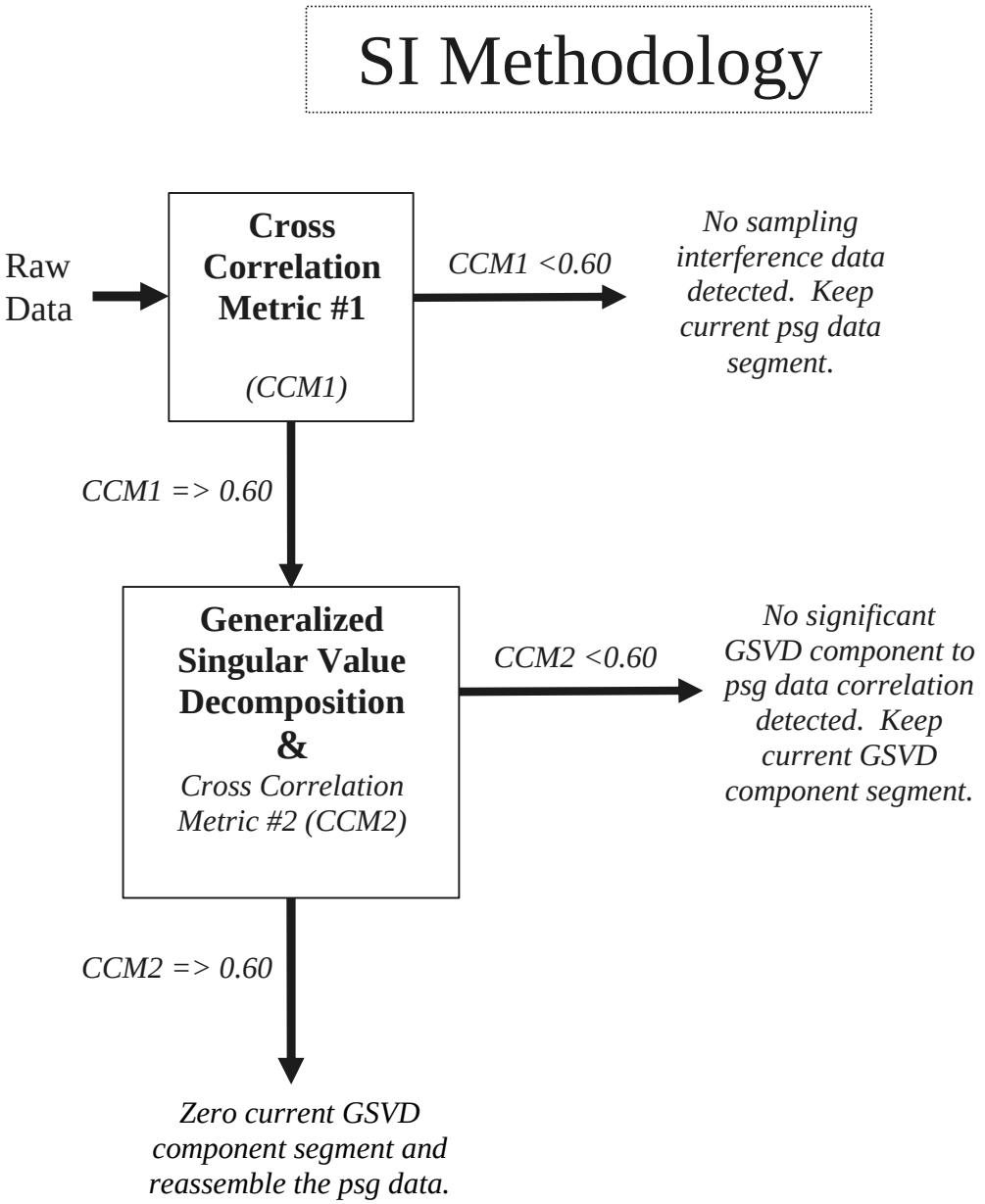

Figure 3.6.1.1 1: Schematic of methodology outlining the SI data compensation module.

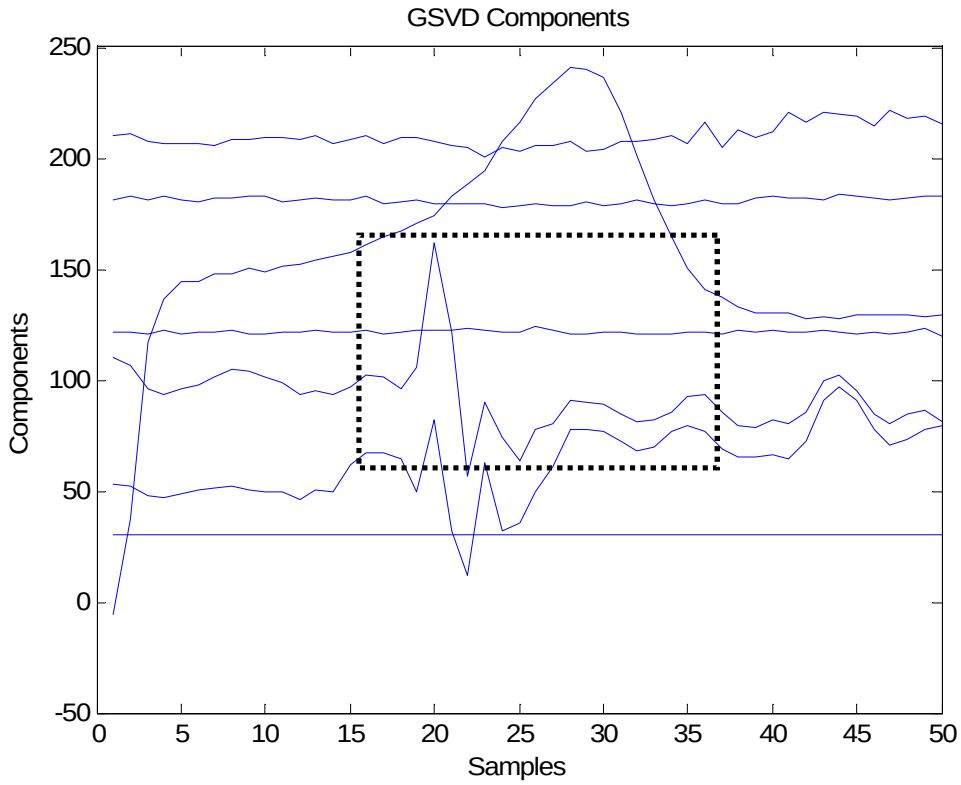

Figure 3.6.1.1 2: GSVD components obtained from preprocessing the window containing SI for subject #4 in Figure 3.6.1 3. Component number four (highlighted with the dashed box) contains a suitable correlation to that of the SI.

Table 3.6.1.1 1: Correlation matrix obtained from the psg of subject #4 corrupted with SI and the GSVD components (CCM2 value shown in bold).

	GSVD COMPONENT						
CHANNEL	1	2	3	4	5	6	7
Chin	0.18477	0.36335	0.41513	0.25307	0.66416	0.64584	0.71353
L Leg	0.29055	0.28317	0.53321	0.24821	0.44068	0.65513	0.51222
EKG	0.19733	0.24611	0.46325	0.53451	0.4011	0.99726	0.70125
R Leg	0.68388	0.6244	0.35109	0.44773	0.3317	0.24033	0.23013
EOG Left	0.30385	0.38085	0.40539	0.40597	0.60807	0.58974	0.78996
EOG Right	0.40128	0.50082	0.39362	**0.62668**	0.3331	0.44771	0.50257
C3-A2	0.4287	0.32625	0.34724	0.92831	0.29943	0.55176	0.44966

The highest CCM1 value (0.69037) in relation to the C3-A2 EEG data channel was found in correlation to the R-EOG channel. Therefore, the R-EOG channel was considered the primary channel for C3-A2 sampling interference contribution. Table 3.6.1.1 1 shows that GSVD component number four, highlighted in bold, meets CCM2

standards (0.62668) for suitable SI correlation to R-EOG channel artifact. GSVD component number four was zeroed for this 0.5 second data segment and results are presented in Figure 3.6.1.1 3. The original C3-A2 EEG data channel information is displayed at the top of the figure and the GSVD processed C3-A2 EEG data set is shown at the bottom. Observation of Figure 3.6.1.1 3 displays the benefits provided by the automated use of the GSVD algorithm in recovering data corrupted by SI artifact sources. Notice the decrease in signal amplitude and subsequent artifact compensation of the GSVD processed signal (bottom) compared to that of the original SI corrupted signal (top) for electrode channel C3-A2.

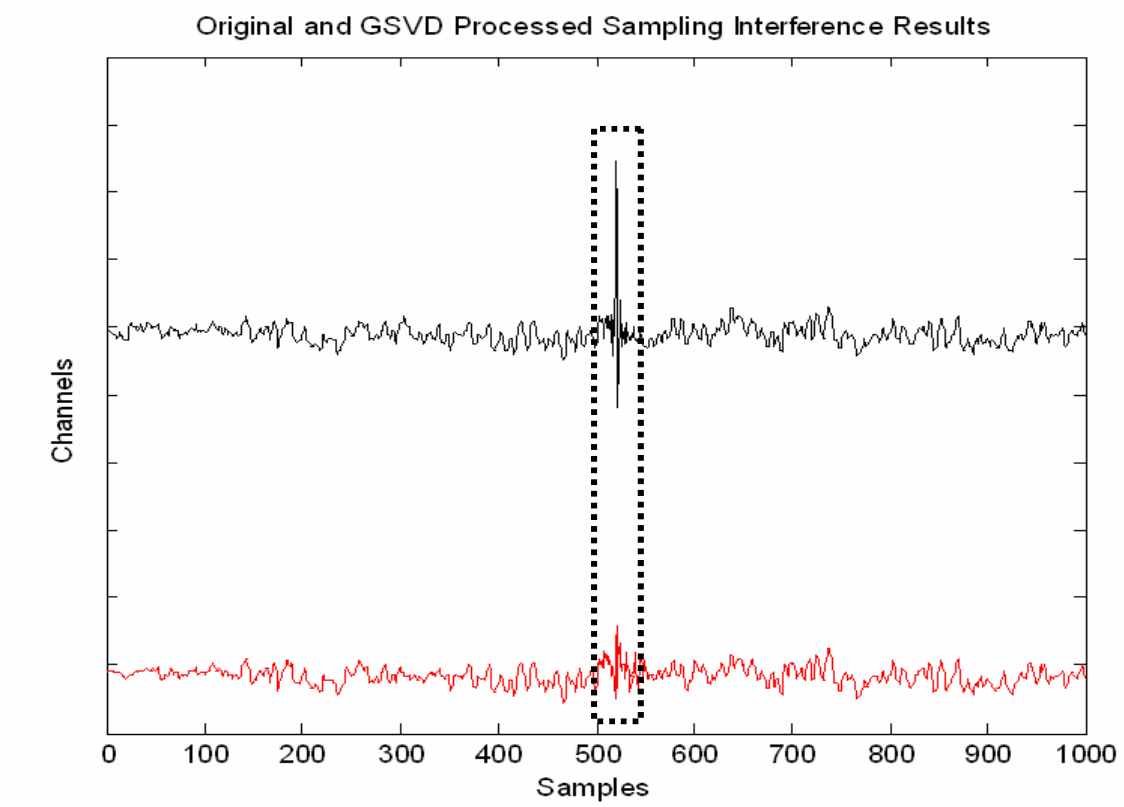

Figure 3.6.1.1 3: Original C3-A2 EEG data set (top) and GSVD processed C3-A2 EEG data set (bottom) for subject #4 from Figure 3.6.1 3. The dashed box displays the 0.5 second processing window.

An illustration of the entire artifact removal and data compensation pre-processing procedure is provided in Figure 3.6.1.1 4.

ARTIFACT PROCESSING METHODOLOGY

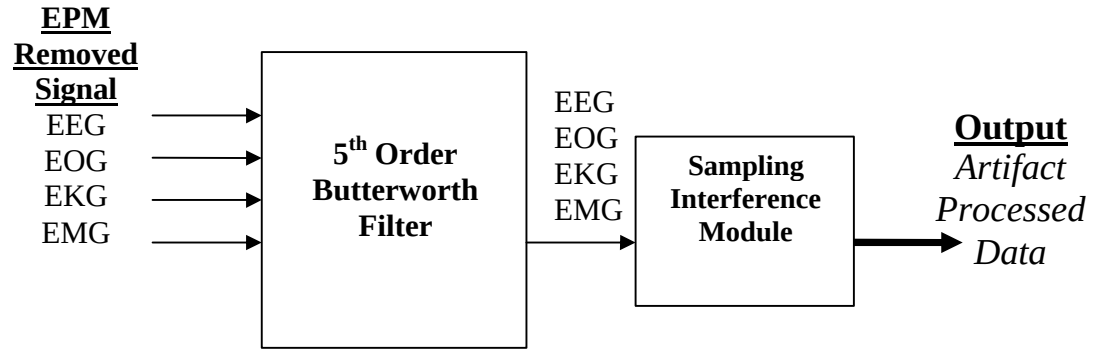

Figure 3.6.1.1 4: Illustration of the preprocessing procedure to remove and compensate for artifacts in the psg data sets.

3.6.2 Feature Selection

3.6.2.1 Sequential Feature Selection

Sequential forward and backward feature selection results were compared to the binary particle swarm optimization (b-PSO) algorithm feature selection results to determine the most suitable feature sub-sets. This allowed for the efficient detection of sleep events modeled in the GOHMM. Results from this comparison are provided in Chapter 4. Feature sub-sets were determined from the feature library displayed in Tables 4.2.1 1- 4.2.1 6. The theoretical background on feature selection described by van der Heijde was utilized in this study[62].

The features extracted from the psg data were represented as an *N*-dimensional feature measurement vector, where *N*=67, with M data windows. The feature vector was described by $x_{i,n}$ with *i* and *n* representing the temporal size and number of psg features respectively. The full feature set, $F(N)$, was described such that $F(N) = \{x_{i,n} | i = 1,\ldots,M;$

n = 0,…, N-1}. The feature sub-set of $F(N)$, $F_j(D)$, was described such that $F_j(D)$ = {$y_{i,d}|i$ =1,…,M; d = 0,…, D-1} with $D<N$. Each element in the feature sub-set, $F_j(D)$, was found in the feature set, $F(N)$, such that $y_{i,d} = x_{i,n}$.

All possible distinct feature subsets for a particular value of D were determined as follows:

$$q(D) = \binom{N}{D} = \frac{N!}{(N-D)!D!}. \qquad (3.6)$$

All unique combinations of N features containing D dimensions were described by q(D). The performance metric, J, was defined as the squared Mahalanobis distance (r^2), which is the distance between the feature vector, **x**, and the mean vector, **μ**, [63] such that

$$r^2 = (\mathbf{x}-\boldsymbol{\mu})'\mathbf{C}^{-1}(\mathbf{x}-\boldsymbol{\mu}), \qquad (3.7)$$

with **C** representing a self-adjoint and positive definite covariance matrix of the training data set. The squared Mahalanobis distance was used to determine which sleep event of interest was nearest to a specific feature vector. This allowed for efficient classification of sleep events of interest using a selected feature subset.

The main objective of feature selection was to find a feature subset $\hat{F}(D)$ that outperformed all other feature subsets with D dimensions such that:

$$\hat{F}(D) = F_i(D) \text{ with: } J(F_i(D)) = J(F_j(D)) \text{ for all } j \in \{1,...,q(D)\}. \qquad (3.8)$$

Pseudo-code for the sequential forward and backward algorithms are included in Figures 3.6.2.1 1 and 3.6.2.1 2 [64].

1. Initialize the feature subset
   $F_0 = \{\emptyset\}$; $j = 0$.

2. Add a feature based on the performance metric results
   $x^+ = \arg \max_{x \notin F_j}[J(F_j + x)]$

3. Update the feature subset
   $F_{j+1} = F_j + x^+$

4. If $j<d$, then
   $j = j + 1$ and go to step 2
   Else
   END

Figure 3.6.2.1 1: Pseudo-code for the sequential forward feature selection algorithm

1. Initialize the feature subset
   $F_0 = F(N)$; $j = 0$.

2. Eliminate a feature based on performance metric results
   $x^- = \arg \max_{x \in F_j}[J(F_j - x)]$

3. Update the feature subset
   $F_{j+1} = F_j - x^{--}$

4. If $j<d$, then
   $j = j + 1$ and go to step 2
   Else
   END

Figure 3.6.2.1 2: Pseudo-code for the sequential backward feature selection algorithm

3.6.2.2 Binary Particle Swarm Optimization Algorithm

The b-PSO algorithm was implemented in this study to provide the most suitable feature subsets for the pre-Parkinsonian disease patient and control subject GOHMMs. This approach was selected based on its direct feature selection approach, which indicates

selected features (1) or removed features (0). Selected features represent the final feature subsets and are included in the feature extraction module in ESAM. The theoretical basis behind the b-PSO is provided by Engelbrecht [65].

The original PSO states that the trajectory, *v*, of each particle is represented by the following equation:

$$v_{ij}(t+1) = w * v_{ij}(t) + c_1 * r\,(p_{ij} - x_{ij}(t)) + c_2 * r\,(p_{gi} - x_{ij}(t)). \quad (3.9)$$

Where w is an inertia weight, c_1 and c_2 are positive constants, r represents a random number in the range [0, 1] sampled from a uniform distribution, p_{ij} is the best state obtained for particle i at dimension j, and p_{gj} is the neighborhood best particle state obtained for the neighborhood g at dimension j.

The inertia weight, *w*, was set to control the exploration and exploitation abilities of the PSO. This parameter controled the amount of influence the previous velocity had on the new velocity. The cognitive component $c_1 * r\,(p_{ij} - x_{ij}(t))$ represented the particle's performance based on its previous best position. Particle performance relative to a group of particles was represented by $c_2 * r\,(p_{gi} - x_{ij}(t))$, which is described as the social component. This component represents the best position found by the particle's neighborhood. To obtain the particles current position, *x*, the following equation was used:

$$x_{ij}(t+1) = x_i(t) + v_i(t+1). \quad (3.10)$$

In b-PSO particles were represented in binary space. The particle position vector was expressed in binary notation having values of 0 or 1 such that

$$x_{ij} \in \{0,1\}. \quad (3.11)$$

Where x_{ij} denoted the position of particle *i* for the j^{th} dimension (number of dimensions was equal to the number of features in the original feature vector).

A particles position was represented by bit flips therefore discretization was necessary to obtain a binary representation for the particle position. As noted previously, particle position was related to particle velocity and particle velocity was described by the amount of bit flips per iteration. Bit flips were tracked by calculating the Hamming distance between the current and previous particle position vector and is described as

$$H(x_i(t), x_i(t-1)), \qquad (3.12)$$

where *t* is the current time step and *t-1* is the previous time step.

When $H(x_i(t), x_i(t-1)) = 0$ no bits were flipped and the particle's position remains unchanged with

$$\|v_i(t)\| = 0. \qquad (3.13)$$

Maximum particle velocity was reached when all bits were flipped such that,

$$\|v_i(t)\| = n_x \qquad (3.14)$$

with n_x representing all the bits for the position particle *x*.

Single dimension particle velocities were defined in terms of probabilities that a bit would take on the value of 0 or 1. Therefore, a velocity of $v_{ij} = 0.60$ represented a 60% chance for the bit to have a value of 1 and a 40% chance of the bit to have the value 0. This requires all particle velocities in the b-PSO to be restricted to the range [0, 1]. To avoid premature convergence to non-optimal solutions from limited exploration we normalized the velocities in this study using the log sigmoid function such that,

$$v'_{ij}(t) = \log sig(v_{ij}(t)) = \frac{1}{1+e^{(-v_{ij}(t))}}. \qquad (3.15)$$

Using, $v'_{ij}(t)$, the normalized velocity, the particle position update equation was

$$x_{ij}(t) = 1 \text{ if } r_j(t) < \log sig(v_{ij}(t)); \qquad (3.16)$$

else,

$$x_{ij}(t) = 0 \qquad (3.17)$$

with $r_j(t) \sim U(0,1)$ representing a random value in the range [0,1], sampled from an uniform distribution. Finally, the probability of bit flipping was expressed as

$$\Pr ob(\Delta) = \log sig(v_{ij}(t))(1 - \log sig(v_{ij}(t)) \qquad (3.18)$$

with Δ representing a bit flip.

In summary the parameters needed for the implementation of the b-PSO algorithm included[66].

- $x_{ij}(t)$ the current position of particle *i* at dimension *j*
- $\Pr ob(\Delta)$ the probability that a bit flip would occur and the particle would change position
- $v'_{ij}(t)$ the measurement of bit flips per iteration of the algorithm for particle *i* at dimension *j*
- p_{ij} the best state obtained for particle *i* at dimension *j* (for example if the best state occurred at $x_{ij}(t)=0$ then $p_{ij}(t)=0$ and if the best state occurred at $x_{ij}(t)=1$ then $p_{ij}=1$)

- p_{gj} the neighborhood best particle state obtained for the neighborhood g at dimension j (for example if the best particle state occurred when a member of the neighborhood was in the state 1 then p_{gj}=0)

The b-PSO algorithm was implemented in this study as follows:

1) *Randomly created a particle swarm/population.*

2) *Initialized the swarm velocities for the population created in step 1.*

3) *Initialized the maximum number of algorithm iterations and minimum fitness value criteria for algorithm termination.*

4) *Calculated the fitness value for each particle in the population using the k-NN algorithm.*

5) *Selected the current best particle position (p_{ij}) based on the fitness value results from step 4.*

6) *Selected the neighborhood best particle position (p_{gj}) based on the results from step 5.*

7) *Updated the population velocity, $v'_{ij}(t)$, and the particle position, $x_{ij}(t)$, for the population.*

8) *Calculated the fitness value for each particle in the population.*

9) *Selected the current best particle position (p_{ij}) based on the fitness value results from step 8.*

10) *Selected the neighborhood best particle position (p_{gj}) based on the results from step 9.*

11) *If algorithm termination requirements from step 3 were met, then continued to step 12 else proceeded to step 7.*

12) *Saved the neighborhood best particle position (p_{gj}) as the global best particle position.*

13) *Selected the user defined number of features using roulette wheel selection (see Appendix A for the roulette wheel selection methodology) from the global best particle position results to form the feature subsets.*

3.6.3 Quantitative Modeling Selection

The primary goal in model selection is to obtain a proper mathematical description of a known physical phenomenon. The physical phenomenon of interest in this study was the human sleep cycle. Model selection based on sleep onset has been presented in the literature since 1988 [49]. However, these models were behavioral based and focused primarily on the transitions between wake-to-sleeping states and did not address transitional occurrences within the sleep process itself. Current models that attempt to address the sleep to wake transitions as well as, incorporate transitions within the sleep process have been cited in the literature by Kemp and Kamphuisen [50]. The current condition of sleep models establishes the need for suitable quantitative representations of transitional stages within the sleep cycle [67]. GOHMM an extension of Markov Modeling utilized by Flexer et al. and has been selected as a basis for this research due to its effectiveness in tracking transitional occurrences within the human sleep cycle[4].

3.6.3.1 Markov Modeling

Markov processes consist of a sequence of repeated experimental trials with outcomes that have the following properties [68]:

(i) Each outcome/observable sequence, $\mathbf{V}^{M}$, belongs to a finite set $\mathbf{V} = \{v_1, v_2,\ldots, v_M\}$, where v_M is the emission value at state M for time *t* and the emission value is equal to the state value.

(ii) The outcome of any trial depends solely on the outcome of the preceding trial and not on previous outcomes.

A Markov process is described by the following parameters [68]:

- A set of N distinct hidden states $\{S_1, S_2,\ldots, S_N\}$, with the state at time t represented by q_t.

An M-by-M transition matrix (**A**) whose i, j entry is the probability of a transition from state i to state j. This matrix corresponds to a state diagram similar to Figure 3.6.3.1 1. The sum of the entries in each row of **A** must equal 1, since it represents a stochastic matrix.

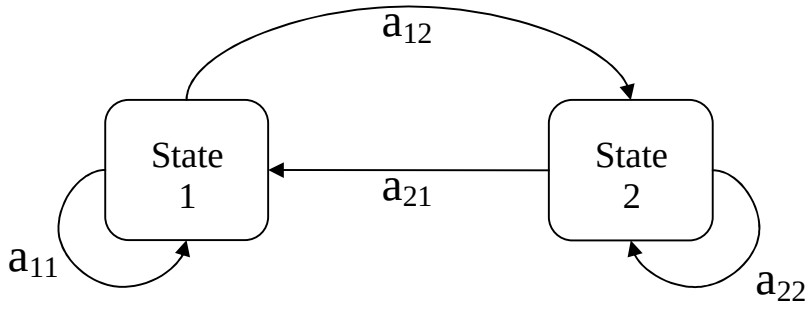

Figure 3.6.3.1 1: Illustration of a two-state Markov model.

A hidden Markov model is considered an extension of the Markovian process. This model is more complex than a Markovian process in that the probability of being in a certain state is not necessarily equal to the model emission(s)/observation(s) probability.

Building upon the Markov model, a discrete hidden Markov model contains the same parameters as a Markov model in addition to the following [69]:

- A set of M distinct observations $\mathbf{V}^M = \{v_1, v_2, \ldots, v_M\}$, where v_M represents a visible symbol/emission at state M for time *t*.
- An observation symbol probability distribution $B = \{b_j(k)\}$ in state j, where

$$b_j(k) = P(v_k \text{ at } t | q_t = S_j), \qquad 1 = j = N, \quad 1 = k = M \tag{3.19}$$

- The initial state distribution $p = \{p_i\}$, where

$$p_i = P(q_i = S_i), \qquad 1 = i = N \tag{3.20}$$

To further our analysis we introduce the variable

$$g_t(i) = P(q_t = S_i \mid O, l), \tag{3.21}$$

where $g_t(i)$ is the probability of being in state S_i at time *t*, given the observation sequence O and the model ?. Where ? is a compact notation used to represent the HMM such that ? = (A, B, p).

We may now define the expected number of occurrences in state S_i at time *t* as,

$$\hat{p}_i = g_t(i), \; 1 = i = N \tag{3.22}$$

The state transition coefficients are calculated as follows

$$\hat{a}_{ij} = \frac{\sum_{t=1}^{T-1} x_t(i, j)}{\sum_{t=1}^{T-1} g_t(i)} \tag{3.23}$$

with,

$$\sum_{t=1}^{T-1} x_t(i, j) \tag{3.24}$$

representing the expected number of transitions from state S_i to state S_j. Observation symbol coefficients are expressed as

$$\hat{b}_{jk} = \frac{\sum_{t=1, O_t = k}^{T} g_t(j)}{\sum_{t=1}^{T} g_t(j)}. \qquad (3.25)$$

According to Duda et al. [27] there exist three primary issues in hidden Markov model analysis:

Evaluation: Given a complete HMM with transition probabilities a_{ij} and b_{jk} determine the probability a particular sequence of visible states, $\mathbf{V}^{M}$, being generated by that model.

Decoding: Provided we are supplied with a HMM and a set of observations/sequences, $\mathbf{V}^{M}$. Obtain the most likely hidden states q_t that produced those observations.

Learning: Assume we are provided with an intelligent estimate regarding the HMM structure (number of hidden states and number of distinct observations) but no information regarding the probabilities a_{ij} and b_{jk}**.** Provided with a set of training observations/sequences and corresponding hidden states determine the unknown probabilities.

The primary focus of this work was to investigate the learning problem present within Flexer's GOHMM. This model provides a continuous perspective in the analysis of the human sleep cycle and represents the classification module in ESAM.

3.6.3.2 Gaussian Observation Hidden Markov Model Methodology

Investigation of the continuous nature of the human sleep cycle was obtained with a continuous GOHMM. The GOHMM was characterized by having a finite number of N states labeled Q:

$$Q = q_1, q_2, \ldots, q_N. \quad (3.26)$$

New states were entered based upon the transition distribution **A** which depended solely on the previous state (the Markovian property):

$$\mathbf{A} = \{ \hat{a}_{ij} \}, \ \hat{a}_{ij} = P(q_j(t+1) | q_i(t)), \quad (3.27)$$

where $t = 1,\ldots,T$ is a time index and T is the length of the observation sequence, i and j were the previous and current states respectively, and P was the probability of being in state q at time t. Each transition was followed by an observation output symbol that was produced according to the probability distribution **B** which depended on the current state j such that:

$$\mathbf{B} = \{ \hat{bj}(\mathbf{O}) \} = c_{jm} N[\mathbf{O}, \boldsymbol{\mu}_{jm}, \mathbf{U}_{jm}], \quad (3.28)$$

where N could represent any log-concave or elliptically symmetric density, in this study a normal density was selected. The mixture coefficient was c_{jm} for the mth mixture in state j, $\boldsymbol{\mu}_{jm}$ and $\mathbf{U}_{jm}$ representing the mean vector and covariance matrix which corresponded to the mth mixture in state j. Furthermore, **O** was considered a random variable that represented the feature vector [69].

The mixture coefficients satisfied the following stochastic constraints.

$$\sum_{m=1}^{M} c_{jm} = 1 \ , \ 1 = j = N, \quad (3.29)$$

$$c_{jm} = 0, \ 1 = j = N, \ 1 = m = M, \quad (3.30)$$

The stochastic constraints ensured that the probability density function (pdf) was normalized such that,

$$\int_{-\infty}^{\infty} b_j(x) dx = 1, \ 1 = j = N. \quad (3.31)$$

The mixture coefficient, mean vector, and covariance matrix were calculated as follows:

$$\bar{c}_{jk} = \frac{\sum_{t=1}^{T} g_t(j,k)}{\sum_{t=1}^{T}\sum_{k=1}^{M} g_t(j,k)}, \qquad (3.32)$$

$$\bar{m}_{jk} = \frac{\sum_{t=1}^{T} g_t(j,k) O_t}{\sum_{t=1}^{T} g_t(j,k)}, \qquad (3.33)$$

$$\bar{U}_{jk} = \frac{\sum_{t=1}^{T} g_t(j,k)(O_t - \bar{m}_{jk})(O_t - \bar{m}_{jk})'}{\sum_{t=1}^{T} g_t(j,k)}, \qquad (3.34)$$

where the prime value in $\bar{U}_{jk}$ indicated the vector transpose.

Initial estimates for the mean vector, $\boldsymbol{\mu}_{jm}$, and the covariance matrix, $\mathbf{U}_{jm}$, were obtained using training data sets. The GOHMM was trained using the expectation-maximization (EM) algorithm to estimate the final model parameters: **A**, **B**, $\boldsymbol{\mu}_{jm}$ and $\mathbf{U}_{jm}$ [70].

The EM algorithm is an iterative method commonly utilized in statistical estimation to obtain the Maximum Likelihood estimates of unknown model parameters for incomplete data sets[63]. Use of the algorithm may be further understood by application to a specific problem. Assume that a complete data set is described by, ***y*** such that

$$\boldsymbol{y} \in Y \subseteq \Re^m, \qquad (3.35)$$

and the associated probability density function (pdf) is denoted by

$$p_{\boldsymbol{y}}(\boldsymbol{y}; \theta), \qquad (3.36)$$

where q represents an unknown parameter vector. In this problem we can not directly observe the samples $\boldsymbol{y}$. In relation to our study the samples $\boldsymbol{y}$ represented the sleep event of interest. Although, the samples $\boldsymbol{y}$ were not directly observable we were able to obtain a subset of the $\boldsymbol{y}$'s corresponding to a specific $\boldsymbol{x}$ such that

$$\boldsymbol{x}=\boldsymbol{g}(\boldsymbol{y})\in X_{ob} \subseteq \Re^{l}, l < m, \qquad (3.37)$$

and the associated pdf was denoted by

$$p\boldsymbol{x}(\boldsymbol{x};q). \qquad (3.38)$$

A *many-to-one mapping* was obtained from the above pdf such that $Y(\boldsymbol{x}) \subseteq Y$ became a subset for all $\boldsymbol{y}$'s corresponding to a particular $\boldsymbol{x}$. The pdf for the incomplete data set was expressed as

$$p\boldsymbol{x}(\boldsymbol{x};q) = \int_{y(x)} py(y;q)dy. \qquad (3.39)$$

The maximum likelihood estimate of the unknown parameter q was denoted as

$$\hat{q}_{ML} : \sum_{k} \frac{\partial \ln(py(y_k;q))}{\partial q} = 0. \qquad (3.40)$$

Recall that the $\boldsymbol{y}$ values could not be directly obtained therefore, we utilized the EM algorithm to maximize our expectation of the log–likelihood function to obtain the unknown parameter values, q. The EM algorithm consisted of two steps. In step one, the E-Step, missing data was estimated from the observed data and current model parameter estimates. Assume that we are at the (t+1) algorithm iteration and $q(t)$ data was available then the expected value of the log-likelihood function, $Q(q;q(t))$, was

$$Q(q;q(t)) \equiv E\left[\sum_{k} \ln(py(y_k;q \mid X;q(t))\right]. \qquad (3.41)$$

We maximized our estimation of the log-likelihood function in the M-Step. Again assuming that we are at the (t+1) algorithm iteration we maximized our estimate of the log-likelihood function $Q(q;q(t))$ as follows

$$q(t+1):\frac{\partial Q(q;q(t))}{\partial q}=0. \qquad (3.42)$$

The EM algorithm was applied in this study as follows:

1) *Initialized the model parameters based on the initialization of the GOHMM parameters(see Method #1 and Method #2 following Figure 3.6.3.2 1).*

2) *Implemented the E-Step by computing the expected value of the log-likelihood function.*

3) *Implemented the M-Step by maximizing the expected value of the log-likelihood function obtained in step 2.*

4) *Repeated steps 2-3 until,* $\|q(t+1)-q(t)\|\le e$, *where* e *represented a predefined stopping criteria (in our case 10,000 iterations were used).*

Testing/performance evaluation on the estimated GOHMM was conducted using Viterbi decoding to determine the most likely state sequence/sleep events from the given observation set/feature set. The Viterbi algorithm found the most likely state sequence, Q, of the GOHMM, l, such that $P(O,Q\mid l)$ was maximized [63]. A diagram displaying an example of the best path selection process is displayed in Figure 3.6.3.2 1. Each row in the diagram represents one of the possible, Q, classes (q_1, q_2, q_{M-1}, q_M). Observations, x_k, are shown in successive columns for sample values k =1, 2, …, N-1, N. Class transitions are illustrated with arrows and represented by known fixed probabilities such that the transition probability from class q_i to q_j is defined as, $P(q_j|q_i)$. We assumed that

these probabilities, $P(q_j|q_i)$, did not change across sample values, k, and that the conditional probability densities $p(\boldsymbol{x}|q_i)$ for i=1,2,…,M were known.

Using Figure 3.6.3.2 1 we observed the feature vector X such that X: x_1, x_2,…,x_N and the observed feature vector with the respective class vector Q_i:q_{i1}, q_{i2},…, q_{iN} was maximized as follows

$$p(X \mid Q_i) = P(q_{i1})\, p(x_1 \mid q_{i1}) \prod_{k=2}^{N} P(q_{ik} \mid q_{i(k-1)})\, p(x_k \mid q_{ik})\,. \tag{3.43}$$

Maximization of $p(X \mid Q_i)$ provided the most likely state sequence/optimal path, Q, of the GOHMM, l , such that $P(O,Q \mid l)$ was maximized. We obtained the optimal path by assigning a cost for each state transition that related to $p(X \mid Q_i)$ and as suggested by Theodoridis [63] we utilized the following cost function

$$\hat{d}(q_{ik}, q_{i(k-1)}) = P(q_{ik} \mid q_{i(k-1)})\, p(x_k \mid q_{ik})\,. \tag{3.44}$$

Using $\hat{d}(q_{ik}, q_{i(k-1)})$ the overall cost was described as

$$\hat{D} \equiv \prod_{k=1}^{N} \hat{d}(q_{ik}, q_{i(k-1)})\,, \tag{3.45}$$

with $\hat{D}$ being maximized as follows

$$\ln(\hat{D}) = \sum_{k=1}^{N} \ln \hat{d}(q_{ik}, q_{i(k-1)}) \equiv \sum_{k=1}^{N} d(q_{ik}, q_{i(k-1)}) \equiv D. \tag{3.46}$$

Using D we associate the cost of being in class q_{ik} at stage k for the path i as

$$D(q_{ik}) = \sum_{r=1}^{k} d(q_{ir}, q_{i(r-1)})\,. \tag{3.47}$$

The Bellman principle was utlized to obtain D_{max} such that

$$D_{max}(q_{ik}) = \max_{i(k-1)} [D_{\max}(q_{i(k-1)}) + d(q_{ik}, q_{i(k-1)})], i_k, i_{k-1} = 1,2,...,M \tag{3.48}$$

and

$$D_{max}(q_{io})=0. \tag{3.49}$$

Using D_{max} the optimal path was related to the final stage N and corresponding class q^*_{iN} as follows

$$q^*_{iN} = \arg\max_{q_{iN}} D_{\max}(q_{iN}). \tag{3.50}$$

From observation of Figure 3.6.3.2 1 each observation k, with k = 1, 2,…, *N*, contained *M* potential transitions to each of the q_{ik} stages. The Viterbi algorithm was iterative, therefore we recursively utilized D_{max} to obtain the corresponding q_{ik} which provided the most likely state sequence/optimal path for the GOHMM. An example tracing of an optimal GOHMM path is displayed in Figure 3.6.3.2 1 with the maximum cost displayed by the thick arrowed lines.

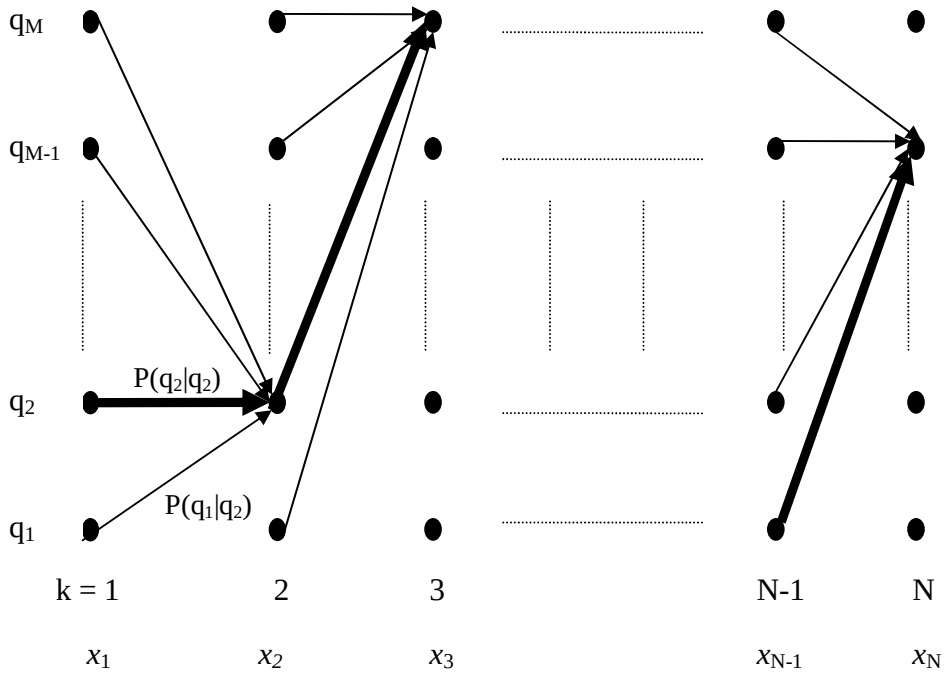

Figure 3.6.3.2 1: Diagram displaying the best path selection in the Viterbi algorithm.

Using the *k*-means, EM and Viterbi algorithms the GOHMM for this study was implemented using two methods. Method #1 utilized a supervised approach to initialize the GOHMM. An unsupervised *k*-means clustering approach was implemented in method #2 to initialize the GOHMM. The procedures executed in each method are described below (note the GOHMM was executed using the software platform MATLAB v. 7.0 and Murphy's Hidden Markov Model Toolbox for MATLAB [71]):

Method #1

1) *Initialized the number of mixture components to one.*

2) *Calculated initial estimates of the mean vector and the covariance matrix for the GOHMM based upon the training data set. A full covariance matrix was used in this study.*

3) *Executed the EM algorithm to optimize the GOHMM model parameters,* ? = (A, B, p), *based on the initial estimates for the mean vector and covariance matrix obtained from step 2.*

4) *Utilized the Viterbi algorithm to obtain the most likely hidden states path* ***(sleep event classification)*** *based on results obtained from step 3.*

5) *Correlated hidden states* ***path*** *obtained in step 4 to the* ***expert's classifications*** *of the data using a* ***confusion matrix****. The confusion matrix showed the level of agreement between the GOHMM and expert classification (in our case the sleep event scoring from the sleep physician/technician represented the expert's classification).*

6) *Selected final GOHMM parameters that provided the optimal performance results* ***(sleep event classification)****.*

Method #2

1) *Initialized the number of mixture components to one.*

2) *Obtained mean/centroid values using the k-means algorithm (See Appendix A). Calculated initial estimates of the mean vector and the covariance matrix for the GOHMM based on the mean/centroid values.*

3) *Executed the EM algorithm to optimize the GOHMM model parameters,* ? = (A, B, p), *based on the initial estimates for the mean vector and covariance matrix obtained from step 2.*

4) *Utilized the Viterbi algorithm to obtain the most likely hidden states path* ***(sleep event classification)*** *based on results obtained from step 3.*

5) *Correlated hidden states* ***path*** *obtained in step 4 to the* ***expert's classifications*** *of the data using a* ***confusion matrix****.*

6) *Selected final GOHMM parameters that provided the optimal performance results* ***(sleep event classification)***.

In this study, two GOHMMs were implemented using method #1 and #2. One GOHMM was based on pre-Parkinsonian detection and the other was based on normal age matched control detection. Model output consisted of individual probability distributions for each sleep event of interest with respect to the observation sequence and the hypnogram. The individual probability distribution for each sleep event was used to create the hypnogram. A summary of sleep event occurrence with respect to sleep recording time was provided by the hypnogram and in clinical practice the physician uses this information to diagnosis the subject/patient.

3.6.4 ESAM Applications and Significance

Research on the mechanisms and quality of sleep also have profound implications for the United States (U.S.) given that approximately 60% of U.S. adults suffer from some type of sleep problem at least a few nights each week [72].

Establishment of a reliable model for human sleep analysis, provided by this research, means improved physician diagnosis and investigation of pathologies within the human sleep cycle specifically for neurodegenerative disorders such as Parkinson's disease. ESAM provides the commonly used hypnogram as a system output to aid the physician in the diagnosis process. Previous sleep models have not focused on neurodegenerative disorder applications[4, 32].

ESAM improves on previous sleep modeling approaches by providing human sleep modeling techniques that are applicable to neurodegenerative disorders commonly correlated to the sleep process. Since ESAM may be applied to specific sleep related disorders it has significant sleep research benefits as well as commercial marketability. ESAM may be adapted for commercial use in clinical settings via an on-line sleep event scoring software system. The latter displays the significance of the ESAM system to the sleep research community.

CHAPTER 4: RESULTS

4.1 Chapter Introduction

Quantitative results are provided in this chapter to answer research questions two and three posed in chapter 1. Investigation of these research questions aid in meeting the specific aims of the study and are included below.

2. What quantitative features should be extracted from the polysomnogram to best describe the human sleep cycle?

3. What GOHMM model parameters should be used to best differentiate between control subjects and pre-Parkinsonian patients?

Section 4.2 entitled *Feature Selection,* provides a detailed overview of the quantitative feature library used in this study. This library is utilized to obtain feature subset selection results using the sequential forward and backward algorithms and b-PSO algorithm; data from these analyses are presented. The feature subsets selected from the latter provide information specific to research question number two. Following the sub-section on *Feature Selection* is section 4.3 entitled *Human Sleep Modeling,* this section provides modeling results used to obtain the pre-Parkinsonian and age matched control GOHMM parameters. Results obtained from section 4.3 provide information to address research question number three. The final section in this chapter entitled *ESAM Output* provides graphical illustrations of the ESAM sleep event classification output as compared to the physicians/technicians labeling. This information is provided as a visual display of ESAM sleep event classification performance.

4.2 Feature Selection

4.2.1 Quantitative Feature Library

In this study, as stated in chapter 2, we utilized feature extraction and selection to reduce the data size, enhance data visualization and data interpretation, and improve classification performance in ESAM. The feature library used in the feature extraction and selection processes are included in Tables 4.2.1 2-Tables 4.2.1 7. Details that include the feature name, mathematical expression, channel extraction, domain, and description are provided in these tables. The feature library consisted of 67 features. Each feature was processed using the sequential forward (sf) and sequential backward (sb) feature selection algorithms, and b-PSO algorithm. Consultation with sleep physicians and an exhaustive review of previous sleep analysis and bio-signal feature extraction approaches resulted in the ESAM feature library. Table 4.2.1 1 displays the feature number and corresponding literature reference for the ESAM feature library.

Table 4.2.1 1: A table displaying the feature number and corresponding reference for the ESAM feature library.

Feature Number	Reference
1-43	Zoubek [35]
44-47, 52-55,60-67	D'Alessandro [73]
48-51	Agarwal [74]
56-59	Smart [75]

The *k*-NN classifier was utilized to measure sleep event detection performance using feature subsets obtained from the sf, sb, and b-PSO algorithms. Tables 4.2.1 8 - 4.2.1 9 include the feature numbers and corresponding feature name and psg channel used to obtain the feature subsets.

Following artifact removal/compensation polysomnogram data was split into 3 second epochs, to meet signal stationarity assumptions, utilizing Tables 4.2.1 2 - 4.2.1 7 for feature extraction. A similar approach for meeting the stationarity assumption has been utilized by Zoubek[35]. The 3 second processing window was selected to obtain optimal resolution in sleep event detection and was verified for practical application by consultation with sleep physicians in agreement with ESAM Module #5. For

performance evaluation purposes the 3 second processing windows were averaged into 30 second epochs to correspond to the sleep technician/physician sleep event labeling.

Table 4.2.1 2: Detailed feature library for features 1:11 used in the development of ESAM.

Feature Name	Feature Equation	Channels	Feature Domain	Feature Description
Power Spectral Density Sub-band (PSD-SB) $0.5 = \| X_m(w_k)^2 \|_m < 4.5$[Hz]{Delta} , $4.5 = \| X_m(w_k)^2 \|_m < 8.5$[Hz]{Theta}, $8.5 = \| X_m(w_k)^2 \|_m <$ 11.5[Hz]{Alpha}, 11.5 $= | X_m(w_k)^2 |_m <$15.5[Hz]{Spindle}, and $15.5 = | X_m(w_k)^2 |_m =$32.5[Hz]{Beta}	PSD-SB $= \| X_m(w_k)^2 \|_m =$ $\left(\frac{1}{M} \sum_{m=0}^{M-1} \| DFT_k(x_m) \|^2 \right)$ DFT = the discrete Fourier transform of the signal x_m time averaged across M blocks k = frequency domain length of the signal x_m	EEG/C3-A2	Frequency	PSD-SB represents the absolute value of the signal power in the frequency band relative to the sampling rate.
Relative Frequency Power (Prel)	$12.5 = | X_m(w_k)^2 |_m <$32[Hz] {Spectral Power (EMG, high)}, $8 = \| X_m(w_k)^2 \|_m <$ 32[Hz] {Spectral Power (EMG, total)}, Prel = $\frac{\{SpectralPower(EMG, high)\}}{\{SpectralPower(EMG, total)\}}$	EMG/CHIN EMG/RL	Frequency	Prel is a measure of the spectral power of the EMG signal in the frequency band 12.5Hz to 32 Hz relative to the total spectral power of the entire EMG signal.
Spectral Edge Frequency (SEF)	SEF = $Max(Frequency\ (x)) < P\{95\}$ x = the data signal $P\{95\}$ = the 95th percentile of the spectral power of the data signal	EEG/C3-A2 EOG/R EMG/CHIN EMG/RL	Frequency	SEF is a calculation of the highest frequency below which 95% of the total spectral power resides.

Table 4.2.1 3: Detailed feature library for features 12:19 used in the development of ESAM.

Feature Name	Feature Equation	Channels	Feature Domain	Feature Description
Standard Deviation (SD)	$\mathrm{SD} = \left(\frac{1}{n-1} \sum_{i=1}^{n} \left(x_i - \bar{x} \right)^2 \right)^2$, with n = the length of the data sample x and $\bar{x}$ is the mean of the data sample	EEG/C3-A2 EOG/R EMG/CHIN EMG/RL	Statistical	SD is a measurement of the spread of the signal's distribution. It is equivalent to the positive square root of the variance of the signal.
Skewness (Skew)	$\mathrm{Skew} = \sum_{i=1}^{n} \frac{\left(E\left(x_i - \bar{x} \right)^3 \right)}{s^3}$, with n = the length of the data sample x, s is the standard deviation of the data sample for all i, and E is the expected value/mean such that $\mathrm{E}(x) = \sum_{i=1}^{n} p_i x_i$, with n = the length of the data sample x and p_i represents the associated probabilities for x_i.	EEG/C3-A2 EOG/R EMG/CHIN EMG/RL	Statistical	Skewness represents the degree of symmetry the signal's distribution is with respect to the mean.

Table 4.2.1 4: Detailed feature library for features 20:31 used in the development of ESAM.

Feature Name	Feature Equation	Channels	Feature Domain	Feature Description
Kurtosis (Kurt)	$\text{Kurt} = \sum_{i=1}^{n} \frac{\left(E(x_i - \bar{x})^4\right)}{s^4}$, with n = the length of the data sample x, s is the standard deviation of the data sample for all i, and E is the expected value.	EEG/C3-A2 EOG/R EMG/CHIN EMG/RL	Statistical	Kurtosis is a measurement of how resilient the signal's distribution is to outliers.
75^{th} Amplitude Percentile (75_Amp)	$75\_\text{Amp} = Max(Amplitude(x)) < P\{75\}$, x = the data signal $P\{75\}$ = the 75^{th} percentile of the amplitude of the data signal	EEG/C3-A2 EOG/R EMG/CHIN EMG/RL	Time/Statistical	75_Amp calculates the highest amplitude value below which 75% of the total signal amplitude resides.
Entropy (Ent)	$\text{Ent} = -\sum_{j=1}^{M} \frac{n_j}{n} \ln\left(\frac{n_j}{n}\right)$, n = the length of the data signal M = number of bins used to estimate the histogram for the data signal n_j = the number of data samples in the j^{th} histogram bin.	EEG/C3-A2 EOG/R EMG/CHIN EMG/RL	Information	Entropy is a measurement of the randomness or unpredictability in the data signal.

Table 4.2.1 5: Detailed feature library for features 32:43 used in the development of ESAM.

Feature Name	Feature Equation	Channels	Feature Domain	Feature Description
Variance (S^2)	$S^2 = \frac{\sum_{i=1}^{n}(x_i - \bar{x})^2}{n-1}$, with n = the length of the data sample x and $\bar{x}$ is the mean of the data sample	EEG/C3-A2 EOG/R EMG/CHIN EMG/RL	Statistical	Variance determines how the signal is dispersed with respect to the value of the mean.
Mobility (Mobi)	$Mobi = \frac{SD(\frac{d(x)}{dt})}{SD(x)}$, SD is the standard deviation and x is the amplitude of data sample	EEG/C3-A2 EOG/R EMG/CHIN EMG/RL	Information	Mobility is a measure of the average slope of the data signal.
Complexity (Comp)	$Comp = \frac{Mobi\left(\frac{d(x)}{dt}\right)}{Mobi(x)}$, x is the amplitude of data sample	EEG/C3-A2 EOG/R EMG/CHIN EMG/RL	Information	Complexity calculates the average slope of the mobility of the data signal.

Table 4.2.1 6: Detailed feature library for features 44:55 used in the development of ESAM.

Feature Name	Feature Equation	Channels	Feature Domain	Feature Description
Curve Length (L)	$L = \sum_{i=1}^{n} \lvert x(i+1) - x(i) \rvert$ with n = the length of the data sample x	EEG/C3-A2 EOG/R EMG/CHIN EMG/RL	Time	Curve length determines the length between consecutive points within the signal.
Mean Absolute Amplitude (MAA)	$MAA = \frac{1}{n} \sum_{i=1}^{n} \lvert x(i) \rvert$ with n = the length of the data sample x	EEG/C3-A2 EOG/R EMG/CHIN EMG/RL	Time	MAA is a nonnegative scalar measurement of the data signals magnitude.
Mean Energy (MnE)	$MnE = \frac{1}{n} \sum_{i=1}^{n} x(i)^2$ with n = the length of the data signal x	EEG/C3-A2 EOG/R EMG/CHIN EMG/RL	Time	MnE represents the potential for causing amplitude changes in the data signal.

Table 4.2.1 7: Detailed feature library for features 56:67 used in the development of ESAM.

Feature Name	Feature Equation	Channels	Feature Domain	Feature Description
Zero Crossings (ZC)	$ZC'(i) = \begin{cases} 1, x(i) \le 0 \cap x(i+1) \\ 1, x(i) \ge 0 \cap x(i+1) \\ 0, otherwise \end{cases}$ $ZC = \sum_{i=1}^{n-1} ZC'(i)$ with n = the length of the data sample x.	EEG/C3-A2 EOG/R EMG/CHIN EMG/RL	Time	ZC is a measurement of how the signal is dispersed with respect to the value zero.
Nonlinear Energy (NE)	$NE = \sum_{i=1}^{n} x^2(i) - x(i-1)\,x(i+1)$ with n = the length of the data sample x.	EEG/C3-A2 EOG/R EMG/CHIN EMG/RL	Time	NE is an instantaneous measurement of the frequency and amplitude envelope of AM-FM signals.
Spectral Entropy (SE)	$PSD = \left(\frac{1}{M} \sum_{m=0}^{M-1} \lvert DFT_k(x_m) \rvert^2 \right)$ PSD = the power spectral density of the signal DFT = the discrete Fourier transform of the signal x_m time averaged across M blocks k = frequency domain length of the signal x_m $SE = -PSD(x) \log_2 PSD(x)$ where x is the data sample.	EEG/C3-A2 EOG/R EMG/CHIN EMG/RL	Frequency	SE determines the degree of disorganization or uncertainty of the signal in the frequency domain.

Table 4.2.1 8: Features 1:30 with corresponding feature name and psg channel.

FEATURE #	FEATURE NAME	CHANNEL
1	Delta Power	EEG/C3-A2
2	Theta Power	EEG/C3-A2
3	Alpha Power	EEG/C3-A2
4	Spindle Power	EEG/C3-A2
5	Beta Power	EEG/C3-A2
6	Relative Frequency Power	EMG/CHIN
7	Relative Frequency Power	EMG/RL
8	Spectral Edge Frequency	EEG/C3-A2
9	Spectral Edge Frequency	EOG/R
10	Spectral Edge Frequency	EMG/CHIN
11	Spectral Edge Frequency	EMG/RL
12	Standard Deviation of Signal Amplitude	EEG/C3-A2
13	Standard Deviation of Signal Amplitude	EOG/R
14	Standard Deviation of Signal Amplitude	EMG/CHIN
15	Standard Deviation of Signal Amplitude	EMG/RL
16	Skewness	EEG/C3-A2
17	Skewness	EOG/R
18	Skewness	EMG/CHIN
19	Skewness	EMG/RL
20	Kurtosis	EEG/C3-A2
21	Kurtosis	EOG/R
22	Kurtosis	EMG/CHIN
23	Kurtosis	EMG/RL
24	75th Amplitude Percentile	EEG/C3-A2
25	75th Amplitude Percentile	EOG/R
26	75th Amplitude Percentile	EMG/CHIN
27	75th Amplitude Percentile	EMG/RL
28	Entropy	EEG/C3-A2
29	Entropy	EOG/R
30	Entropy	EMG/CHIN

Table 4.2.1 9: Features 31:67 with corresponding feature name and psg channel.

FEATURE #	FEATURE NAME	CHANNEL
31	Entropy	EMG/RL
32	Variance	EEG/C3-A2
33	Variance	EOG/R
34	Variance	EMG/CHIN
35	Variance	EMG/RL
36	Mobility	EEG/C3-A2
37	Mobility	EOG/R
38	Mobility	EMG/CHIN
39	Mobility	EMG/RL
40	Complexity	EEG/C3-A2
41	Complexity	EOG/R
42	Complexity	EMG/CHIN
43	Complexity	EMG/RL
44	Curve Length	EEG/C3-A2
45	Curve Length	EOG/R
46	Curve Length	EMG/CHIN
47	Curve Length	EMG/RL
48	Mean Absolute Amplitude	EEG/C3-A2
49	Mean Absolute Amplitude	EOG/R
50	Mean Absolute Amplitude	EMG/CHIN
51	Mean Absolute Amplitude	EMG/RL
52	Energy	EEG/C3-A2
53	Energy	EOG/R
54	Energy	EMG/CHIN
55	Energy	EMG/RL
56	Zero Crossing	EEG/C3-A2
57	Zero Crossing	EOG/R
58	Zero Crossing	EMG/CHIN
59	Zero Crossing	EMG/RL
60	Non-Linear Energy	EEG/C3-A2
61	Non-Linear Energy	EOG/R
62	Non-Linear Energy	EMG/CHIN
63	Non-Linear Energy	EMG/RL
64	Spectral Entropy	EEG/C3-A2
65	Spectral Entropy	EOG/R
66	Spectral Entropy	EMG/CHIN
67	Spectral Entropy	EMG/RL

4.2.2 Sequential Feature Selection Results

An embedded feature selection approach, as described in Section 2.4.2, is implemented using the Mahalanobis distance as the objective function for the sf and sb algorithms. Classification was conducted with the *k*-NN classifier (see Appendix A for the *k*-NN methodology) utilizing test data sets to evaluate the performance of feature subsets obtained during sf and sb processing on training data sets. Data contained in the test set was not included in the training set and vice versa. To preserve the structure of the sleep process, training and testing data sets were not randomized within subjects and patients. Due to the small number of psg data sets for both normal/control subjects (3) and Parkinsonism patients (3) two psg data sets were used as training data and one as testing data. Tables 4.2.2 1 - 4.2.2 2 display how normal/control subject and Parkinsonism patient datasets were split into training and testing data for this study. All sequential feature selection results were obtained using PR Tools, a MATLAB based toolbox for pattern recognition analysis[62].

Table 4.2.2 1: Normal/control subject training and testing data set configurations.

Data Set	**Training Data (Subject Numbers)**	**Testing Data (Subject Number)**
A	1, 2	3
B	1,3	2
C	2,3	1

Table 4.2.2 2: Parkinsonism patient training and testing data set configurations.

Data Set	Training Data (Subject Numbers)	Testing Data (Subject Number)
D	6,5	4
E	4,6	5
F	4,5	6

The ultimate goal in this study was to incorporate the optimal feature subsets obtained from the sf and sb algorithm into ESAM for sleep event detection, therefore algorithm performance was defined by the following function, a similar approach in subset feature selection evaluation was utilized by Firpi [44]:

$$Accuracy = \left(\frac{\sum (P_{algorithm} = P_{expert})}{P_{total}} \right) * 100 , \qquad (4.1)$$

where $P_{algorithm}$ was the sleep event epoch classification based on processing of the subset feature testing data in the *k*-NN classifier, P_{expert} was the corresponding physician/technician's sleep event epoch labeling and P_{total} represented the total number of sleep event epochs. An accuracy value of 100% represented perfect sleep event detection by the *k*-NN classifier. The number of sleep event epochs (1 epoch = 30 seconds) contained in the training and testing data sets are displayed in Tables 4.2.2 3 – 4.2.2 4.

Table 4.2.2 3: A table display of the number of sleep event epochs within each training data set.

Data Set	Training Data					
[redacted]	Wake	Stage 1	Stage 2	Stage 3&4	REM	Total # Epochs
A	448	152	691	240	178	1709
B	332	91	714	211	182	1530
C	298	127	791	267	138	1621
D	467	153	777	73	192	1662
E	652	170	683	94	214	1813
F	643	265	548	101	184	1741

Table 4.2.2 4: A table display of the number of sleep event epochs for each testing data set.

Data Set	Testing Data					
[redacted]	Wake	Stage 1	Stage 2	Stage 3&4	REM	Total # Epochs
A	91	33	407	119	71	721
B	207	94	384	148	67	900
C	241	58	307	92	111	809
D	414	141	227	61	103	946
E	229	124	321	40	81	795
F	238	29	456	33	111	867

Feature selection algorithms sf and sb were executed for varying *k*-NN nearest neighbor values (k = 1:20), feature subset sizes (F = 2:11), and sleep event combinations. The inputs to the sf and sb algorithms included the training data feature vector obtained from Tables 4.2.1 2 - 4.2.1 7, the objective function, and the corresponding physician/technician's sleep event classification. Sequential feature selection algorithm output included the optimal feature subsets. To provide sleep event detection performance results *k*-NN classification was conducted on the test data set utilizing the optimal feature subsets obtained from the sequential feature selection algorithms.

Sleep event combinations, for sleep event detection, were established based upon review of the sleep literature and consultation with a sleep physician. The sleep event combinations used in this study are displayed in Table 4.2.2. 5. Combination one represents the classical definition of the six sleep stages as described in Section 1.7.2. Stages 3 and 4 were joined in all combinations to reflect the sleep technician/physician labeling. Combinations two and three represented the possibilities of misclassification of Stage 1 as a transitional sleep stage between Stage Wake and Stage 2 sleep, a common case shown in the literature and defined by Agarwal as pseudo-natural sleep patterns [67].

Table 4.2.2 5: Sleep stage event combinations investigated in ESAM performance evaluation

Combination Number	Sleep Events
1	Wake, Stage 1, Stage 2, Stage 3 & Stage 4, REM
2	Wake & Stage 1, Stage 2, Stage 3 & Stage 4, REM
3	Wake, Stage1 & Stage 2, Stage 3 & Stage 4, REM

Maximum classification accuracy across *k*-NN values, feature subset amount, and sleep event combination number were searched for data sets A-F. Figures 4.2.2 1- 4.2.2 2 provide graphical depictions of the search surface for data set A and sleep event combination 1 using the sequential backward and forward feature selection algorithm respectively. Table 4.2.2 6 indicate the maximum classification accuracies as 70.874% and 67.961%, these values are marked in the figure with an encircled x. All maximum classification accuracy sequential feature selection results for normal/control subject data and Parkinsonism patient data (data sets A-F) are displayed in Tables 4.2.2 6 – 4.2.2 7, respectively. The highest maximum accuracy values obtained for each sleep event combination are shown in gray. Appendix B displays the search space and maximum classification accuracy for the sequential feature selection algorithms for data sets B-F.

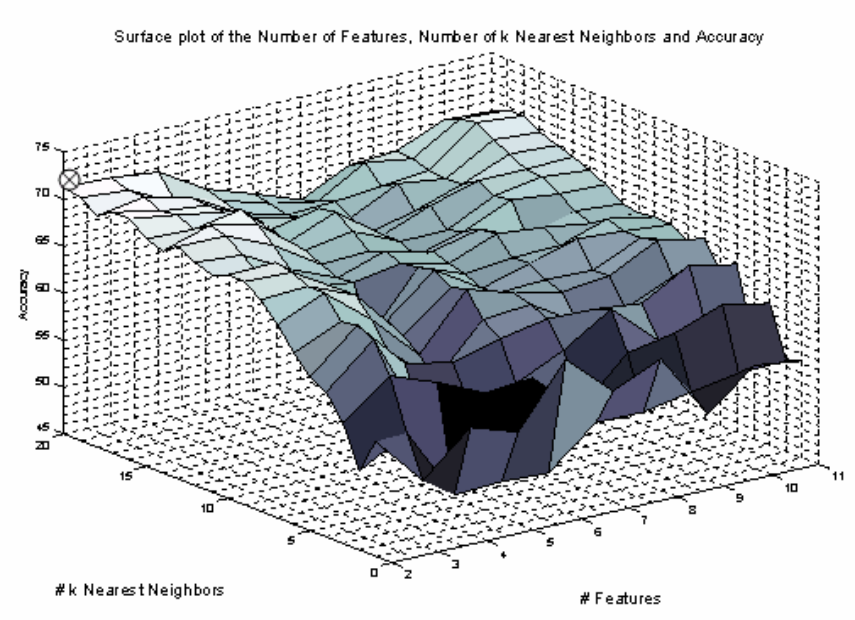

Figure 4.2.2 1: Surface plot of the search space for data set A and sleep event combination 1 using the sequential backward algorithm to obtain the maximum classification accuracy across *k*-NN values and feature subset amount.

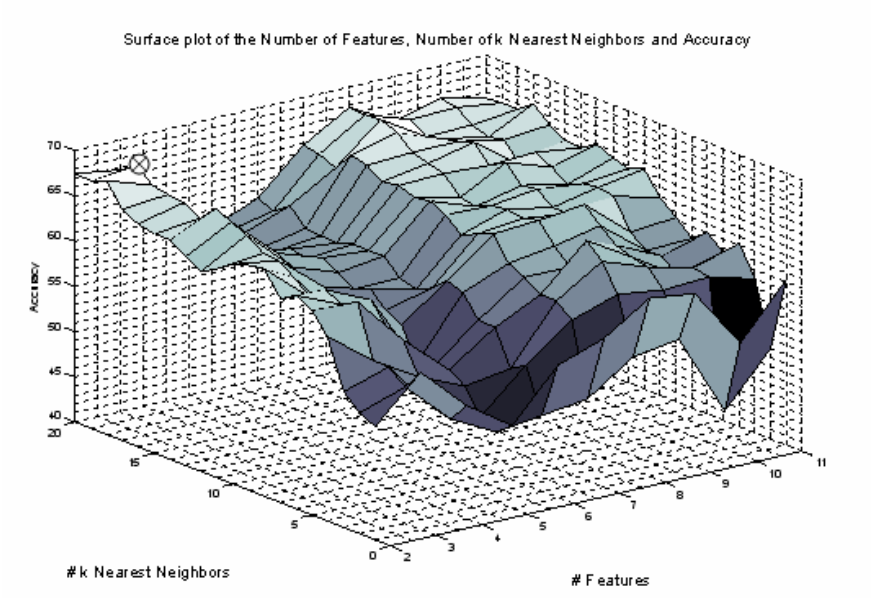

Figure 4.2.2 2: Surface plot of the search space for data set A and sleep event combination 1 using the sequential forward algorithm to obtain the maximum classification accuracy across *k*-NN values and feature subset amount.

Table 4.2.2 6: Sequential feature subset selection results for normal/control subject data.

Combination #	k-NN Value	# Features	Accuracy	Algorithm	Data Set
1	19	2	70.874	Backward	A
1	19	3	67.961	Forward	A
1	11	8	69.556	Backward	B
1	19	8	67	Forward	B
1	19	8	56.737	Backward	C
1	11	2	56.613	Forward	C
2	15	7	70.042	Backward	A
2	15	10	70.042	Forward	A
2	3	10	71.222	Backward	B
2	19	5	71.333	Forward	B
2	9	2	61.557	Backward	C
2	13	2	59.827	Forward	C
3	17	10	77.115	Backward	A
3	5	8	74.202	Forward	A
3	19	5	78.333	Backward	B
3	19	9	75.889	Forward	B
3	15	8	64.895	Backward	C
3	13	3	63.288	Forward	C

Table 4.2.2 7: Sequential feature subset selection results for Parkinsonism patient data.

Combination #	k-NN Value	# Features	Accuracy	Algorithm	Data Set
1	9	8	67.336	Backward	D
1	7	3	72.939	Forward	D
1	7	11	69.308	Backward	E
1	15	9	68.679	Forward	E
1	11	3	74.1674	Backward	F
1	3	8	74.74	Forward	F
2	1	8	73.256	Backward	D
2	9	3	80.655	Forward	D
2	11	11	77.736	Backward	E
2	15	5	77.987	Forward	E
2	7	3	75.548	Backward	F
2	3	8	77.97	Forward	F
3	9	7	79.07	Backward	D
3	7	3	81.184	Forward	D
3	19	8	75.723	Backward	E
3	5	11	78.742	Forward	E
3	11	3	84.083	Backward	F
3	15	5	85.236	Forward	F

Table 4.2.2 6 indicates that a *k*-NN nearest neighbor value of 19 provided the highest accuracy values (displayed in gray) across all sleep event combinations and data sets for normal/control subjects. The sb algorithm outperformed the sf algorithm in sleep event combinations 1 and 3. In sleep event combination 2 the sf marginally outperformed the sb algorithm (1.3%). The highest number of features selected across all sleep event combinations included 5 and the lowest number included 2.

The *k*-NN nearest neighbor values varied across all sleep event combinations and data sets for pre-Parkinsonian patient data (see Table 4.2.2 7), however higher accuracy values were achieved with lower nearest neighbor values, maximum value at 15 and minimum value at 3, when compared to the normal/control subject sequential feature selection results. When comparing sequential selection algorithms the sf outperformed the sb across all sleep event combinations and data sets. In both normal/control subject data and pre-Parkinsonian patient data the highest accuracy values, 78.333 and 85.236 respectively, were obtained for sleep event combination 3.

4.2.3 Binary Particle Swarm Optimization Feature Selection Results

Suitable feature subsets obtained from the b-PSO algorithm for sleep event classification using k-NN classification are presented in this section. Data set formulation, sleep event combinations, and performance evaluation criteria are identical to that used in the sequential feature selection algorithm experiments. A matrix containing the parameters used in the b-PSO algorithm to obtain feature subset selection results are displayed in Table 4.2.3 1. Parameters were selected based on promising results from previous feature subset selection techniques using b-PSO obtained by Firpi and Agrafiotis [44, 45]. Accuracy results for normal/control subject data and pre-Parkinsonian patient data are displayed in Tables 4.2.3 2 – 4.2.3 3, respectively. The highest accuracy values for each sleep event combination are shown in gray.

Table 4.2.3 1: Parameters used in the b-PSO algorithm to obtain feature selection results.

# Particles	**# Iterations**	**Maximum Velocity (v_{max})**	**Minimum Velocity (v_{min})**
50	20	6	-6
c_1	**c_2**	**Weight (w)**	**k-NN Value**
2	2	1	5

Table 4.2.3 2: b-PSO feature subset selection results for normal/control subject data.

Combination #	Total Accuracy	Data Set
1	62.552	A
1	62.33	B
1	60.198	C
2	58.807	A
2	66.00	B
2	41.286	C
3	78.086	A
3	70.56	B
3	63.041	C

Table 4.2.3 3: b-PSO feature subset selection results for Parkinsonism patient data.

Combination #	Total Accuracy	Data Set
1	61.628	D
1	60.881	E
1	72.549	F
2	80.867	D
2	70.82	E
2	63.899	F
3	79.704	D
3	67.421	E
3	81.661	F

Table 4.2.3 2 indicates that the highest b-PSO accuracy is obtained in sleep event combination 3 when compared across all sleep event combinations for normal/control subjects. Efficient sleep event classification was not obtained for sleep event combinations 1 (62.552%) and 2 (66.00%). When compared to sequential subset feature selection a decrease in accuracy of 8.3% and 5.3% was found for sleep event combinations 1 and 2, respectively.

Similar to the sequential feature selection results the highest sleep event classification accuracy was also obtained in sleep event combination 3 when compared

across all sleep event combinations for the b-PSO processed pre-Parkinsonian patient data (see Table 4.2.3 3). Favorable sleep event classification was obtained for sleep event combinations 1 (72.549%) and 2 (80.867%) when compared to sequential subset feature selection. A decrease in accuracy of sleep event combination 1 (2.191%) and an increase in accuracy of sleep event combination 2 (0.2%) was obtained.

Although, the b-PSO was limited to a *k*-NN nearest neighbor value of 5 and a feature subset number of 8, using roulette wheel selection (See Appendix A), it performed comparatively well for the most favorable sleep event combination (sleep event combination 3). Sequential subset feature selection results indicated that higher *k*-NN nearest neighbor values (19) displayed higher classification rates for sleep event combination number 1 and 2 for the normal/control subject data. The latter may be the contributing factor for the inefficient sleep event combination classification results obtained in the fixed *k*-NN nearest neighbor (k=5) classifier used in the b-PSO processing. Favorable results were obtained when comparing sequential subset and b-PSO feature selection for pre-Parkinsonian data.

4.2.4 Statistical Significance of Feature Selection Results

Non-parametric repeated measurement comparisons were conducted to determine the statistical significance of the feature selection results obtained from the feature selection algorithms used in this study. Non-parametric test instead of parametric (e.g., ANOVA or paired t-test) test were employed because data distributions (i.e., normality) could not be assumed. The Lilliefor's test for normality was utilized to confirm that data sets in this study did not follow a normal distribution[76].

Friedman's non-parametric Chi-Square test with two degrees of freedom and 95% confidence were utilized[77]. Friedman's test provided statistically significant information to aid in determining whether one feature selection algorithm (sf, sb, or b-PSO) provided more efficient sleep event classification results when compared to the other algorithms.

Table 4.2.4 1: Friedman's non-parametric test results for statistical significance determination across feature selection algorithm experiments.

Data Set Type	Sleep Event Combination #	Friedman's P-value	Chi-Square Value
Normal/Control	1	0.8459	0.33
Normal/Control	**2**	**0.0366**	**6.61**
Normal/Control	3	0.7091	0.69
pre-Parkinsonian	1	0.3959	1.85
pre-Parkinsonian	2	0.8685	0.28
pre-Parkinsonian	3	0.3486	2.11

The Chi-Square value in Table 4.2.4 1 displayed a significant difference between the sequential algorithms and the b-PSO algorithm at a 95% significance level for the normal/control subject data sets for sleep event combination 2 illustrated in bold (the minimum value of Chi-Square for statistical significance at two degrees of freedom with 95% confidence was approximately 5.99[77]). Therefore, with 95% confidence we observed a significant increase in sleep event detection using features selected from the sf and sb algorithms as compared to the b-PSO algorithm. Box plots for the normal/control subject data sets for sleep event combination 2 are displayed in Figure 4.2.4 1. The median box plot sleep event detection accuracy for each data set for the sf and sb algorithms were shown to be significantly higher than that of the b-PSO algorithm, which

graphically agreed with the quantitative Friedman's non-parametric Chi-Square test results. Significant differences between the sb and sf algorithms were not found in this case.

Chi- Square value statistical significance for feature selection algorithm results for normal/control subjects across sleep event combinations 1 and 3 and all pre-Parkinsonian patient sleep event combinations were not observed. The box plots for these cases are displayed in Appendix B.

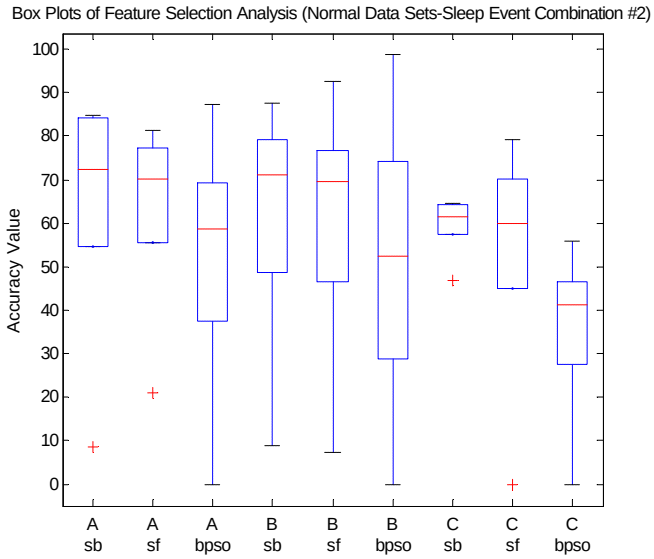

Figure 4.2.4 1: Box plot display of the lower quartile, median, and upper quartile values for normal/control subject data for sleep event combination #2 across all data sets and feature selection algorithms.

4.3 Human Sleep Modeling

4.3.1 GOHMM vs. *k*-NN classification

GOHMM sleep event classification results from suitable feature subsets obtained from the sf and sb feature selection algorithms and the b-PSO algorithm are discussed in this section. Subset features from Tables 4.2.2 6-4.2.2 7 and 4.2.3. 2- 4.2.3 3 were processed utilizing the GOHMM due to their potential representation as optimal feature sub-sets. Figure 4.3.1 provides a graphical display of the number of occurrences (count) for each feature selected across all feature selection techniques. Table 4.3. 2 displays the maximum number of selections for the same feature to be five. Features with the maximum number of selections included: Delta Power-EEG (1), Beta Power-EEG (5), Mobility-EEG (36), and Complexity-EOG/R (41).

Table 4.3 1 provides a list of the selected feature subsets, respective feature selection algorithm, data set and sleep event combination number and corresponding experiment code for processing in the GOHMM. This experimental look-up table was utilized as a reference in the presentation of the GOHMM sleep event classification performance. The feature subsets that provide the near optimal description of the human sleep cycle based upon the total sleep event accuracy value for pre-Parkinsonian patients and normal control subjects are shown in gray in Table 4.3 1. Feature subsets shown in gray addressed research question two (What quantitative features should be extracted from the psg to best describe the human sleep cycle?) by providing the quantitative

features that best described the human sleep cycle for normal/control subjects and pre-Parkinsonian patients across all sleep event combinations.

Table 4.3 1: Experimental lookup table for feature subsets processed with the GOHMM.

Experiment Code	Combination #	Feature Subset	Algorithm	Data Set	Total Acc.
sbn1	1	36,50	Backward	A	70.874
sfab1	1	1,2,5,24,38,40,41,56	Forward	F	74.740
bpson1	1	2,7,10,13,18,26,30,51	b-PSO	A	62.552
bpab1	1	4,5,8,11,12,26,28,34	b-PSO	E	72.549
sfn2	2	3,5,36,41,44	Forward	B	71.333
sfab2	2	40,56,58	Forward	D	80.655
bpson2	2	1,11,21,35,36,45,50,64	b-PSO	B	66.00
bpab2	2	1,5,36,38,41,42,44,58	b-PSO	D	80.867
sbn3	3	1,2,14,36,41	Backward	B	78.333
sfab3	3	1,24,38,40,41	Forward	F	85.236
bpson3	3	3,11,28,30,45,46,48,50	b-PSO	A	78.086
bpab3	3	5,8,12,45,50,55,56,63	b-PSO	F	81.661

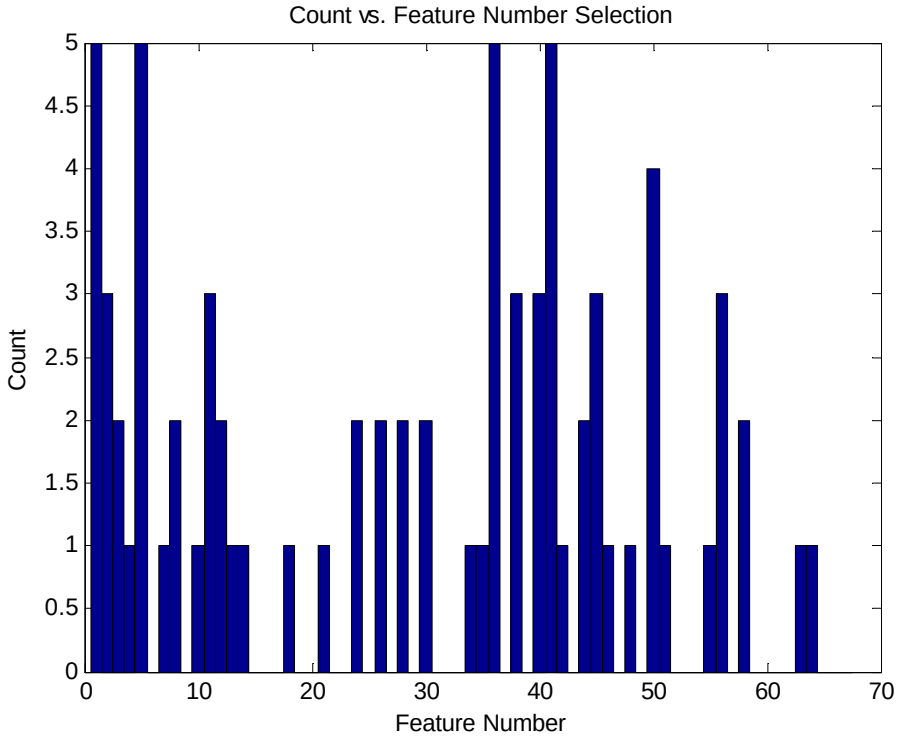

Figure 4.3 1: This figure displays the number of occurrences (count) for each feature selected in Table 4.3.1.

Table 4.3 2: A table display of all selected features along with the number of occurrences (count). The maximum number of occurrences was five and features meeting this selection amount are shown in gray.

Feature Number	Count
1	5
2	3
3	2
4	1
5	5
7	1
8	2
10	1
11	3
12	2
13	1
14	1
18	1
21	1
24	2
26	2
28	2
30	2
34	1
35	1
36	5
38	3
40	3
41	5
42	1
44	2
45	3
46	1
48	1
50	4
51	1
55	1
56	3
58	2
63	1
64	1

Feature subsets displayed in Table 4.3 1 for sleep event classification were processed in the GOHMM using method #1 and #2 from section 3.6.3.2. Results from GOHMM method #2, unsupervised GOHMM initialization, are displayed in Table 4.3 3

with individual sleep event accuracies shown in parenthesis. GOHMM method #2 used 100 *k*-means iterations and ten runs for each experiment code. Total classification performance did not exceed 38% for all experiments. Therefore, further exploration of the unsupervised GOHMM for normal/control subject and pre-Parkinsonian patient human sleep modeling were discontinued.

Classification results from GOHMM method #1, supervised GOHMM initialization, are displayed in Table 4.3. 4. Individual sleep event accuracies are shown in parenthesis. GOHMM results were compared to *k*-NN classification for comparison purposes. The highest classification accuracies for the GOHMM and *k*-NN classifier across each experiment code are shown in the "Total Accuracy" column. Cases where the GOHMM outperformed or displayed equal performance results compared to the *k*-NN classifier are shown in bold. Sleep event combination 1 displayed higher GOHMM accuracy results compared the *k*-NN classifier in the normal data sets for both the sf algorithm (74.064% GOHMM and 70.874% *k*-NN) and the b-PSO (67.129% GOHMM and 62.552% *k*-NN) algorithm. The *k*-NN classifier outperformed the GOHMM in all cases for sleep event combination 2. The binary particle swarm algorithm performed similar for both the GOHMM and the *k*-NN classifier for the normal data sets for sleep event combination 3.

Table 4.3 3: Classification results from 10 runs of the GOHMM using method #2 with 100 iterations of the *k*- means algorithm.

Exp. Code	Mean Unsupervised GOHMM Classification	Total Mean Accuracy	Standard Deviation
sbn1	S1(0),S2(30),S3&S4(20),REM(20),W(24.84)	25.34	31.86
sfab1	S1(0),S2(20),S3&S4(0),REM(10),W(17.48)	16.59	22.43
bpson1	S1(0),S2(30),S3&S4(20),REM(0),W(22.75)	23.11	24.97
bpab1	S1(0),S2(20),S3&S4(0),REM(0),W(16.29)	12.77	17.69
sfn2	S1&W(19.60),S2(20),S3&S4(30),REM(15.07)	21.14	22.59
sfab2	S1&W(21.49),S2(50),S3&S4(0),REM(30)	27.88	31.91
bpson2	S1&W(36.15),S2(10),S3&S4(10),REM(6.27)	18.47	15.92
bpab2	S1&W(37.84),S2(20),S3&S4(0),REM(20.29)	29.21	23
sbn3	W(20),S1&S2(36.07),S3&S4(30),REM(22.54)	30.37	19.87
sfab3	W(10.71),S1&S2(58.21),S3&S4(0),REM(19.99)	38.06	29.66
bpson3	W(28.02),S1&S2(19.25),S3&S4(20),REM(20.14)	20.57	22.26
bpab3	W(18.66),S1&S2(10.59),S3&S4(0),REM(21.98)	13.86	14.84

Table 4.3 4: GOHMM classification results using method #1 and *k*-NN classification.

Exp. Code	GOHMM Classification	Total Accuracy	*k*-NN Classification	Total Accuracy
sbn1	S1(6.06),S2(74.45), S3&S4(100.00), REM(98.59), W(43.96)	**74.064**	S1(15.15),S2(72.97), S3&S4(84.03), REM(49.29), W(81.32)	**70.874**
sfab1	S1(51.72),S2(50.44), S3&S4(100.00), REM(94.59), W(60.50)	60.784	S1(41.38),S2(77.41), S3&S4(6.06), REM(70.27), W(85.29)	74.74
bpson1	S1(3.03),S2(75.18), S3&S4(98.32), REM(50.70), W(26.37)	**67.129**	S1(15.15),S2(72.73), S3&S4(74.79), REM(12.68), W(57.14)	**62.552**
bpab1	S1(26.61),S2(30.22), S3&S4(.95.00), REM(82.72), W(13.10)	33.333	S1(34.48),S2(74.34), S3&S4(0.00), REM(55.86), W(91.59)	72.549
sfn2	W&S1(42.19),S2(73.95), S3&S4(100.00), REM(32.84)	64.556	W&S1(59.47),S2(92.45), S3&S4(69.59), REM(7.46)	71.333
sfab2	W&S1(81.98),S2(26.43), S3&S4(100.00), REM(92.23)	70.93	W&S1(82.70),S2(91.63), S3&S4(42.62), REM(67.96)	80.655
bpson2	W&S1(21.26),S2(73.96), S3&S4(99.32),REM(4.48)	55.333	W&S1(52.49),S2(98.69), S3&S4(38.51),REM(0.00)	66.00
bpab2	W&S1(25.22),S2(16.74), S3&S4(100.00), REM(88.35)	34.884	W&S1(83.42),S2(85.90), S3&S4(47.54), REM(75.73)	80.867
sbn3	W(84.54),S1&S2(66.32),S3&S4(100.00), REM(25.37)	73.00	W(73.43),S1&S2(89.54), S3&S4(78.38), REM(13.43)	78.33
sfab3	W(27.31),S1&S2(53.81), S3&S4(100.00), REM(99.09)	54.095	W(84.03),S1&S2(91.96), S3&S4(0.00), REM(83.78)	85.236
bpson3	W(34.07),S1&S2(78.64), S3&S4(98.32),REM(97.18)	**78.086**	W(65.93),S1&S2(81.36), S3&S4(81.51),REM(67.61)	**78.086**
bpab3	W(9.66),S1&S2(28.45), S3&S4(100.00),REM(92.79)	34.256	W(95.38),S1&S2(82.47), S3&S4(0.00),REM(72.97)	81.661

4.3.2 Age Matched Controls Gaussian Observation Hidden Markov Model Parameters

This section provides the GOHMM models parameters from method #1 that outperformed the *k*-NN classifier for the age matched control subjects. Tables 4.3.2 1-4.3.2 3 display the experiment code and sleep event combination numbers that

correspond to the GOHMM parameters. These tables addressed research question three (What GOHMM parameters should be used to best discriminate between control subjects and pre-Parkinsonian patients?) by providing the GOHMM parameters specific to normal/control subjects for sleep event combinations 1-3.

Table 4.3.2 1: GOHMM parameters for experiment sbn1.

Exp. Code	**Sleep Event Combination #**	**GOHMM Parameters**
sbn1	1	$A = \begin{bmatrix} .91709 & .032048 & 0 & 1.52e-25 & .050865 \\ .000407 & .94783 & .021687 & .0072859 & .022795 \\ 0 & .00564 & .96573 & 0 & .028708 \\ 7.96e-21 & .017932 & 0 & .96381 & .018256 \\ .1117 & .15372 & 0 & .035764 & .69882 \end{bmatrix}$ $p = \begin{bmatrix} 1 \\ 1.09e-97 \\ 2.5197e-322 \\ 4.54e-110 \\ 8.16e-9 \end{bmatrix}$ $\overline{m} = \begin{bmatrix} 1.2518 & .015677 & -1.2071 & .6508 & .64258 \\ .39908 & -.12738 & -.44312 & -.53631 & 1.8997 \end{bmatrix}$

Table 4.3.2 2: GOHMM parameters for experiment sfn2.

Exp. Code	**Sleep Event Combination #**	**GOHMM Parameters**
sfn2	2	$A = \begin{bmatrix} .75149 & .13585 & 3.15e-73 & .11266 \\ .03115 & .95293 & .010396 & .005522 \\ .012126 & .00404 & .98383 & 0 \\ .12946 & 0 & 0 & .87054 \end{bmatrix}$ $p = \begin{bmatrix} .000108 \\ 3.42e-213 \\ 0 \\ .99989 \end{bmatrix}$ $\overline{m} = \begin{bmatrix} .1667 & .421 & -.92303 & .42572 \\ 1.5893 & -.37023 & -.72083 & .67133 \\ 1.4912 & -.21158 & -.96959 & .79043 \\ .26128 & -.60856 & .64284 & .11808 \\ 1.4523 & -.28497 & -.42466 & -.24174 \end{bmatrix}$

Table 4.3.2 3: GOHMM parameters for experiment bpson3.

Exp. Code	**Sleep Event Combination #**	**GOHMM Parameters**
bpson3	3	$A = \begin{bmatrix} .53392 & .40982 & 0 & .056263 \\ .031994 & .94325 & .022213 & .002541 \\ .027771 & .01336 & .95887 & 0 \\ .033201 & .01485 & 0 & .95195 \end{bmatrix}$ $p = \begin{bmatrix} 6.85e-18 \\ 1 \\ 2.81e-109 \\ 1.04e-68 \end{bmatrix}$ $\bar{m} = \begin{bmatrix} -.09911 & .47063 & -.4427 & -.61642 \\ 1.9175 & -.15713 & -.16678 & -.13685 \\ -.06447 & .46654 & -.81749 & .37603 \\ -.5539 & .16492 & -.073 & -.028 \\ .22662 & -.14213 & .35704 & -.81974 \\ 2.3092 & .012195 & -.4751 & -.42684 \\ .5072 & -.37823 & .78734 & -1.273 \\ 2.1411 & .01709 & -.41296 & -.58407 \end{bmatrix}$

4.3.3 Pre-Parkinsonian Gaussian Observation Hidden Markov Model Parameters

This section provides the GOHMM models parameters from method #1 that outperformed the *k*-NN classifier for the pre-Parkinsonian patients. Tables 4.3.3 1-4.3.3 3 display the experiment code and sleep event combination number that corresponds to the GOHMM parameters. These tables addressed research question three (What GOHMM parameters should be used to best discriminate between control subjects and pre-Parkinsonian patients?) by providing the GOHMM parameters specific to pre-Parkinsonian patients for sleep event combinations 1-3.

Table 4.3.3 1: GOHMM parameters for experiment sfab1.

Exp. Code	Sleep Event Combination #	GOHMM Parameters
sfab1	1	$A = \begin{bmatrix} .78394 & .18927 & 0 & .006415 & .02037 \\ .077458 & .80736 & .086072 & 9.51e-37 & .029108 \\ 0 & .0302 & .9201 & 0 & .049705 \\ 2.20e-07 & 0 & 0 & .94438 & .055616 \\ .101081 & .033027 & 0 & .036588 & .82857 \end{bmatrix}$ $p = \begin{bmatrix} 2.12e-164 \\ 0 \\ 0 \\ 0 \\ 1 \end{bmatrix}$ $\overline{m} = \begin{bmatrix} -.57002 & .51797 & 1.1076 & -.41678 & -1.2544 \\ .041745 & -.30776 & -.90934 & 1.0264 & .86188 \\ 1.1097 & -.47838 & -.85257 & -.39116 & .92233 \\ .065345 & -.074827 & .15642 & -.40152 & -.00085 \\ .86907 & .54272 & -.23713 & -1.2762 & -.08373 \\ -.71206 & .31467 & 1.2655 & -.62355 & -.90777 \\ -.42748 & -.36432 & .41307 & .40666 & -.11442 \\ 1.0089 & -.44754 & -1.1128 & -.00955 & 1.0585 \end{bmatrix}$

Table 4.3.3 2: GOHMM parameters for experiment sfab2.

Exp. Code	**Sleep Event Combination #**	**GOHMM Parameters**
sfab2	2	$A = \begin{bmatrix} .90877 & .083755 & 0 & .007376 \\ .24525 & .70186 & .022273 & .030624 \\ .016695 & .0066504 & .97665 & 0 \\ .037286 & 0 & 0 & .96271 \end{bmatrix}$ $p = \begin{bmatrix} 1 \\ 1.10e-22 \\ 0 \\ 1.24e-295 \end{bmatrix}$ $\overline{m} = \begin{bmatrix} -.71402 & .64857 & 1.7381 & .15303 \\ .72934 & -.3127 & -1.7081 & -.44552 \\ .65437 & .29279 & -1.0693 & -1.0675 \end{bmatrix}$

Table 4.3.3 3: GOHMM parameters for experiment sfab3.

Exp. Code	Sleep Event Combination #	GOHMM Parameters
sfab3	3	$A = \begin{bmatrix} .36613 & .51782 & 0 & .11605 \\ .075502 & .83119 & .085812 & .007493 \\ .075295 & .00059486 & .92411 & 0 \\ .048801 & 1.37e-16 & 0 & .9512 \end{bmatrix}$ $p = \begin{bmatrix} 6.39e-97 \\ 5.55e-193 \\ 0 \\ 1 \end{bmatrix}$ $\overline{m} = \begin{bmatrix} -.54425 & .16457 & 1.0563 & -1.1082 \\ .84081 & -.12527 & .13652 & -.38271 \\ .56106 & .29117 & .085602 & -.49051 \\ -.47068 & -.1345 & 1.179 & -.96475 \\ .43891 & -.57773 & .322 & .006406 \end{bmatrix}$

4.4 ESAM Output

This section provides graphical displays of the ESAM sleep event classification output compared to the physician/technician labeling for the GOHMMs from method #1 presented in sections 4.3.2-4.3.3. Figures 4.4 1-4.4 6 display the hypnograms and Tables 4.4 4-4.4 9 show the corresponding confusion matrices (classification matches between the GOHMM and the physician/technician labeling are shown in bold). Tables 4.4 1-4.4 3 show the relationship between the sleep event and sleep event classification number displayed in Figures 4.4 1-4.4 6 for each sleep event combination.

Table 4.4 1: Relationship between sleep event and sleep event classification number for sleep event combination 1 (experiments sbn1 and sfab1).

Sleep Event	Sleep Event Classification Number
Stage 1	1
Stage 2	2
Stage 3 and Stage 4	3
REM	4
Wake	5

Table 4.4 2: Relationship between sleep event and sleep event classification number for sleep event combination 2 (experiments sfn2 and sfab2).

Sleep Event	**Sleep Event Classification Number**
Wake & Stage 1	1
Stage 2	2
Stage 3 and Stage 4	3
REM	4

Table 4.4 3: Relationship between sleep event and sleep event classification number for sleep event combination 3 (experiments bpson3 and sfab3).

Sleep Event	**Sleep Event Classification Number**
Wake	1
Stage 1 & Stage 2	2
Stage 3 and Stage 4	3
REM	4

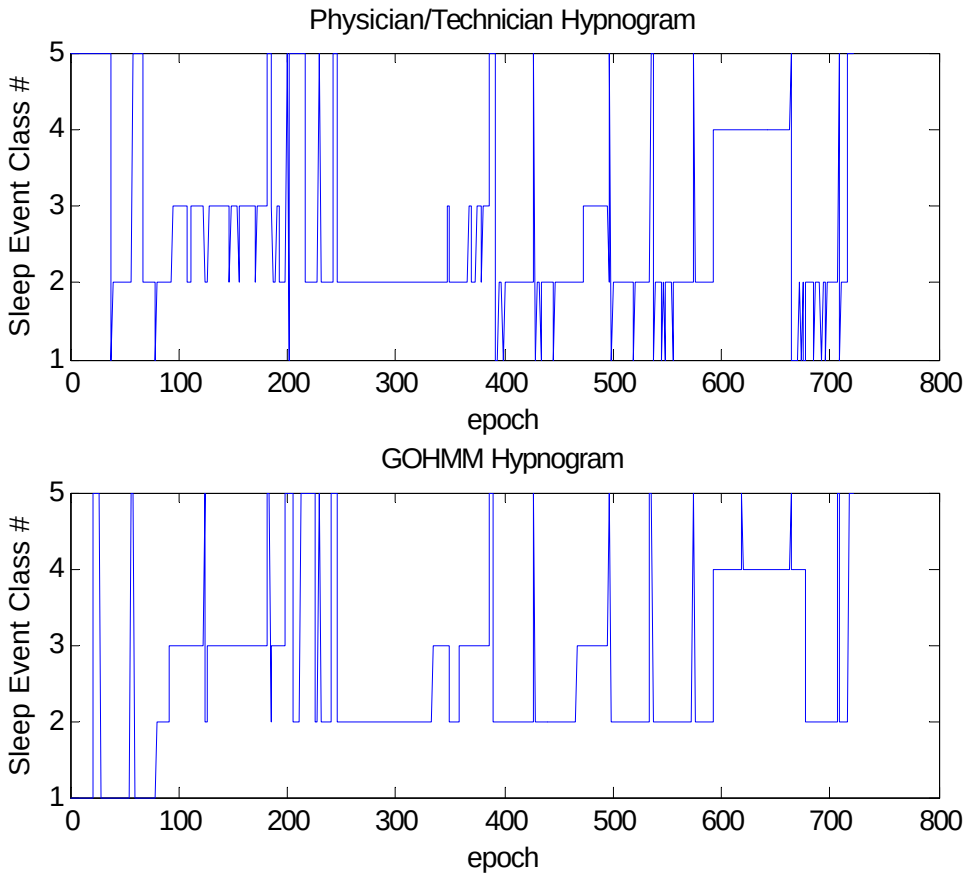

Figure 4.4 1: Hypnograms of GOHMM and physician/technician labeling for experiment sbn1.

Table 4.4 4: Confusion matrix of GOHMM and physician/technician labeling for experiment sbn1.

	GOHMM Labeling				
Technician/Physician Labels	1	2	3	4	5
1	**2**	20	0	10	1
2	28	**303**	54	3	19
3	0	0	**119**	0	0
4	0	0	0	**70**	1
5	40	11	0	0	**40**

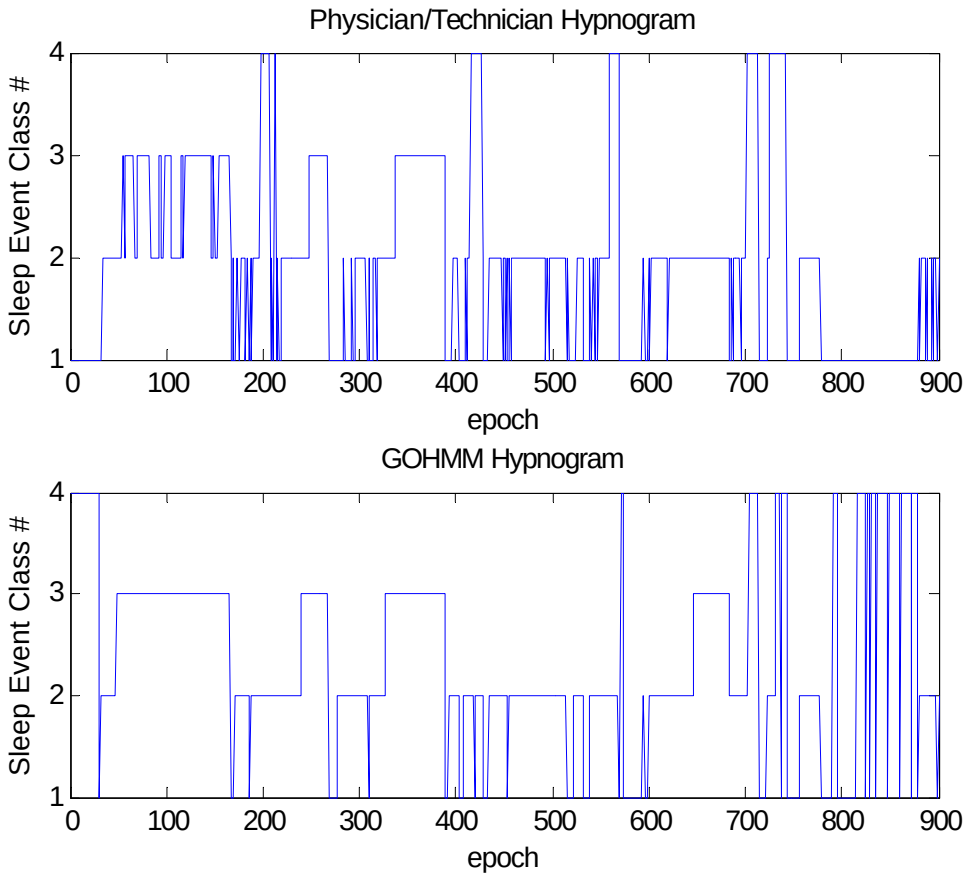

Figure 4.4 2: Hypnograms of GOHMM and physician/technician labeling for experiment sfn2.

Table 4.4 5: Confusion matrix of GOHMM and physician/technician labeling for experiment sfn2.

	GOHMM Labeling			
Technician/Physician Labels	1	2	3	4
1	**127**	77	0	97
2	3	**284**	97	0
3	0	0	**148**	0
4	3	42	0	**22**

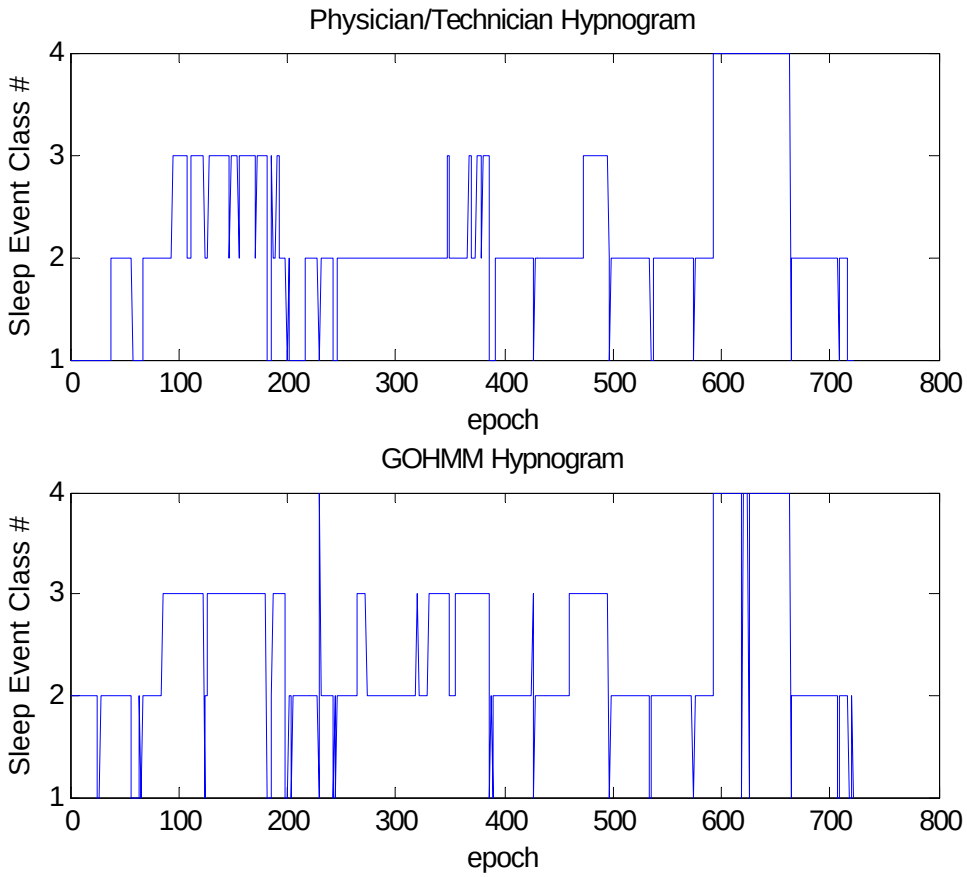

Figure 4.4 3: Hypnograms of GOHMM and physician/technician labeling for experiment bpson3.

Table 4.4 6: Confusion matrix of GOHMM and physician/technician labeling for experiment bpson3.

	GOHMM Labeling			
Technician/Physician Labels	1	2	3	4
1	**31**	59	0	1
2	7	**346**	87	0
3	1	1	**117**	0
4	2	0	0	**69**

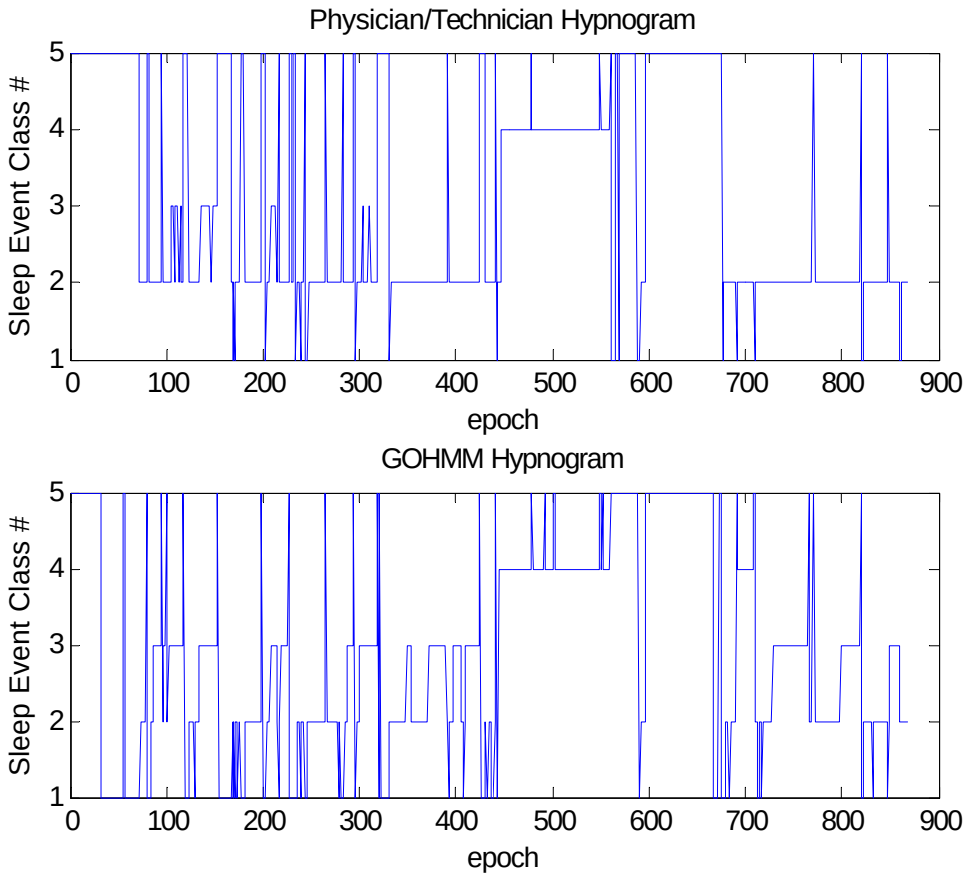

Figure 4.4 4: Hypnograms of GOHMM and physician/technician labeling for experiment sfab1.

Table 4.4 7: Confusion matrix of GOHMM and physician/technician labeling for experiment sfab1.

	GOHMM Labeling				
Technician/Physician Labels	1	2	3	4	5
1	**15**	4	0	0	10
2	32	**230**	169	20	5
3	0	0	**33**	0	0
4	0	0	0	**105**	6
5	93	1	0	0	**144**

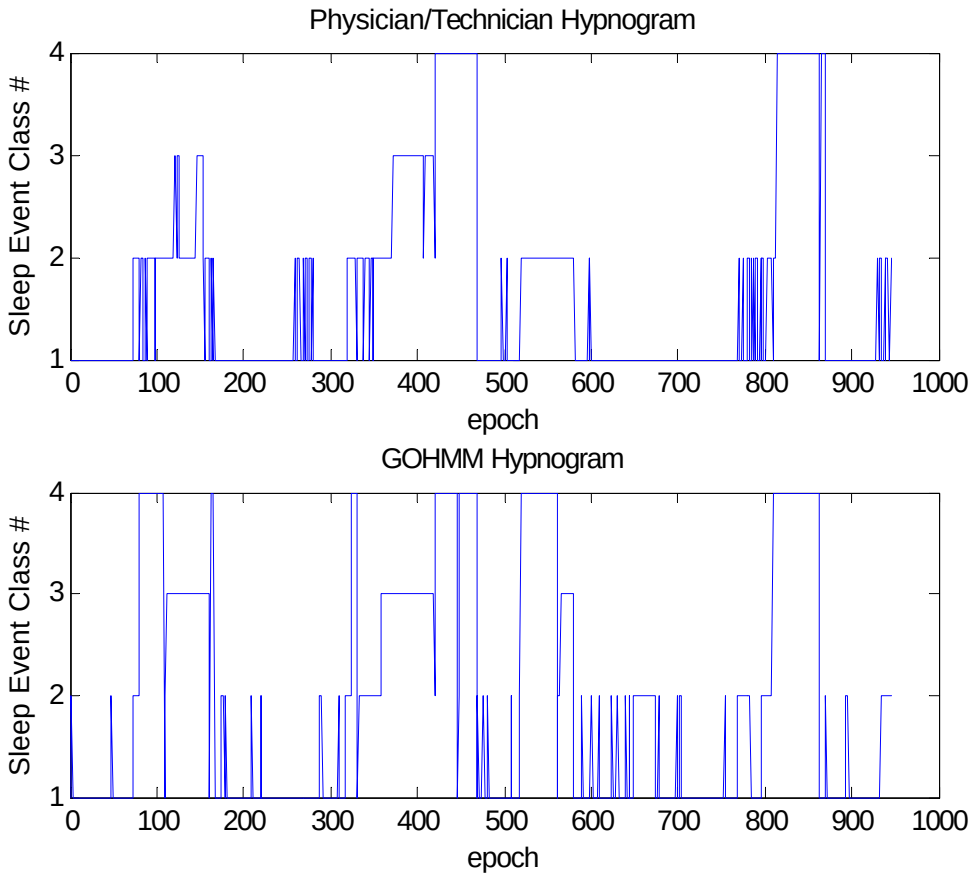

Figure 4.4 5: Hypnograms of GOHMM and physician/technician labeling for experiment sfab2.

Table 4.4 8: Confusion matrix of GOHMM and physician/technician labeling for experiment sfab2.

	GOHMM Labeling			
Technician/Physician Labels	1	2	3	4
1	**455**	90	1	9
2	26	**60**	63	78
3	0	0	**61**	0
4	7	1	0	**95**

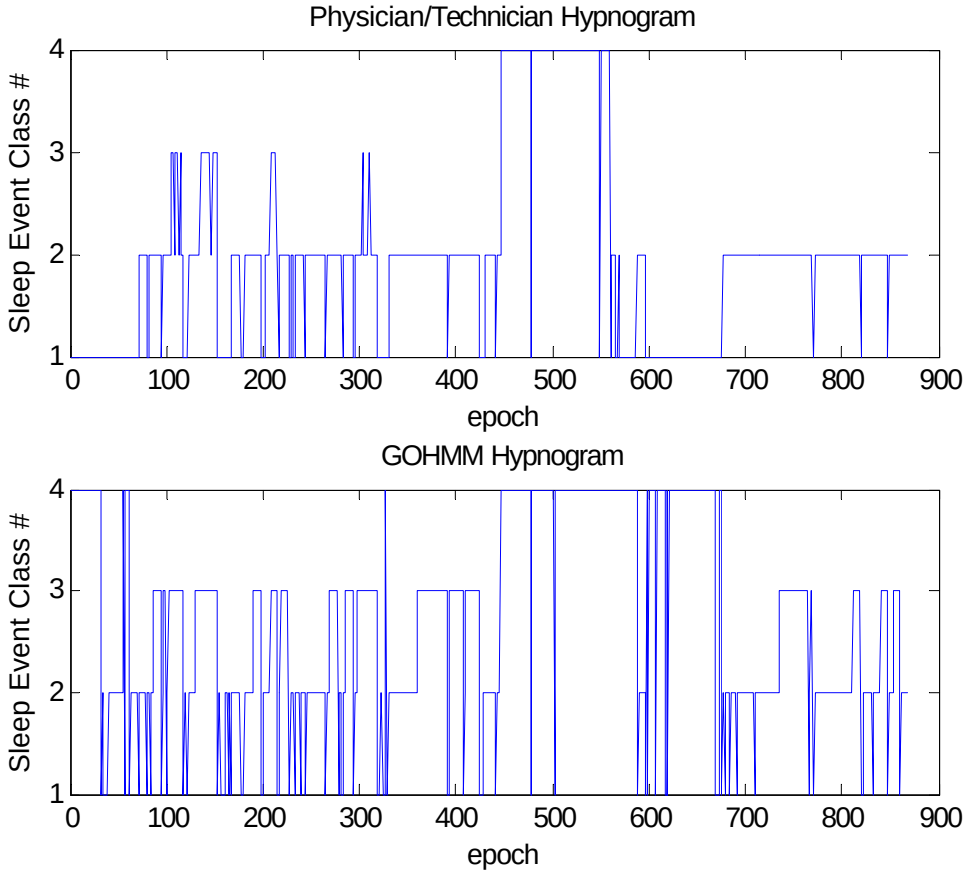

Figure 4.4 6: Hypnograms of GOHMM and physician/technician labeling for experiment sfab3.

Table 4.4 9: Confusion matrix of GOHMM and physician/technician labeling for experiment sfab3.

	GOHMM Labeling			
Technician/Physician Labels	1	2	3	4
1	**65**	45	0	128
2	21	**261**	195	8
3	0	0	**33**	0
4	1	0	0	**110**

4.5 Chapter Summary

This chapter provided quantitative results to address research questions two and three posed in section 1.3. In section 4.3.1 the quantitative features extracted from the psg to best describe the human sleep cycle were indicated providing insight on research question number two. Research question three was addressed in sections 4.3.2-4.3.3 by

providing the GOHMM parameters that represented the sleep cycles for the normal/control subjects and pre-Parkinsonian patients. Graphical illustrations and tables were provided in section 4.4 displaying ESAM performance using the selected feature subsets and GOHMM parameters. Interpretation of the presented results and a summary relating these findings to current sleep research are provided in Chapter 5.

CHAPTER 5: CONCLUSIONS

5.1 Chapter Introduction

This chapter presents four topics: the research study summary, research findings and their relation to the literature, study surprises, and study conclusions. Research conclusions specifically address implications for action and further research based upon results presented in Chapter 4.

5.2 Study Summary

5.2.1 Problem Overview

The main objective of this work was the development of a computer-based ESAM to aid sleep care physicians in the diagnosis of Pre-Parkinson's disease symptoms utilizing psg data. ESAM displays significant promise in streamlining the analysis of the human sleep cycle to aid physicians in the identification, treatment, and prediction of sleep disorders.

In this work four aspects of computer-based human sleep analysis were investigated that included psg interpretation, pre-processing, sleep event classification and abnormal sleep detection. In Chapter 2 a review of previous developments in these four areas were provided along with their relationship to the establishment of ESAM.

The technical approach in this work used psgs of control subjects and pre-Parkinsonian disease patients obtained from the ECDC as inputs into ESAM. The engineering tools employed during the development of ESAM included the GSVD, sequential forward and backward feature selection algorithms, the b-PSO algorithm, *k*-NN classification, and GOHMM. Details regarding the specific implementation and

methodology behind these engineering and statistical analysis tools were provided in Chapter 3. Experimental results obtained from the methodology implemented in Chapter 3 were provided in Chapter 4.

Contributions of this work included a methodology for automatic removal/compensation of specific artifacts within the human psg, quantitative based feature sub-sets for sleep event classification, and human sleep models representing pre-Parkinsonian disease patients and normal age matched control subjects. The contributions from this work are significant in understanding the human sleep cycle and aiding physicians in the identification, treatment, and prediction of sleep disorders.

5.2.2 Statement of Purpose and Research Questions

Quantitative sleep methodologies have been difficult to establish since sleep has been traditionally defined with quantitatively ambiguous rules. The goal of this study was to bypass the need for ambiguous rule use in sleep analysis by establishing a computer-based expert decision system built upon sleep physician knowledge and a quantitative methodology.

This study contained three aims to meet the established research goal. Aim one was the development of an automated computer-based artifact removal/compensation methodology for specific artifacts within human psgs. The second aim involved the development of a quantitative computer-based sleep model based on human psgs. The third and final aim was the application of the quantitative sleep model obtained in aim two towards a clinically relevant sleep problem.

5.2.3 Methodology Review

An illustration of the methodology used in ESAM to meet the three aims described in section 5.2.2 is provided in Figure 5.2 3 1(module #1 reprinted with the author's permission [1]). The five module process implemented in ESAM is described in the bulleted list below:

- **MODULE#1**: Psg data collection, for both control subjects and pre-Parkinsonian disease patients, conducted at ECSDC
- **MODULE#2**: Pre-processing of psg data using noise reduction/artifact removal methods that include band-pass filtering and the GSVD
- **MODULE#3**: Psg processing window selection and feature extraction with window selection obtained from physician consultation and feature extraction conducted using sequential forward and backward feature selection algorithms, b-PSO algorithm, and *k*-Nearest Neighbor classification.
- **MODULE#4**: Sleep stage classification implemented using GOHMM's constructed for both control subjects and pre-Parkinsonian disease patients
- **MODULE#5**: Expert prior knowledge of the human sleep cycle provided by the sleep physician to enhance ESAM performance

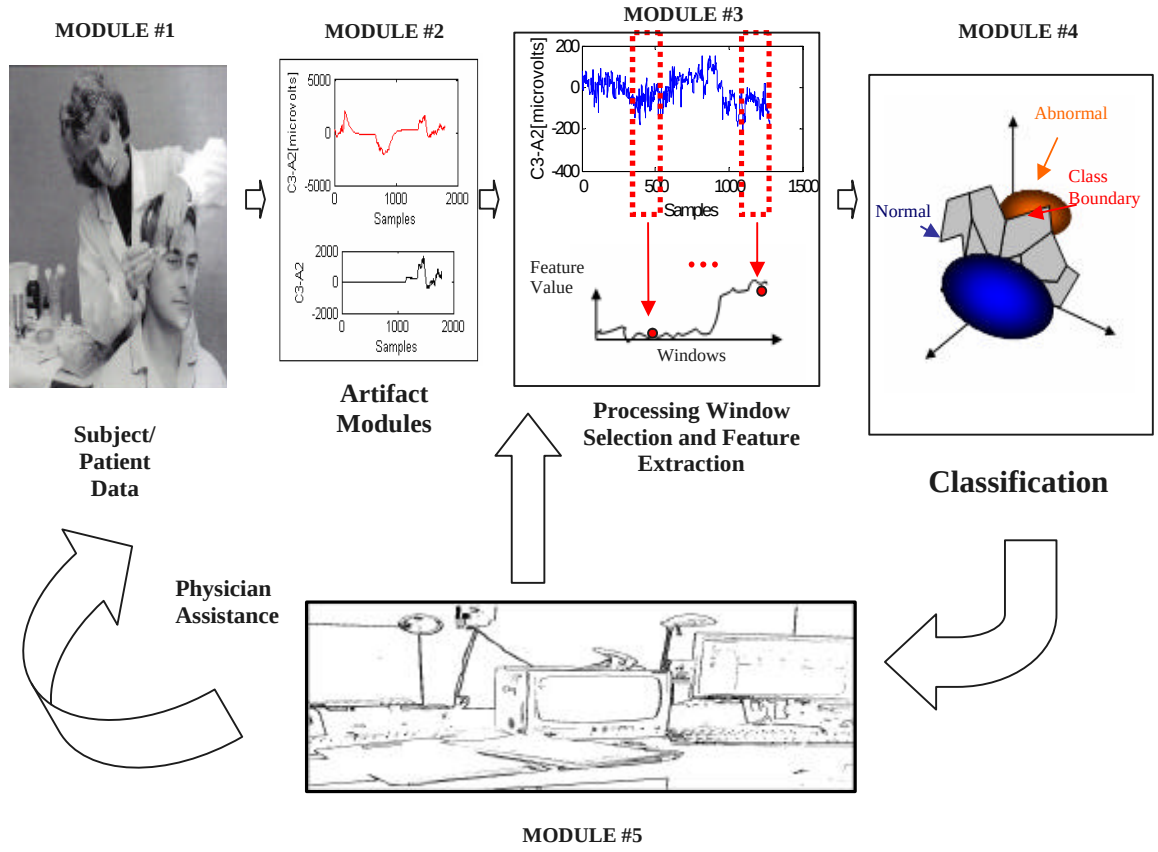

Figure 5.2.3 1: Illustration of the expert sleep analysis methodology (ESAM).

5.2.4 Major Findings

A brief overview of the major study findings entitled *Study Overview* are provided in this section. This overview is followed by two sub sections entitled *Study Contrast and Contributions compared to Previous Works* and *Study Relationships with the Literature*. The subsection entitled *Study Contrast and Contributions compared to Previous Works* was explored by answering the following questions:

**What are the differences between this study and previous studies?*

**How does this study contribute to the current knowledge base?*

Questions investigated in the subsection entitled *Study Relationships with the Literature* included:

**How do the study findings compare with those in the literature?*

** How do these results fit or not fit into the findings of previous studies?*

**Do these findings have any special importance, either as improvements on previous findings or in breaking new ground?*

The questions explored in both subsections were adapted from Roberts[78].

Study Overview

This study presented a methodology to aid physicians in the analysis of psg data for the diagnosis of patient's with Pre-Parkinson's disease symptoms. The primary areas of investigation in this study included preprocessing techniques, and feature and model selection. Pre-processing techniques were conducted to eliminate and compensate for artifacts within the human polysomnogram data sets as presented in section 3.6.1. Feature and model selection experiments were conducted on the psg data sets across three types of sleep cycle combinations as described in section 4.2.2.

The pre-processing methodology presented in this study addressed 50Hz and 60 Hz line power absorption, EPM activity, and SI artifact removal/compensation. Automated methods were presented using excessive amplitude detection, band pass filtering, and GSVD processing for artifact removal/compensation. Visual inspection

methods showed that the presented artifact removal/compensation methods were efficient in removing/compensating for the artifacts of interest.

The analysis of feature selection results showed highest performance ratings for sleep event combination three across all feature selection techniques for both normal/control subject and pre-Parkinsonian patient data. Performance ratings for sleep event combination one were the lowest across all feature selection techniques for both normal/control subject and pre-Parkinsonian patient data. Sequential forward and backward feature selection algorithms out performed the proposed b-PSO algorithm for sleep event combination two for the normal/control subject data with 95% statistical confidence.

The analysis of model selection results showed that the normal/control subject GOHMM performed best in sleep combination three using the b-PSO selected features. pre-Parkinsonian patient data analysis showed highest GOHMM performance results for sleep combination two using the sf selected features.

Study Contrast and Contributions compared to Previous Works

What are the differences between this study and previous studies?

This study was innovative via the automated application of the GSVD algorithm for psg artifact compensation and the b-PSO algorithm for feature selection in human sleep cycle analysis along with the investigation of the presented sleep cycle combinations. To the author's knowledge no other study has presented findings regarding the investigation of the automated use of the GSVD algorithm for artifact compensation and the b-PSO algorithm for feature selection in human psg analysis.

Again, to the author's knowledge, the literature does not indicate other study findings investigating human sleep analysis using the defined sleep cycle combinations.

How does this study contribute to the current knowledge base?

Contributions of this study include: the automated application of the GSVD algorithm for artifact compensation; the b-PSO algorithm for feature selection in human sleep cycle analysis; and the examination of the proposed sleep cycle combinations.

Study Relationships with the Literature

How do the study findings compare with those in the literature?

Two study findings can be directly related to the literature. The two findings of interest included the most selected features across feature selection experiments and the sleep cycle combination investigation results. Both findings are addressed in the order presented.

Table 5.2.4 1 displays the top eleven features chosen across all feature selection experiments. Zoubek found using sequential forward feature selection that the top seven relevant features for normal human psg analysis to include: Beta Power-EEG, Entropy-EMG, Sigma Power-EEG, Entropy-EOG, Alpha Power-EEG, and Delta Power-EEG [35]. Two of Zoubek's selected features were found to be in the top eleven features selected in this study and are shown highlighted in gray in Table 5.2.4 1. Alpha-EEG and Entropy-EEG, included in Zoubek's top seven features, were only selected twice during the features selection experiments in this study, hence their exclusion from the top eleven selected features Table 5.2.4 1.

Table 5.2.4 1: A table of the top eleven features chosen across all feature selection experiments.

Feature #	Feature Name	Channel	# of Selections
1	Delta Power	EEG	5
5	Beta Power	EEG	5
36	Mobility	EEG	5
41	Complexity	EOG/R	5
50	Mean Absolute Amplitude	EMG/CHIN	4
2	Theta Power	EEG	3
11	Spectral Edge Frequency	EMG/RL	3
38	Mobility	EMG/CHIN	3
40	Complexity	EEG	3
45	Curve Length	EOG/R	3
56	Zero Crossing	EEG	3

Other relevant findings included low feature selection performance results (across all feature selection experiments) for sleep event combination one (67.261% ± 6.629%), the classical definition of sleep, compared to that of sleep event combinations two and three (77.771% ± 6.201%) for both normal/control subjects and pre-Parkinsonian patients. These findings agreed with the results in the literature which indicated problems in the classical approach for the identification of sleep stage 1[9].

How do these results fit or not fit into the findings of previous studies?

The importance of the Delta-EEG and Beta-EEG features, for normal psg analysis, found in this study fit within the findings of Zoubek's work.

Low feature selection performance results for sleep event combination one fits in the works of Whitney and Kubicki which noted application of the classical human sleep cycle toward the identification of stage 1 sleep may hinder optimal sleep analysis[9, 10].

Do these findings have any special importance, either as improvements on previous findings or in breaking new ground?

The labeling of Delta-EEG and Beta-EEG as highly relevant features show importance in normal/control subject human sleep analysis and pre-Parkinsonian patient analysis. This is the first, to the author's knowledge, in depth analysis validating Delta-EEG and Beta-EEG features as significant quantitative features in pre-Parkinsonian human sleep analysis have not been conducted. Results from this study break new ground in establishing the importance of these features in pre-Parkinsonian human sleep analysis.

Investigation of varying sleep cycle combinations are of special importance in breaking new ground toward the identification of new perspectives on pathological human sleep cycle analysis. The quantitative results displayed in this study offer promising perspectives regarding sleep classification for both normal/control subjects and pre-Parkinsonian patients. Features obtained in this study may be utilized as benchmarking tools for the discrimination of pre-Parkinsonism symptoms from normal sleep characteristics in future psg analysis studies.

5.3 Study Surprises

Surprisingly the GOHMM classification rate, in experiment sbn1, for sleep cycle combination one (74.064%) were higher than that of the GOHMM classification rate, in experiment sfn2, for sleep cycle combination two (64.556%). This observation was not found in the *k*-NN classification. The observation of the higher GOHMM classification rate for experiment sbn1 may be due to the GOHMM, in experiment sfn2, inefficiently classifying 32% of the Wake&S1 epochs as REM epochs. This surprise observation may also be contributed to the inability of the GOHMM to efficiently characterize REM sleep

with a small number of S1 epochs in the training data set (B). It should be noted that the training data set (B) for experiment sfn2 contained the lowest number of S1 epochs (91) when compared to the other training datasets (A; C-F). This surprise observation displays the limitations of the GOHMM with respect to training data set size for sleep classification when compared to the *k*-NN classifier. Suggestions to possibly correct for this observation are provided in section 5.4.2.

5.4 Study Conclusions

5.4.1 Implications for Action

Based on findings from this study the following recommendations are suggested to make ESAM more accessible and significant to the sleep research community:

- Implementation of a graphical user interface (GUI) encapsulating the pre-processing, feature selection, and sleep modeling methods presented in this study
- The facilitation of clinical setting tests of the GUI using sleep practitioners and researchers to obtain feedback on the relevance of ESAM in clinical applications

5.4.2 Recommendations for Further Research

Recommendations for improvements of this study and future studies based upon this work and how they might contribute to the field are discussed in this section. Three recommendations are suggested to improve this study and further explore the presented work. The recommendations include large data studies, b-PSO *k*-NN implementation optimization, and model based sleep illness prediction.

A major limitation in this work included the polysomnogram data set size. The small data set size of normal/control subject data (3) and pre-Parkinsonian patient data (3) prevented an in-depth validation of the GOHMMs implemented. According to Becq et al. in order to eliminate classifier bias a minimum training data set size of 500 samples/epochs should be used for each classification label [79]. This information should be considered in the further development of training data sets for ESAM. Adherence to the training data set criteria established by Becq et al. might prevent study surprises such as those encountered in section 5.3. Therefore, large size data studies containing training data sets greater than or equal to 500 epochs for each classification label are recommended as a future work.

In this study the optimal sub-set feature selection performance of the b-PSO algorithm (66.793%±9.875%) compared to the sequential feature selection algorithms (72.245%±7.083%) was extremely low. The low performance rate of the b-PSO algorithm may be due to the lack of a rigorous survey of the optimal b-PSO parameters. Increased computational costs of using the b-PSO coupled with the *k*-NN classifier as a fitness function prevented a rigorous survey of the optimal b-PSO parameters. Since normality could not be assumed with the data sets in this study other classifiers that offered improved computational speed such as the linear and quadratic discriminant classifiers were not applicable. Another future work for this study includes using efficient machine learning routines in open source programs such FASTlib to improve *k*-NN classifier computational speed [80]. Increased *k*-NN classifier computational speed will permit a rigorous survey of the optimal b-PSO parameters for optimal sub-set feature selection.

An aim of this study was the formulation of GOHMM models for normal/control subjects and pre-Parkinsonian patients. As a future work the normal/control and pre-Parkinsonian prediction rates for the models should be tested using a large size data set. Information from these tests will provide insight on the relevance of ESAM as a sleep illness diagnostic aid in clinical applications.

5.4.3 Concluding Remarks

The main objective of this work to develop a computer-based ESAM to aid sleep care physicians in the diagnosis of pre-Parkinson's disease symptoms using polysomnogram data has been met. Contributions of this work included a methodology for automatic removal/compensation of specific artifacts within the human polysomnogram, a quantitative based feature library for sleep event classification, and sleep models representing pre-Parkinsonian disease patients and normal age matched control subjects.

The results presented in this study provided a quantitative methodology for stream-lining the analysis of the human sleep cycle to aid physicians in the identification, treatment, and prediction of sleep disorders. Implications for action and future works were recommended to make ESAM more accessible and significant to the sleep research community.

It is the author's hope that sharing the results from this study will advance the field of sleep research and aid physicians to better assist patients suffering from sleep pathologies that hinder their quality of life.

APPENDIX A

A.1 *k*-NN Methodology

The primary basis of the k-NN algorithm is that similar observations belong to similar classes. This algorithm is an extension of the nearest neighbor rule. The number of nearest neighbors was selected by setting the value of k. Classification occurred when observations, ***x***, were inputted into the algorithm and corresponding class labels, *c*, of the k nearest neighbor, ***x'***, were outputted. The observations of interest were features extracted from the psg.

The nearest neighbor was selected by calculating the Euclidean distance. For example, let **x** and **y** be **d**-dimensional vectors. So, the distance from a point in **x** to **y** using the Euclidean distance (*d*) was expressed as

$$d(\mathbf{x}, \mathbf{y}) = ((\mathbf{x}- \mathbf{y})^{\mathrm{T}}(\mathbf{x}- \mathbf{y}))^{1/2}, \qquad \text{(A.1)}$$

where superscript T represented the transpose operation.

The k-NN algorithm consisted of two phases: training and testing. Feature values and corresponding class labels of the data were stored to create the training set. Classification of features with unknown class labels were obtained during the testing phase. Testing was implemented when the k-NN algorithm searched for the nearest k values to the unknown data within the training data with respect to the testing data.

A simple graphical representation of the testing process for "Stage 2" and "REM" sleep classification is displayed in Figure A.1 1. In this illustration k equaled five nearest neighbor candidates. The training set is shown by the red and black circles. The feature with an unknown class label is shown by the white circle and labeled with a question mark. Connecting lines represent the Euclidean distance from the feature to nearest

neighbor candidates. In this example the unknown value fell within the "Stage 2" sleep category and the *k*-NN classifier labeled the unknown data segment as "Stage 2" sleep.

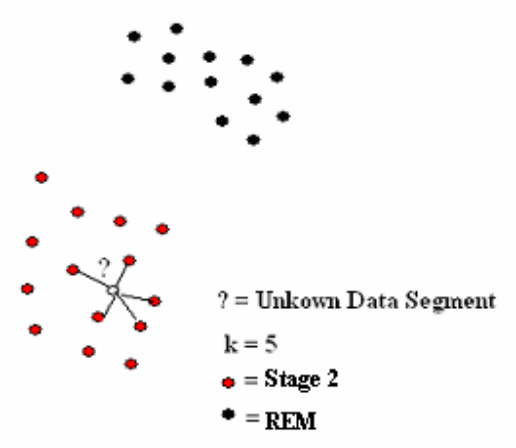

Figure A.1 1: Illustration of the testing processes for the *k*-NN classifier.

A.2 Roulette Wheel Selection Methodology

Roulette wheel selection is a proportional selection routine that focuses on selecting the most-fit individuals, in our case features, in a population based on the sampling distribution of the data set. Roulette wheel selection was defined by the following fitness expression[65]:

$$P_s(x_i) = \frac{f(x_i)}{\sum_{j=1}^{n_p} f(x_j)}, \qquad \text{(A.2)}$$

where n_p was the total number of individuals (features) in the population, and $P_s(x_i)$ was the probability that x_i , a particular feature, would be selected. The probability distribution may be viewed as a roulette wheel with the size of each roulette slice proportional to the normalized selection probability value of each individual/feature. Selection may be viewed as spinning the roulette wheel and recording the

individual/feature corresponding to the selected slice. Individual/feature fitness was directly proportional to selection probability ensuring that optimal individuals/features were more likely to be selected.

A.3 *k*-Means Methodology

The k-Means clustering algorithm is a commonly used unsupervised learning algorithm for the classification of a given data set into a pre-defined set of k clusters[63]. Centroids were defined for each cluster based upon a distance metric, in our case we utilized the squared Euclidean distance, and the following objective function, $J(q,U)$, was minimized

$$J(q,U) = \sum_{i=1}^{N}\sum_{j=1}^{m} u_{ij}\left\|x_i - q_j\right\|^2, \qquad \text{(A.3)}$$

where, u_{ij} was a membership function such that each data point i=1,2,…N was classified as belonging to any j=1,2,…m clusters, and $\left\|x_i - q_j\right\|^2$ represented the squared Euclidean distance between the data point x_i and the cluster center q_j for the N data points and their respective m cluster centers. The k-Means algorithm was executed as follows:

1) *K cluster points/centroids were defined representing the initial cluster centers based upon the sleep event combination number.*
2) *Each data point/epoch was assigned to a cluster based on the closest cluster centroid/mean cluster value.*
3) *The positions of the K cluster centroids/mean cluster values were recalculated based on the new cluster classifications.*
4) *Steps 2 and 3 were repeated until the cluster centroids did not change.*

5) *The cluster centroid values that minimized the objective function $J(q, U)$ were used to calculate the initial parameters of the GOHMM.*

APPENDIX B

B.1 Sequential Feature Selection Search Spaces

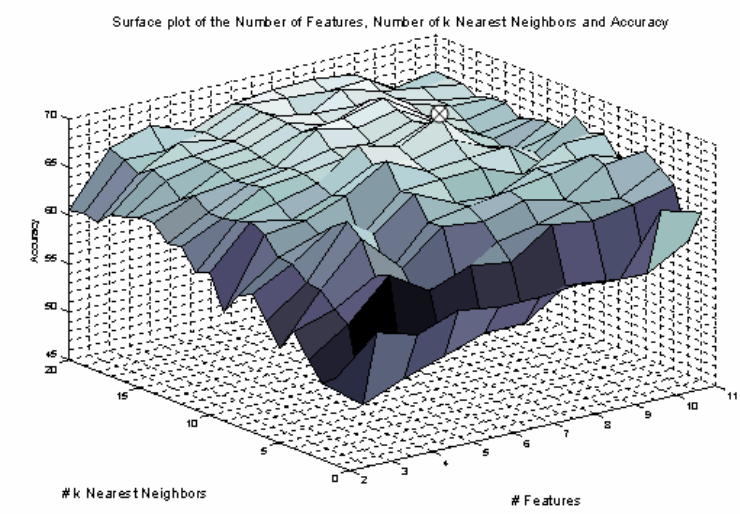

Figure B.1 1: Surface plot of the search space for data set B and sleep event combination 1 using the sequential backward algorithm to obtain the maximum classification accuracy across *k*-NN values and feature subset amount.

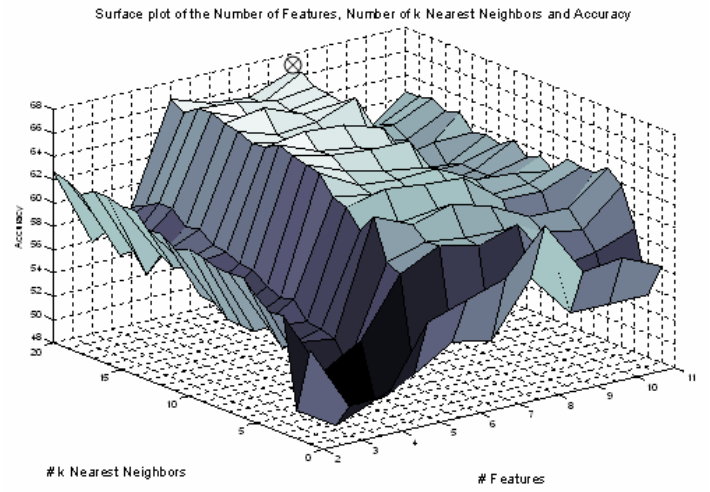

Figure B.1 2: Surface plot of the search space for data set B and sleep event combination 1 using the sequential forward algorithm to obtain the maximum classification accuracy across *k*-NN values and feature subset amount.

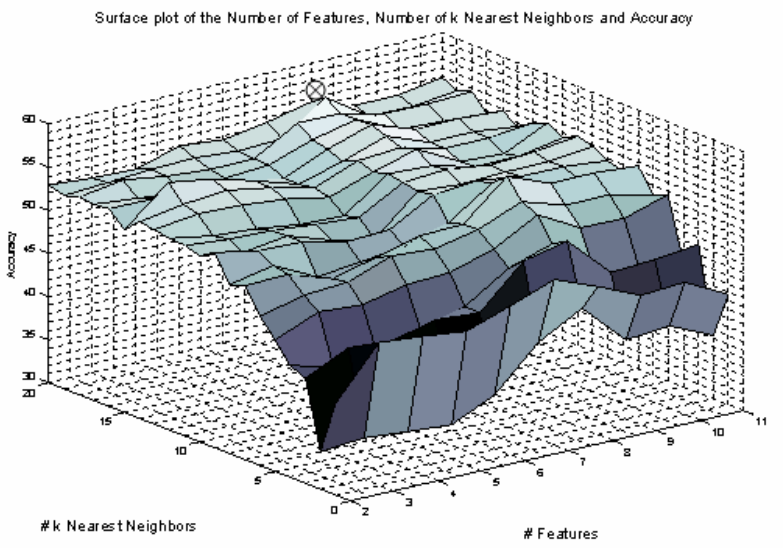

Figure B.1 3: Surface plot of the search space for data set C and sleep event combination 1 using the sequential backward algorithm to obtain the maximum classification accuracy across *k*-NN values and feature subset amount.

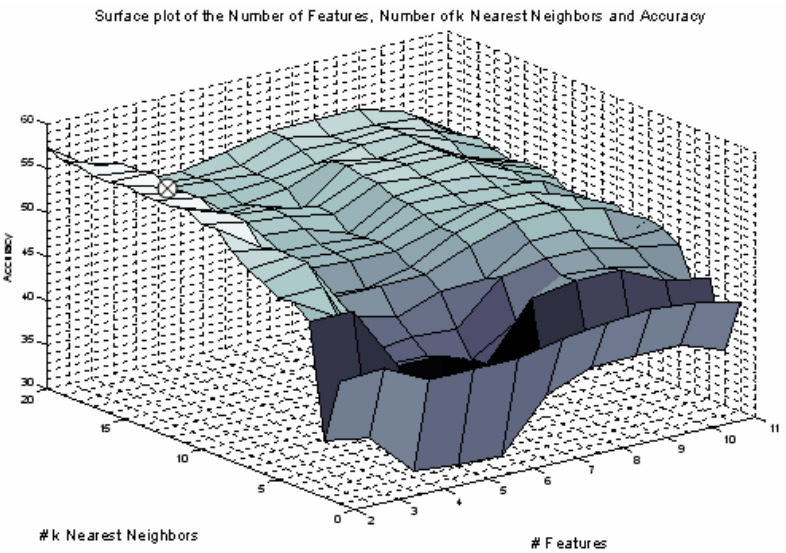

Figure B.1 4: Surface plot of the search space for data set C and sleep event combination 1 using the sequential forward algorithm to obtain the maximum classification accuracy across *k*-NN values and feature subset amount.

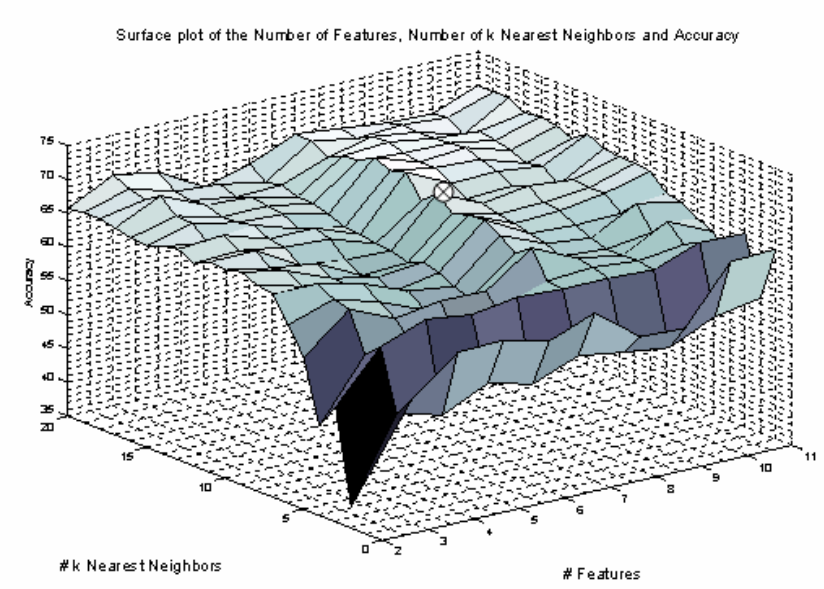

Figure B.1 5: Surface plot of the search space for data set A and sleep event combination 2 using the sequential backward algorithm to obtain the maximum classification accuracy across *k*-NN values and feature subset amount.

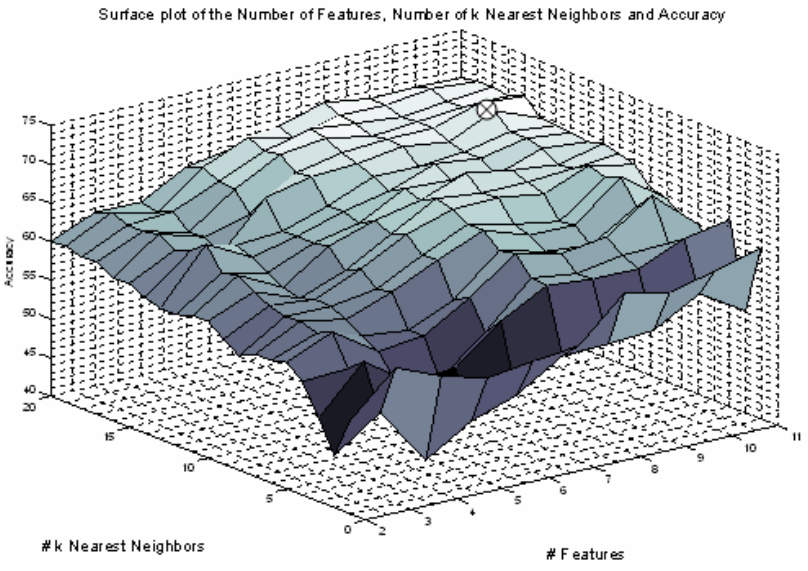

Figure B.1 6: Surface plot of the search space for data set A and sleep event combination 2 using the sequential forward algorithm to obtain the maximum classification accuracy across *k*-NN values and feature subset amount.

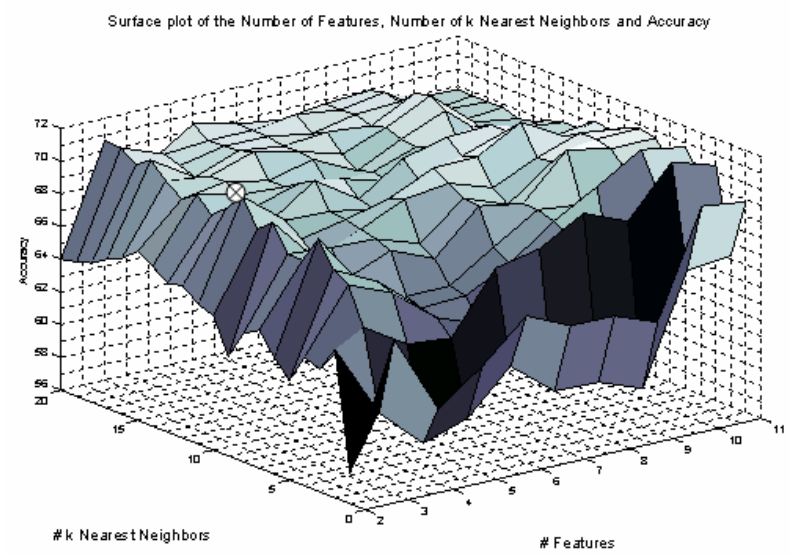

Figure B.1 7: Surface plot of the search space for data set B and sleep event combination 2 using the sequential backward algorithm to obtain the maximum classification accuracy across *k*-NN values and feature subset amount.

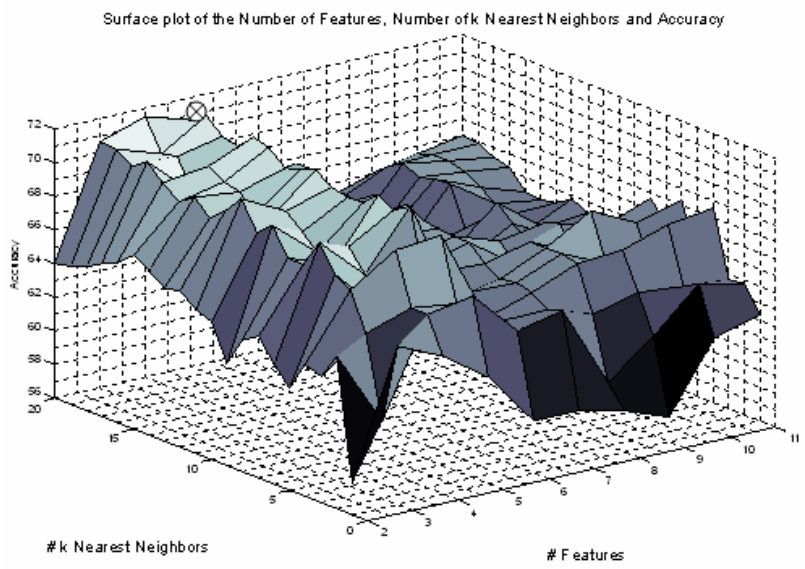

Figure B.1 8: Surface plot of the search space for data set B and sleep event combination 2 using the sequential forward algorithm to obtain the maximum classification accuracy across *k*-NN values and feature subset amount.

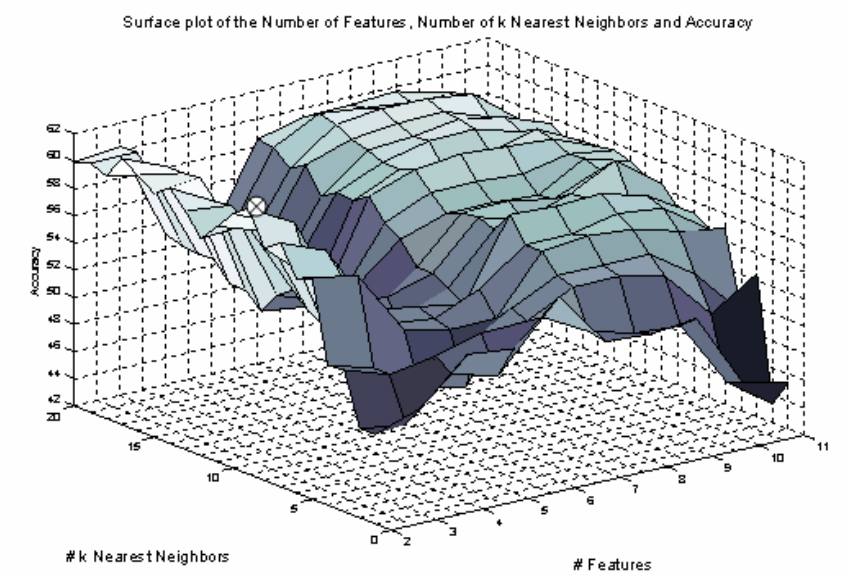

Figure B.1 9: Surface plot of the search space for data set C and sleep event combination 2 using the sequential backward algorithm to obtain the maximum classification accuracy across *k*-NN values and feature subset amount.

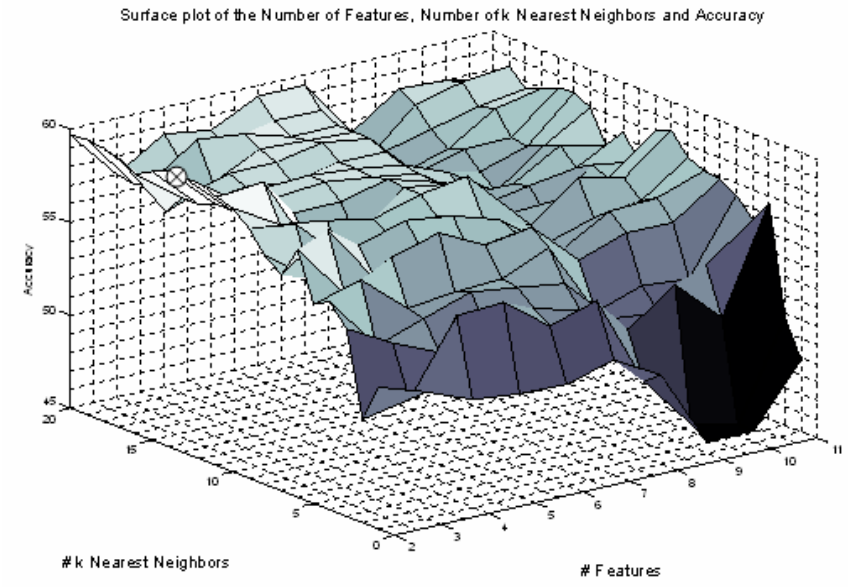

Figure B.1 10: Surface plot of the search space for data set C and sleep event combination 2 using the sequential forward algorithm to obtain the maximum classification accuracy across *k*-NN values and feature subset amount.

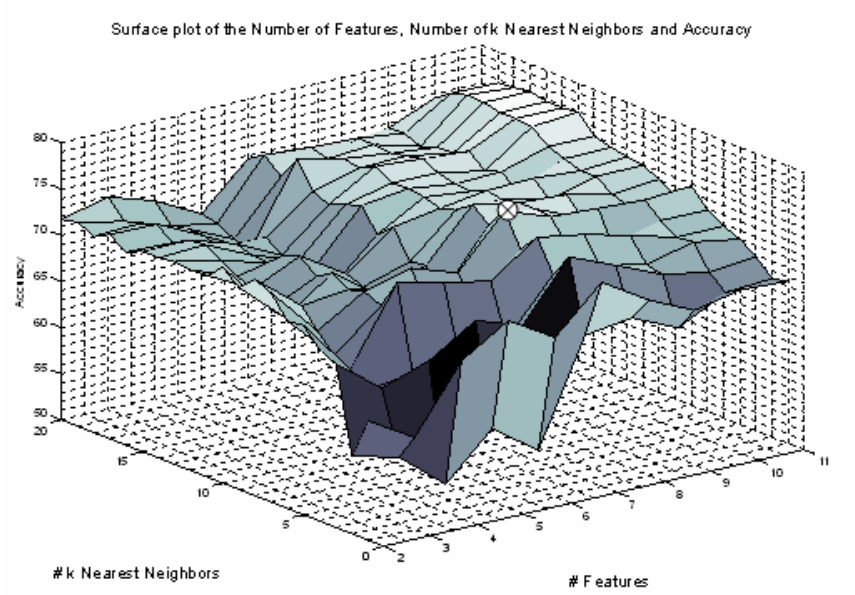

Figure B.1 11: Surface plot of the search space for data set A and sleep event combination 3 using the sequential backward algorithm to obtain the maximum classification accuracy across *k*-NN values and feature subset amount.

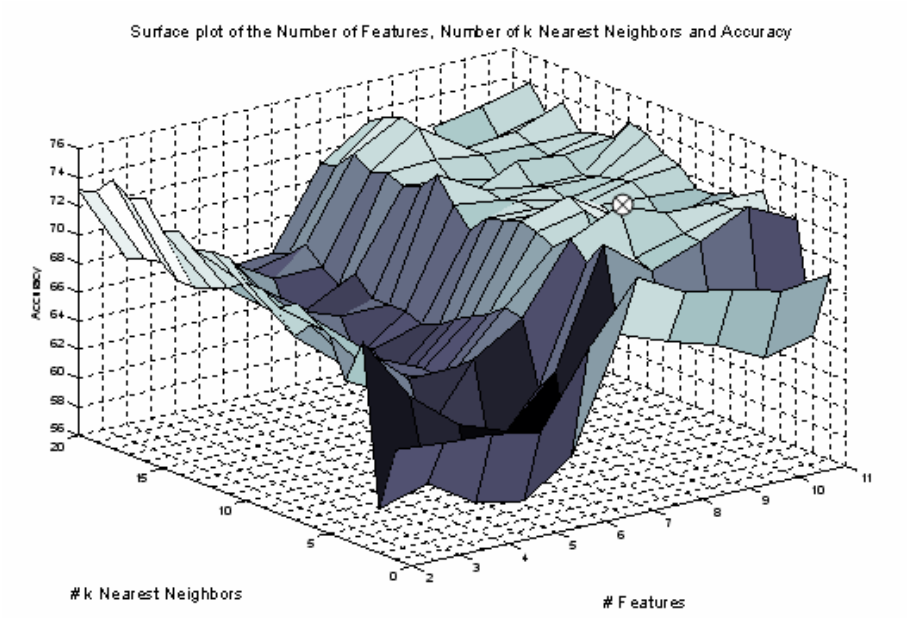

Figure B.1 12: Surface plot of the search space for data set A and sleep event combination 3 using the sequential forward algorithm to obtain the maximum classification accuracy across *k*-NN values and feature subset amount.

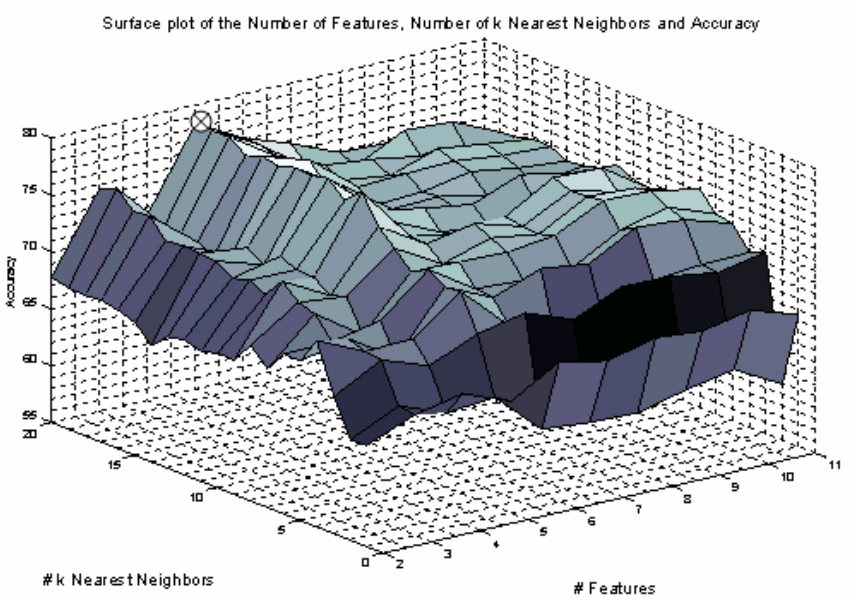

Figure B.1 13: Surface plot of the search space for data set B and sleep event combination 3 using the sequential backward algorithm to obtain the maximum classification accuracy across *k*-NN values and feature subset amount.

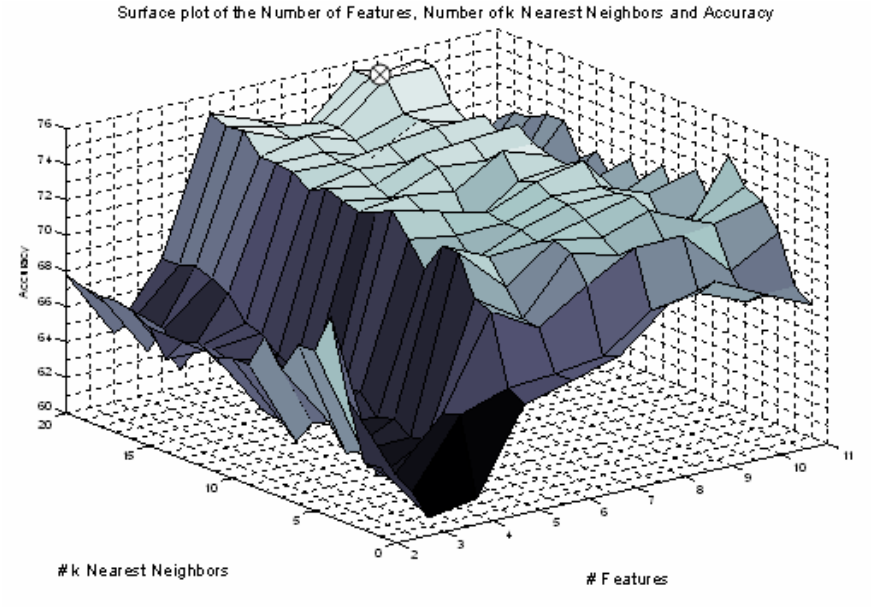

Figure B.1 14: Surface plot of the search space for data set B and sleep event combination 3 using the sequential forward algorithm to obtain the maximum classification accuracy across *k*-NN values and feature subset amount.

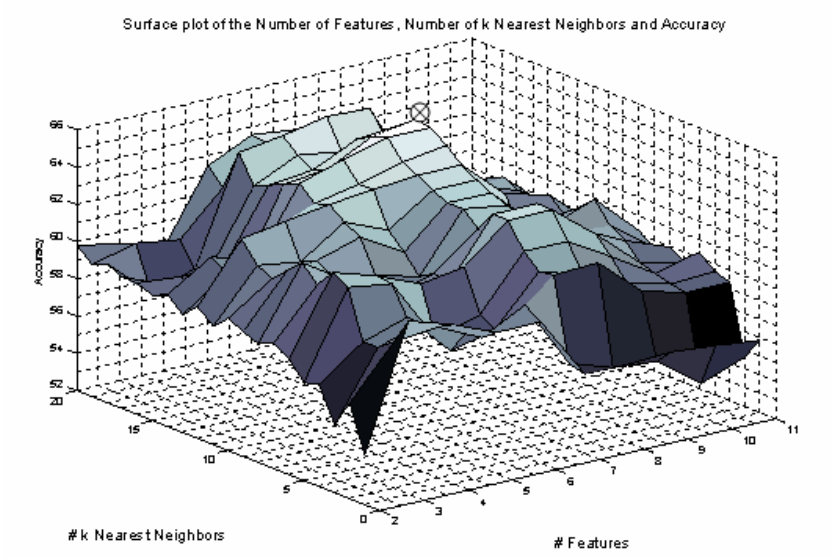

Figure B.1 15: Surface plot of the search space for data set C and sleep event combination 3 using the sequential backward algorithm to obtain the maximum classification accuracy across *k*-NN values and feature subset amount.

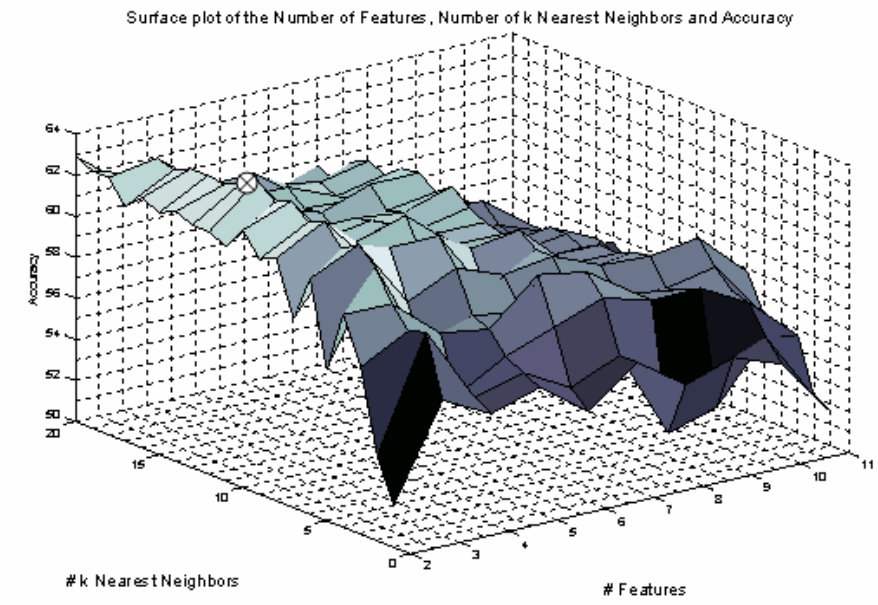

Figure B.1 16: Surface plot of the search space for data set C and sleep event combination 3 using the sequential forward algorithm to obtain the maximum classification accuracy across *k*-NN values and feature subset amount.

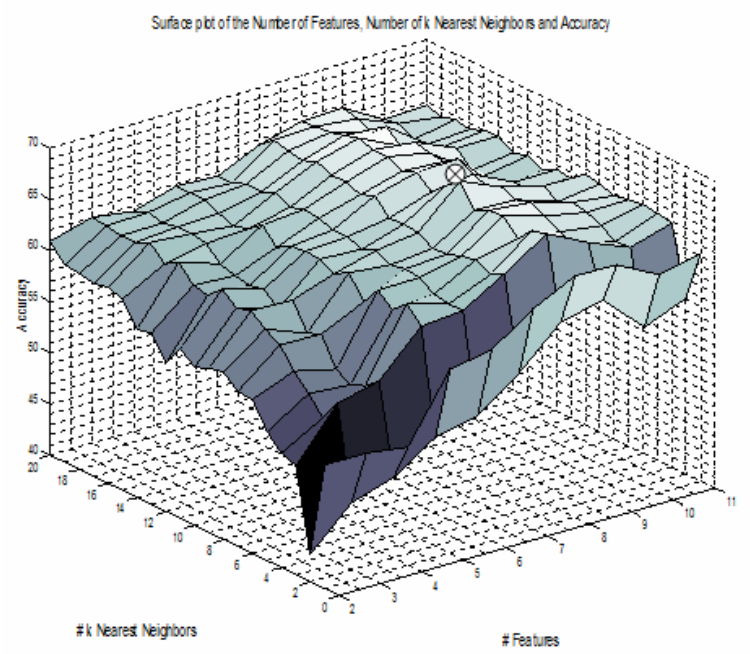

Figure B.1 17: Surface plot of the search space for data set D and sleep event combination 1 using the sequential backward algorithm to obtain the maximum classification accuracy across *k*-NN values and feature subset amount.

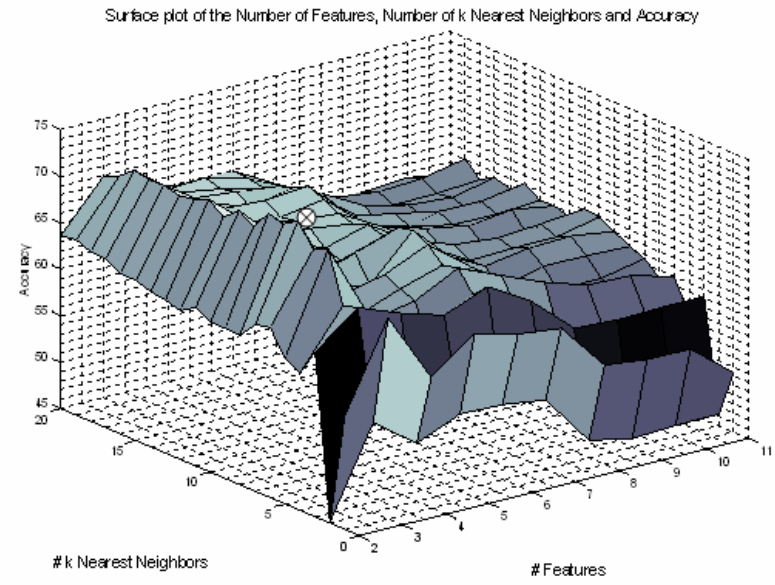

Figure B.1 18: Surface plot of the search space for data set D and sleep event combination 1 using the sequential forward algorithm to obtain the maximum classification accuracy across *k*-NN values and feature subset amount.

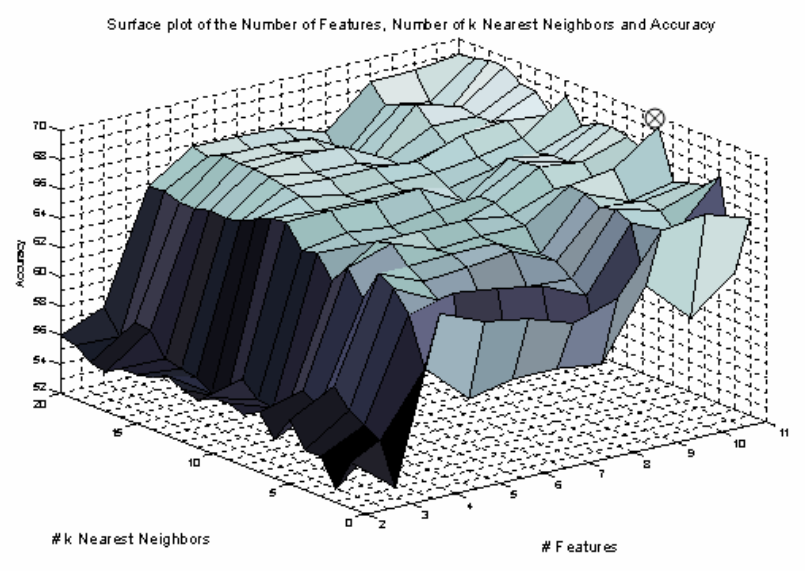

Figure B.1 19: Surface plot of the search space for data set E and sleep event combination 1 using the sequential backward algorithm to obtain the maximum classification accuracy across *k*-NN values and feature subset amount.

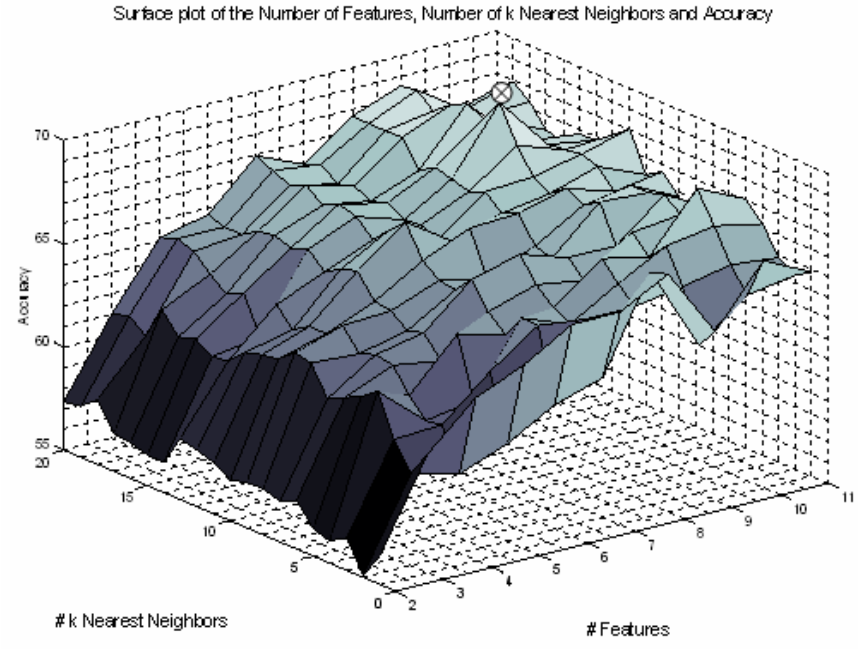

Figure B.1 20: Surface plot of the search space for data set E and sleep event combination 1 using the sequential forward algorithm to obtain the maximum classification accuracy across *k*-NN values and feature subset amount.

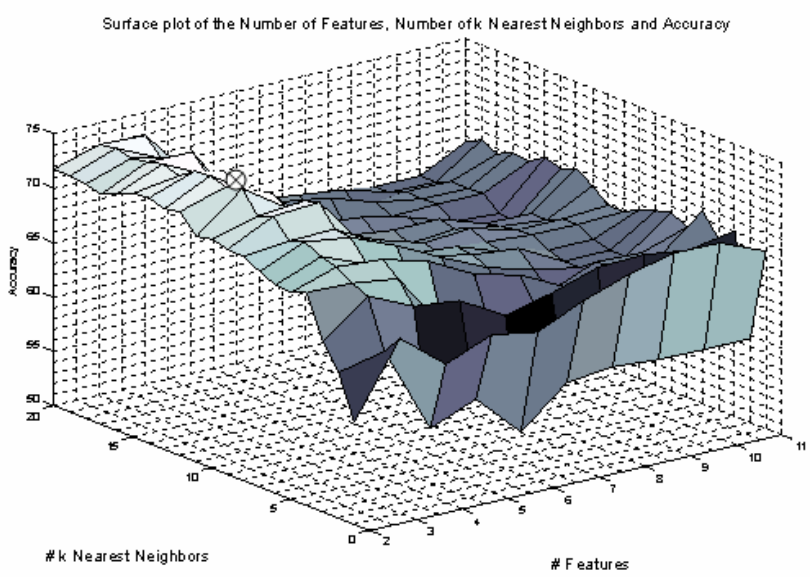

Figure B.1 21: Surface plot of the search space for data set F and sleep event combination 1 using the sequential backward algorithm to obtain the maximum classification accuracy across *k*-NN values and feature subset amount.

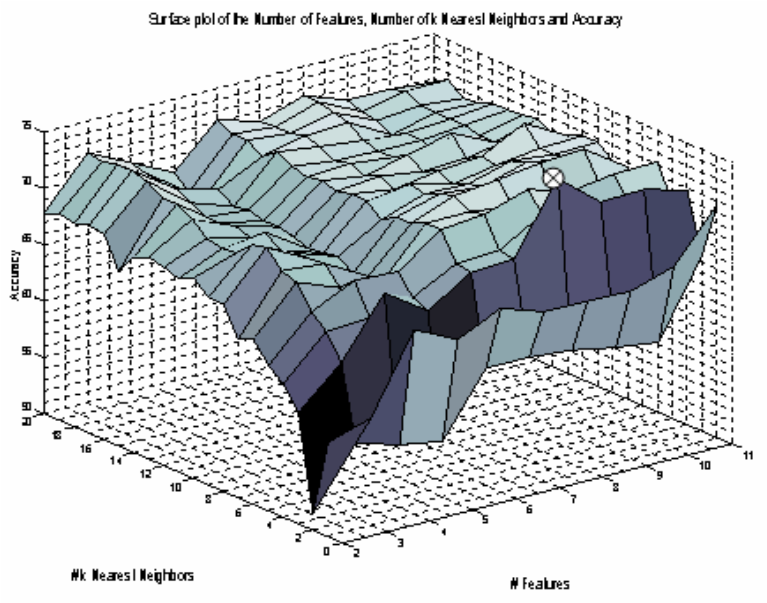

Figure B.1 22: Surface plot of the search space for data set F and sleep event combination 1 using the sequential forward algorithm to obtain the maximum classification accuracy across *k*-NN values and feature subset amount.

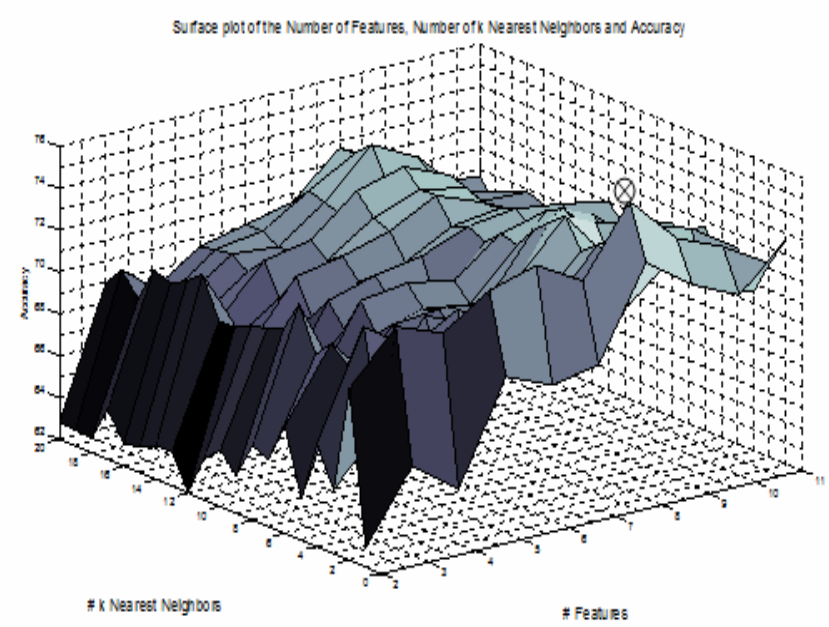

Figure B.1 23: Surface plot of the search space for data set D and sleep event combination 2 using the sequential backward algorithm to obtain the maximum classification accuracy across *k*-NN values and feature subset amount.

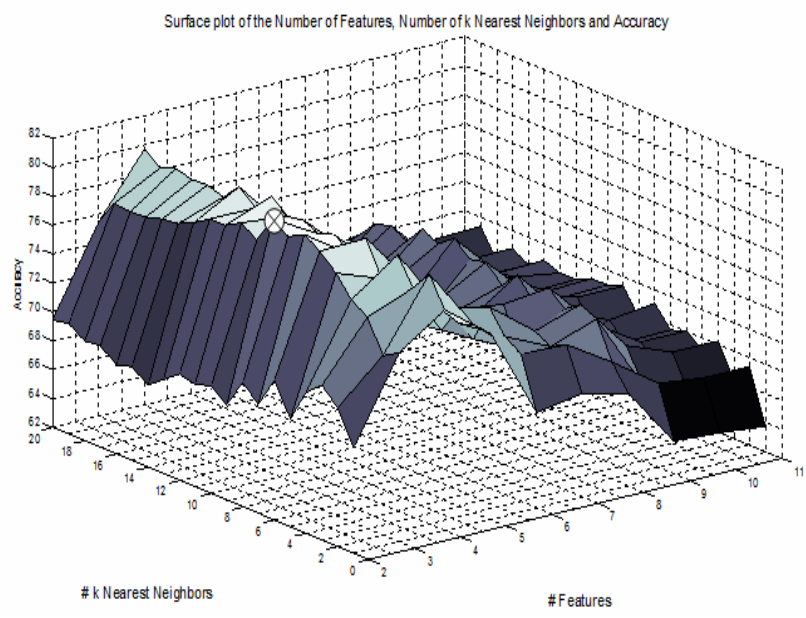

Figure B.1 24: Surface plot of the search space for data set D and sleep event combination 2 using the sequential forward algorithm to obtain the maximum classification accuracy across *k*-NN values and feature subset amount.

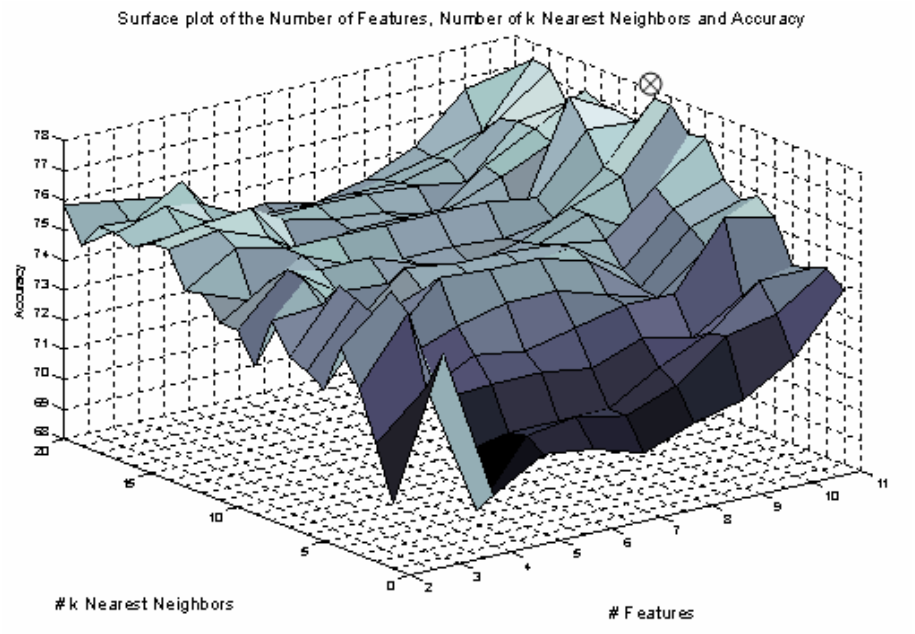

Figure B.1 25: Surface plot of the search space for data set E and sleep event combination 2 using the sequential backward algorithm to obtain the maximum classification accuracy across *k*-NN values and feature subset amount.

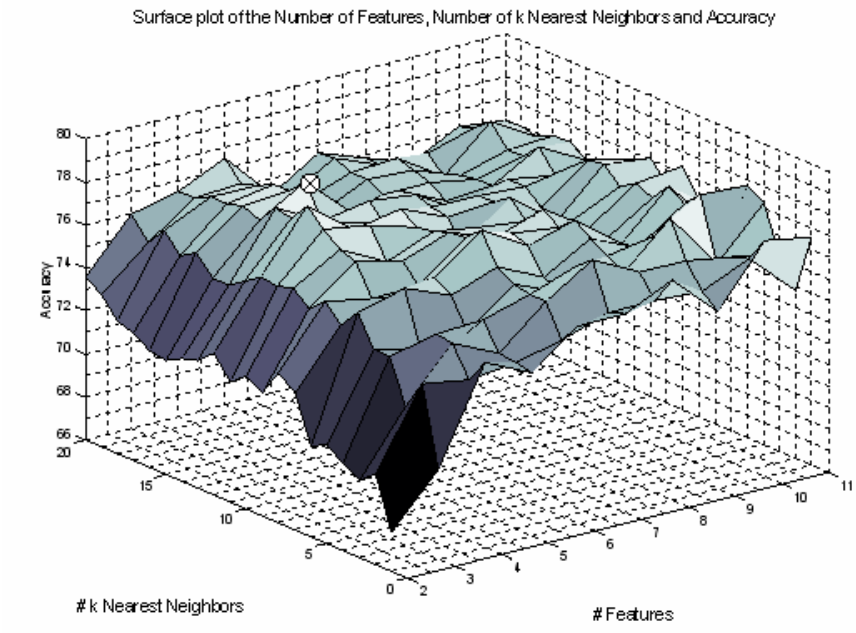

Figure B.1 26: Surface plot of the search space for data set E and sleep event combination 2 using the sequential forward algorithm to obtain the maximum classification accuracy across *k*-NN values and feature subset amount.

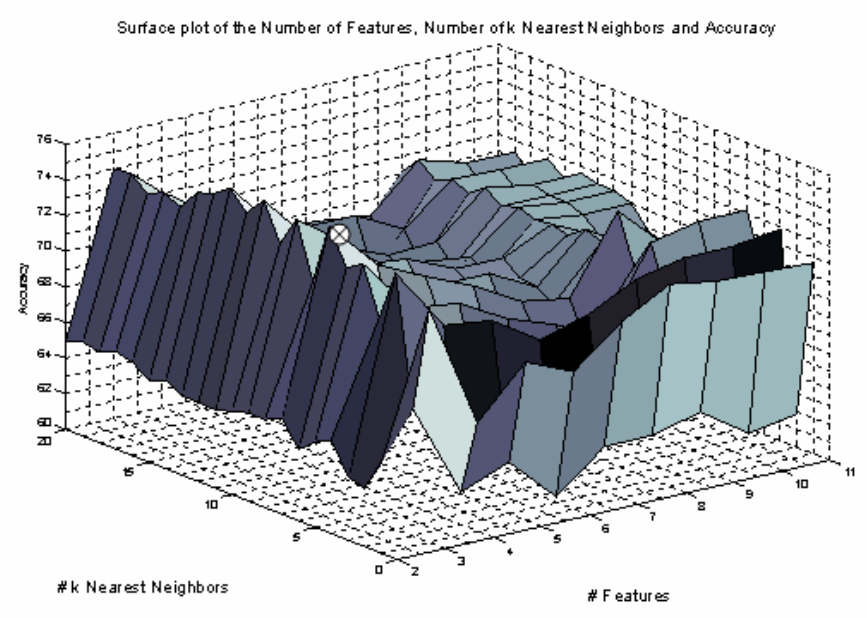

Figure B.1 27: Surface plot of the search space for data set F and sleep event combination 2 using the sequential backward algorithm to obtain the maximum classification accuracy across *k*-NN values and feature subset amount.

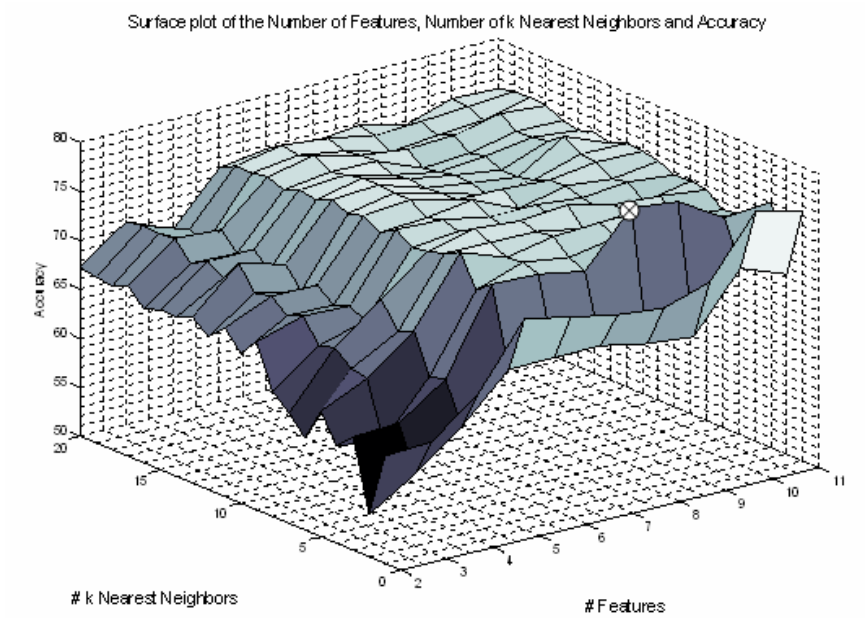

Figure B.1 28: Surface plot of the search space for data set F and sleep event combination 2 using the sequential forward algorithm to obtain the maximum classification accuracy across *k*-NN values and feature subset amount.

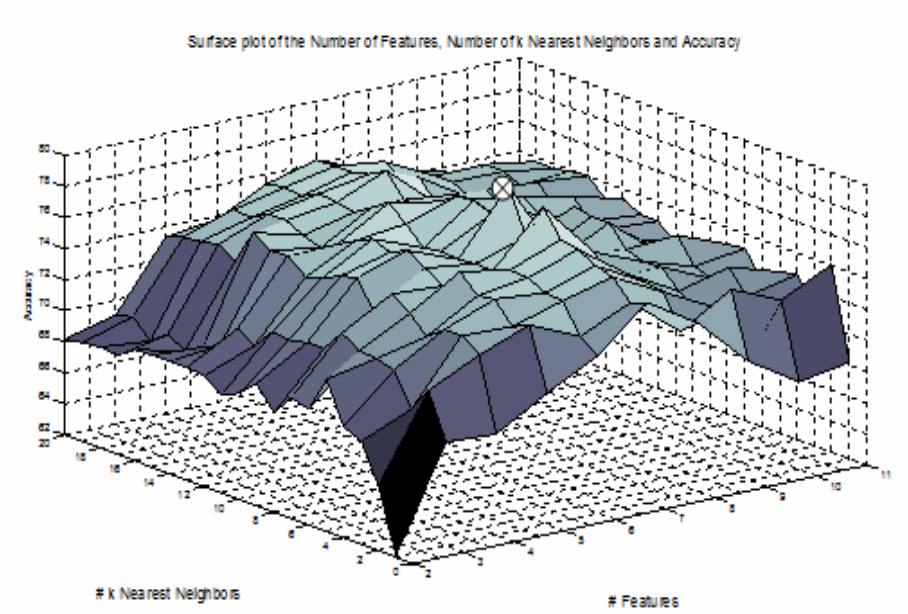

Figure B.1 29: Surface plot of the search space for data set D and sleep event combination 3 using the sequential backward algorithm to obtain the maximum classification accuracy across *k*-NN values and feature subset amount.

Figure B.1 30: Surface plot of the search space for data set D and sleep event combination 3 using the sequential forward algorithm to obtain the maximum classification accuracy across *k*-NN values and feature subset amount.

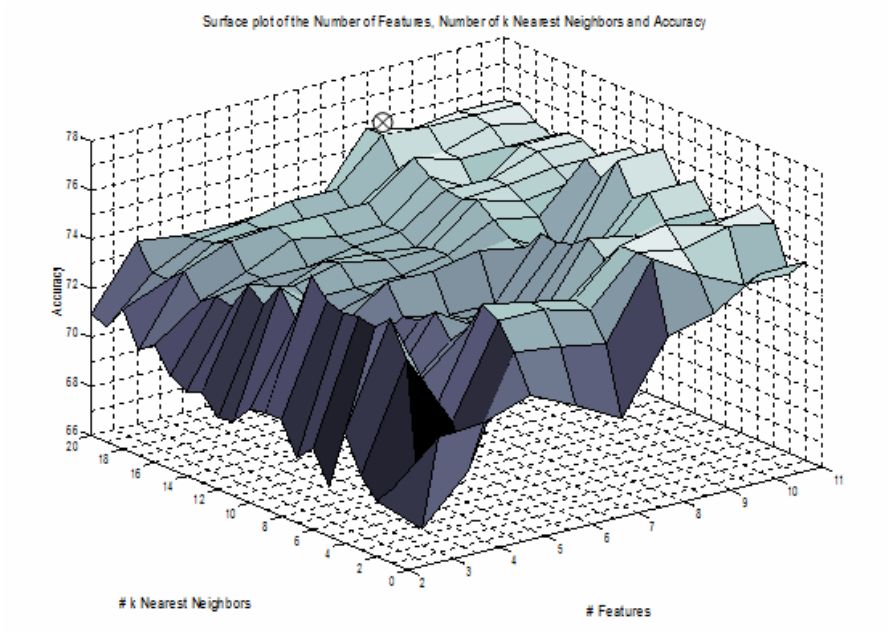

Figure B.1 31: Surface plot of the search space for data set E and sleep event combination 3 using the sequential backward algorithm to obtain the maximum classification accuracy across *k*-NN values and feature subset amount.

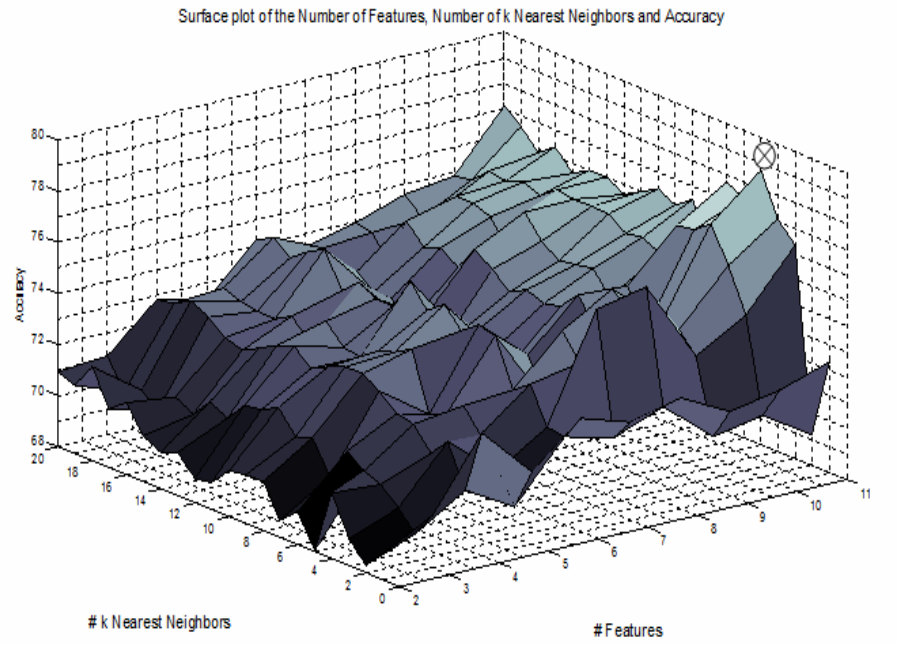

Figure B.1 32: Surface plot of the search space for data set E and sleep event combination 3 using the sequential forward algorithm to obtain the maximum classification accuracy across *k*-NN values and feature subset amount.

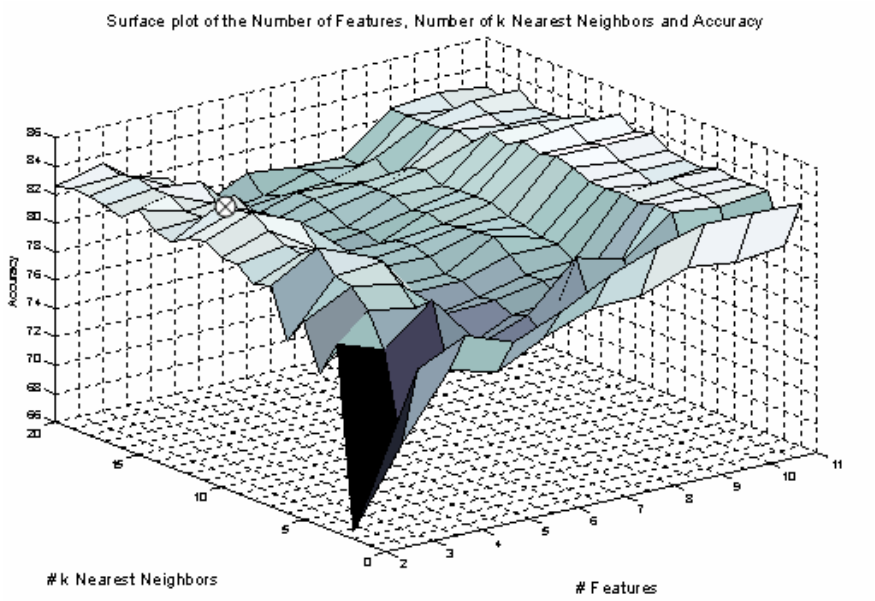

Figure B.1 33: Surface plot of the search space for data set F and sleep event combination 3 using the sequential backward algorithm to obtain the maximum classification accuracy across *k*-NN values and feature subset amount.

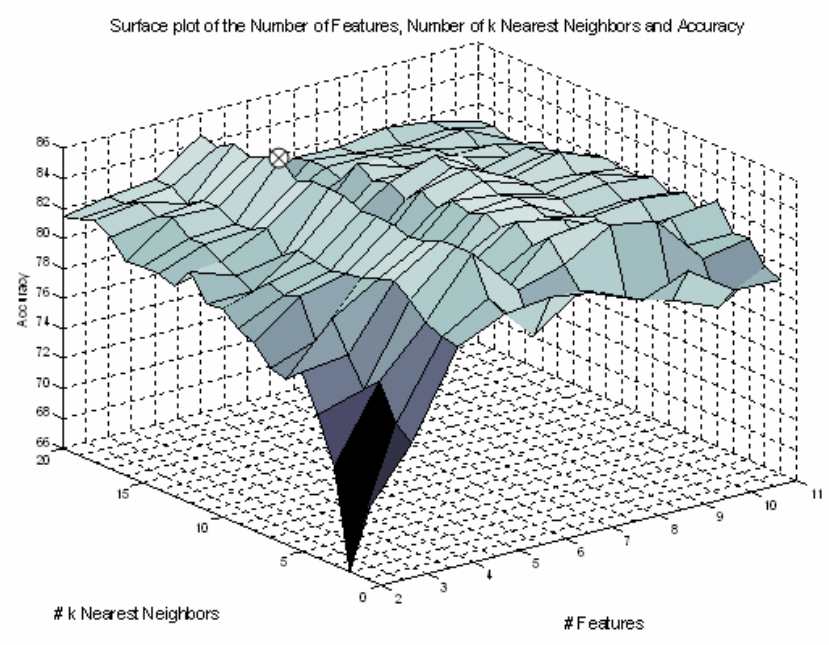

Figure B.1 34: Surface plot of the search space for data set F and sleep event combination 3 using the sequential forward algorithm to obtain the maximum classification accuracy across *k*-NN values and feature subset amount.

B.2 Box Plots of Feature Selection Analysis

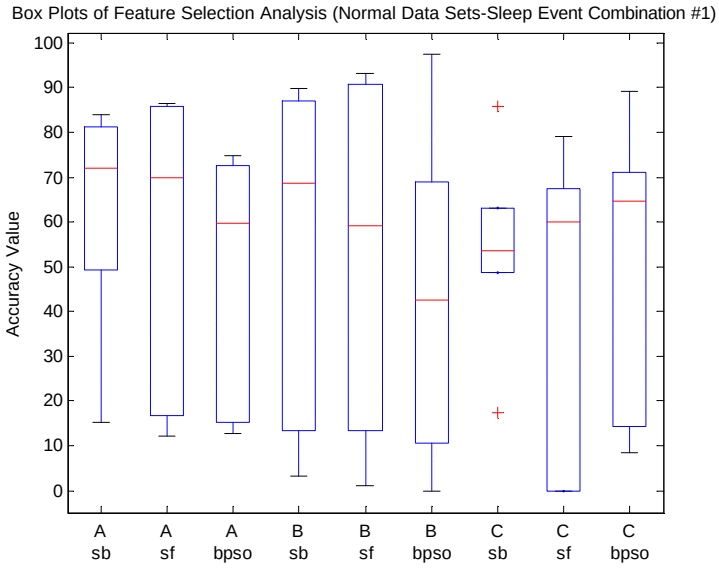

Figure B.2 1: Box plot display of the lower quartile, median, and upper quartile values for normal/control subject data for sleep event combination #1 across all data sets and feature selection algorithms.

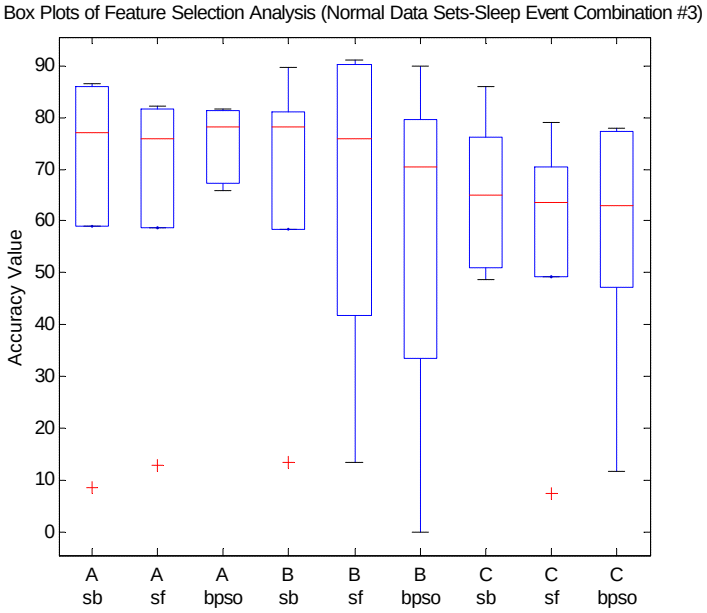

Figure B.2 2: Box plot display of the lower quartile, median, and upper quartile values for normal/control subject data for sleep event combination #3 across all data sets and feature selection algorithms.

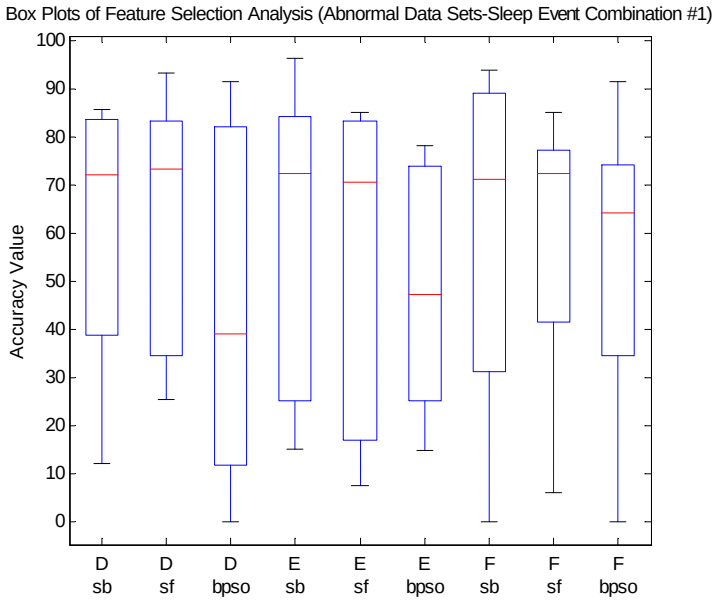

Figure B.2 3: Box plot display of the lower quartile, median, and upper quartile values for Parkinsonism patient data for sleep event combination #1 across all data sets and feature selection algorithms.

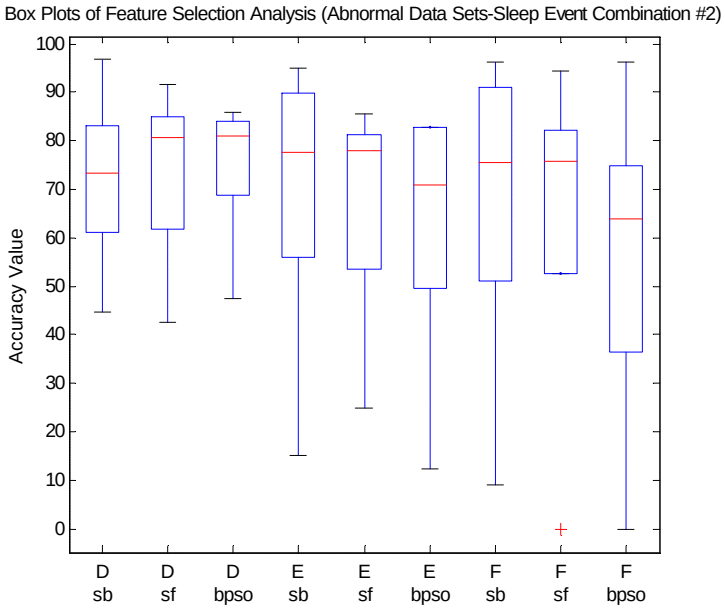

Figure B.2 4: Box plot display of the lower quartile, median, and upper quartile values for Parkinsonism patient data for sleep event combination #2 across all data sets and feature selection algorithms.

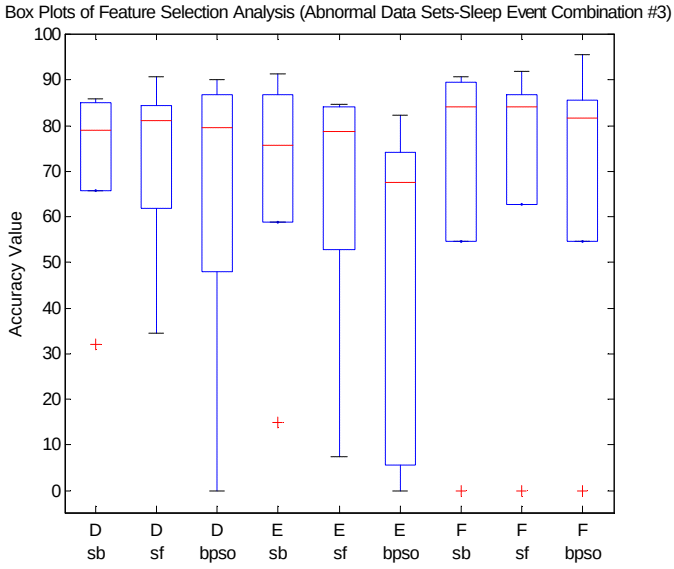

Figure B.2 5: Box plot display of the lower quartile, median, and upper quartile values for Parkinsonism patient data for sleep event combination #3 across all data sets and feature selection algorithms.

REFERENCES

1. Butkov, N., *Atlas of Clinical Polysomnography*. Vol. I. 1996, Ashland: Synapse Media Inc.
2. Rechtschaffen A. and K. A., *A Manual of Standardized Terminology, Techniques and Scoring System for Sleep Stages of Human Subjects*, B.I.S.B.R. Institute, Editor. 1968, University of California, Los Angeles.
3. Parrino, L., et al., *Is insomnia a neurophysiological disorder? The role of sleep EEG microstructure.* Brain Research Bulletin, 2004. **63**(5): p. 377-383.
4. Flexer, A., G. Gruber, and G. Dorffner, *A reliable probabilistic sleep stager based on a single EEG signal.* Artificial Intelligence in Medicine, 2005. **33**(3): p. 199-207.
5. Foundation, N.S., *Sleep in America Poll*, W.A.M. Research, Editor. 2005, National Sleep Foundation: Washington, DC.
6. Carskadon, M. and A. Rechtschaffen, *Monitoring and Staging Human Sleep*, in *Principles and Practice of SLEEP MEDICINE*, M. Hirshkowitz, Editor. 2005, Elsevier Saunders: Philadelphia.
7. Rechtschaffen, A. and J.M. Siegel, *Sleep and Dreaming*. 4 ed. Principles of Neuroscience, ed. E.R. Kandel, J.H. Schwartz, and T.M. Jessel. 2000, New York: McGraw-Hill. 936-947.
8. Himanen, S.L. and J. Hasan, *Limitations of Rechtschaffen and Kales.* Sleep Med Rev, 2000. **4**(2): p. 149-167.
9. Whitney, C.W., et al., *Reliability of scoring respiratory disturbance indices and sleep staging.* Sleep, 1998. **21**(7): p. 749-757.
10. Kubicki, S. and W.M. Herrmann, *The future of computer-assisted investigation of the polysomnogram: sleep microstructure.* J Clin Neurophysiol, 1996. **13**(4): p. 285-94.
11. Crowley, K., et al., *The effects of normal aging on sleep spindle and K-complex production.* Clinical Neurophysiology, 2002. **113**(10): p. 1615-1622.
12. Wauquier, A. and B. Vansweden, *Aging of Core and Optional Sleep.* Biological Psychiatry, 1992. **31**(9): p. 866-880.
13. Suzuki, M., et al., *Discrepancy in polysomnography scoring for a patient with obstructive sleep apnea hypopnea syndrome.* Tohoku Journal of Experimental Medicine, 2005. **206**(4): p. 353-360.
14. Bliwise, D.L., et al., *Inter-rater reliability for identification of REM sleep in Parkinson's disease.* Sleep, 2000. **23**(5): p. 671-6.
15. Hirshkowitz, M., *R&K Manual Update*, in *Sleep Review*. 2005.
16. Iber, C., et al., *AASM Manual for the Scoring of Sleep and Associated Events: Rules, Terminology and Technical Specifications*. 2007, Westchester, Ill.
17. Shumard, T., *Sleep Scoring: Playing by the New Rules*, in *Sleep Review:THE JOURNAL FOR SLEEP SPECIALISTS*. 2007.
18. Anderer, P., et al., *Artifact processing in computerized analysis of sleep EEG - a review.* Neuropsychobiology, 1999. **40**(3): p. 150-7.

19. Klass, D.W., *The continuing challenge of artifacts in the EEG.* American Journal of Eeg Technology, 1995. **35**(4): p. 239-269.
20. Hasan, J., *Automatic analysis of sleep recordings: a critical review.* Ann Clin Res, 1985. **17**(5): p. 280-7.
21. Hallschmid, M., et al., *Transcortical direct current potential shift reflects immediate signaling of systemic insulin to the human brain.* Diabetes, 2004. **53**(9): p. 2202-2208.
22. Erfanian, A. and B. Mahmoudi, *Real-time ocular artifact suppression using recurrent neural network for electro-encephalogram based brain-computer interface.* Medical & Biological Engineering & Computing, 2005. **43**(2): p. 296-305.
23. Allen, P.J., et al., *Identification of EEG events in the MR scanner: The problem of pulse artifact and a method for its subtraction.* Neuroimage, 1998. **8**(3): p. 229-239.
24. Anderer, P., et al., *Artifact Processing in Topographic Mapping of Electroencephalographic Activity in Neuropsychopharmacology.* Psychiatry Research-Neuroimaging, 1992. **45**(2): p. 79-93.
25. Berg, P. and M. Scherg, *A Multiple Source Approach to the Correction of Eye Artifacts.* Electroencephalography and Clinical Neurophysiology, 1994. **90**(3): p. 229-241.
26. Casarotto, S., et al., *Principal component analysis for reduction of ocular artefacts in event-related potentials of normal and dyslexic children.* Clinical Neurophysiology, 2004. **115**(3): p. 609-619.
27. Duda, R., P. Hart, and D. Stork, *Pattern Classification*. 2nd ed. 2001, New York: John Wiley & Sons, Inc. 11-12.
28. Vigario, R.N., *Extraction of ocular artefacts from EEG using independent component analysis.* Electroencephalography and Clinical Neurophysiology, 1997. **103**(3): p. 395-404.
29. Estrada, E., et al. *EEG Feature Extraction for Classification of Sleep Stages*. in *26th Annual International Conference of the IEEE Engineering in Medicine and Biology Society* 2004. San Francisco, CA, USA: IEEE.
30. Subasi, A., *Automatic recognition of alertness level from EEG by using neural network and wavelet coefficients.* Expert Systems with Applications, 2005. **28**(4): p. 701-711.
31. He, W.-X., et al. *Nonlinear Feature Extraction of Sleeping EEG Signals*. in *IEEE Transactions on Engineering in Medicine and Biology 27th Annual Conference* 2005. Shanghai, China.
32. Flexer, A., et al., *An automatic, continuous and probabilistic sleep stager based on a hidden Markov model.* Applied Artificial Intelligence, 2002. **16**(3): p. 199-207.
33. Acir, N. and C. Guzelis, *Automatic recognition of sleep spindles in EEG via radial basis support vector machine based on a modified feature selection algorithm.* Neural Computing & Applications, 2005. **14**(1): p. 56-65.
34. Rezek, I.A. and S.J. Roberts, *Stochastic complexity measures for physiological signal analysis.* Ieee Transactions on Biomedical Engineering, 1998. **45**(9): p. 1186-1191.

35. Zoubek, L., *Automatic Classification of Human Sleep Recordings Combining Artifact Identification and Relevant Features Selection*, in *Measurement and Control*. 2008, Universite Joseph Fourier-Grenoble and VSB-Technical University of Ostrava: Gernoble. p. 144.
36. Agarwal, R. and J. Gotman, *Computer-assisted sleep staging.* Ieee Transactions on Biomedical Engineering, 2001. **48**(12): p. 1412-1423.
37. Park, H.J., et al., *Automated sleep stage scoring using hybrid rule- and case-based reasoning.* Computers and Biomedical Research, 2000. **33**(5): p. 330-349.
38. Durka, P.J., et al., *A simple system for detection of EEG artifacts in polysomnographic recordings.* IEEE Trans Biomed Eng, 2003. **50**(4): p. 526-8.
39. Guyon, I. and A. Elisseeff, *An Introduction to Variable and Feature Selection.* Journal of Machine Learning Research, 2003. **3**: p. 1157-1182.
40. Holder, L.B., et al., *Current and future trends in feature selection and extraction for classification problems.* International Journal of Pattern Recognition and Artificial Intelligence, 2005. **19**(2): p. 133-142.
41. Sykacek, P., et al. *Bayesian wrappers versus conventional filters: Feature subset selection in the Siesta project.* . in *Proceedings of the European Medical & Biomedical Engineering Conference*. 1999. Tallinn, Estonia.
42. Hu, X., R. Eberhart, and Y. Shi. *Recent Advances in Particle Swarm*. in *IEEE Congress on Evolutionary Computation*. 2004. Portland, Oregon,USA.
43. Shi, Y. and R.C. Eberhart. *Parameter selection in particle swarm optimization*. in *Evolutionary Programming VII: Proc. EP 98* 1998. New York: Springer-Verlag.
44. Firpi, H. and E. Goodman. *Swarmed Feature Selection*. in *33rd Applied Imagery Pattern Recognition Workshop*. 2004: IEEE Computer Society.
45. Agrafiotis, D.K. and W. Cedeno, *Feature selection for structure-activity correlation using binary particle swarms.* Journal of Medicinal Chemistry, 2002. **45**(5): p. 1098-1107.
46. Caffarel, J., et al., *Comparison of manual sleep staging with automated neural network-based analysis in clinical practice.* Med Biol Eng Comput, 2006. **44**(1-2): p. 105-10.
47. Geva, A.B. *Unsupervised hierarchical fuzzy clustering methods in forecasting medical events from biomedical signals*. in *IEEE International Conference on Systems, Man, and Cybernetics*. 1997. Orlando, FL, USA: IEEE.
48. Nicolaou, N. and S. Nasuto. *Temporal Independent Component Analysis for Automatic Artefact Removal from EEG*. in *2nd International Conference on Medical Signal and Information Processing*. 2004. Malta, G.C.
49. Ogilvie, R. and J. Harsh, eds. *Sleep Onset: Normal and Abnormal Processes*. 1994, American Psychological Association: DC. 397.
50. Kemp, B. and H.A. Kamphuisen, *Simulation of human hypnograms using a Markov chain model.* Sleep, 1986. **9**(3): p. 405-14.
51. Happe, S. and C. Trenkwalder, *Movement disorders in sleep: Parkinson's disease and restless legs syndrome.* Biomedizinische Technik, 2003. **48**(3): p. 62-67.
52. Scaravilli, T., et al., *Health-related quality of life and sleep disorders in Parkinson's disease.* Neurol Sci, 2003. **24**(3): p. 209-10.

53. Oerlemans, W.G. and A.W. de Weerd, *The prevalence of sleep disorders in patients with Parkinson's disease. A self-reported, community-based survey.* Sleep Med, 2002. **3**(2): p. 147-9.
54. Trenkwalder, C., *Parkinsonism*, in *Principles and Practice of SLEEP MEDICINE*, M. Kryger, T. Roth, and W. Dement, Editors. 2005, Elsevier Saunders: Philadelphia. p. 801-810.
55. Bliwise, D.L., et al., *Quantification of electromyographic activity during sleep: a phasic electromyographic metric.* J Clin Neurophysiol, 2006. **23**(1): p. 59-67.
56. Susan Herman, M.D., *Blankhead Montage*, B. Montage, Editor. 2005: Philadelphia.
57. deRijk, M.C., et al., *Prevalence of parkinsonism and Parkinson's disease in Europe: The EUROPARKINSON collaborative study.* Journal of Neurology Neurosurgery and Psychiatry, 1997. **62**(1): p. 10-15.
58. Knight, J., *Signal Fraction and Artifact Removal in EEG*, in *Department of Computer Science*. 2003, Colorado State University: Fort Collins.
59. Green, A.A., et al., *A Transformation for Ordering Multispectral Data in Terms of Image Quality with Implications for Noise Removal.* Ieee Transactions on Geoscience and Remote Sensing, 1988. **26**(1): p. 65-74.
60. Hundley, D., M. Kirby, and M. Anderle, *A Solution Procedure for Blind Signal Separation using the Maximum Noise Fraction Approach: Algorithms and Examples* Proceedings of the Conference on Independent Component Analysis, 2001: p. 337-342.
61. Park, H.J., et al., *Automated sleep stage scoring using hybrid rule- and case-based reasoning.* Comput Biomed Res, 2000. **33**(5): p. 330-49.
62. van der Heijden F., D.R., de Ridder D., Tax D., *Classification, Parameter Estimation and State Estimation An Engineering Approach using MATLAB* 2004, West Sussex, England: John Wiley & Sons, Ltd. 423.
63. Theodoridis, S. and K. Koutroumbas, *Pattern Recognition*, ed. 3rd. 2006: Elsevier.
64. Burrell, L.S., et al. *Evaluation of Feature Selection Techniques for Analysis of Functional MRI and EEG*. in *International Conference on Data Mining* 2007. Las Vegas, Nevada.
65. Engelbrecht, A.P., *Fundamentals of Computational Swarm Intelligence*. 2005, Hoboken: John Wiley & Sons, Ltd.
66. Kennedy, J.F., R.C. Eberhart, and Y. Shi, *Swarm intelligence*. 2001, San Francisco: Morgan Kaufmann Publishers.
67. Agarwal, R. and J. Gotman, *Digital tools in polysomnography.* J Clin Neurophysiol, 2002. **19**(2): p. 136-43.
68. Lipschutz, S. and M. Lipson, *Probability* Schaums Outline 2000, New York: McGraw-Hill.
69. Rabiner, L.R., *A Tutorial on Hidden Markov-Models and Selected Applications in Speech Recognition.* Proceedings of the Ieee, 1989. **77**(2): p. 257-286.
70. Dugad, R. and U.B. Desai, *A Tutorial on Hidden Markov Models.* 1996, Indian Institute of Technology-Bombay: Powai, Mumbai. p. 16.
71. Murphy, K., *Hidden Markov Model Toolbox for Matlab*. 2005, http://www.cs.ubc.ca/~murphyk/Software/HMM/hmm.html.

72. Gelula, R., *Why sleep is important and what happens when you don't get enough*, in *American Psychological Association Online*, O.o.P. Communications, Editor. 2006: Washington,DC.
73. D'Alessandro, M.M., *The Utility of Intracranial EEG Feature and Channel Synergy for Evaluating the Spatial and Temporal Behavior of Seizure Precursors*, in *Electrical and Computer Engineering*. 2001, Georgia Institute of Technology: Atlanta. p. 177.
74. Agarwal, R., et al., *Automatic EEG analysis during long-term monitoring in the ICU*. Electroencephalography and Clinical Neurophysiology, 1998. **107**(1): p. 44-58.
75. Smart, O.L., *Evolutionary Algorithms and Frequent Itemset Mining for Analyzing Epileptic Oscillations*, in *Electrical and Computer Engineering*. 2007, Georgia Institute of Technology: Atlanta. p. 202.
76. Abdi, H.M., Paul, *Lilliefors/Van Soest's test of normality*, in *Encyclopedia of Measurement and Statistics*, N.J. Salkind, Editor. 2007, SAGE. p. 540-544.
77. Hayter, A., *Probability and Statistics for Engineers and Scientists*. 2 ed, ed. C. Reitz. 2002, Pacific Grove,CA: Duxbury. 916.
78. Roberts, C., *The Dissertation Journey: A Practical and Comprehensive Guide to Planning, Writing, and Defending Your Dissertation*. 2004, Thousand Oaks, CA: Corwin Press. 225.
79. Becq, G., et al., *Comparison Between Five Classifiers for Automatic Scoring of Human Sleep Recordings*, in *Classification and Clustering of Knowledge Discovery*. 2005, Springer Berlin / Heidelberg: Berline Heidelberg. p. 113-127.
80. Gray, A., *FASTlib*, in *Efficient Implementation of Machine Learning Algorithms*. 2008, Georgia Institute of Technology: Atlanta, GA.

VITA

JACQUELINE A. FAIRLEY

Jacqueline was born in Springfield, Missouri (MO). She was raised in Kansas City, MO by her mother Paula Ann Fairley and maternal grandmother Bennie Mae Rayford. She attended Van Horn High School in Independence, MO where she graduated as class valedictorian. Jacqueline is an alumnus of the University of Missouri-Columbia which she attended as a George C. Brooks scholar and graduated with a B.S. in Electrical Engineering and a Minor in Mathematics.

Upon completion of her bachelor's degree she obtained a graduate fellowship from the National Consortium for Graduate Degrees for Minorities in Engineering and Science and Motorola Inc., to pursue graduate education at the Georgia Institute of Technology (GaTech). At GaTech she obtained a M.S. in Electrical and Computer Engineering with a minor in Industrial and Systems Engineering prior to pursuing her doctorate in Electrical and Computer Engineering. During her doctoral studies Jacqueline researched projects utilizing image processing techniques for micro-array gene expression data and pattern recognition techniques for processing human polysomnograms.

Her research interest consists of machine learning, statistical modeling, and evolutionary computation. She is a member of IEEE, Eta Kappa Nu, Tau Beta Pi, and NSBE. When she is not working on her research, Ms. Fairley enjoys volunteering in after school engineering clubs, playing the piano, drawing, Inline skating, and spending time with friends and family.